Impact of high penetration of solar PV generation on transient- and voltage stability of the Dutch high voltage grid

Nikhil Kalloe

Technische Universiteit Delft

TUDelft

Impact of high penetration of solar PV generation on transient- and voltage stability of the Dutch high voltage grid

by

Nikhil Kalloe

in partial fulfilment of the requirements for the degree of

Master of Science

in Electrical Engineering

at the Delft University of Technology,
to be defended publicly on Wednesday September 9, 2020 at 14:00.

This thesis is confidential and cannot be made public until September 9, 2022.

An electronic version of this thesis is available at http://repository.tudelft.nl/.

T̃U Delft

Abstract

The last decade has experienced an immense growth in renewable energy sources such as solar PV parks and wind parks. The staggering rise of these generation units has increased primarily due to environmental concerns and climate change policies. This increase has been brought on to reduce the emission of GHGs from the energy sector. On the other hand, the increase has brought with it several technical challenges concerning the power system stability of the electrical network. In the current TenneT dynamic grid model, PV systems are modelled by way of negative load with low level of detail, while synchronous generation units and aggregated on-shore wind parks are modelled with their dynamic models with a high level of detail. As the growth of PV generation units is constantly rising, these systems are starting to have a larger effect on the stability of the power system thus their dynamic behaviour cannot be neglected.

The focus of this thesis is to propose a dynamic model with parameter set to represent PV systems in the transmission network. Additionally, to implement the dynamic models with the proposed parameter set in the TenneT dynamic grid model and then evaluate the transient- and short-term voltage stability for networks with a high penetration of PV systems. The selection of dynamic models and the assignment of a parameter set required literature research on the requirements for generators, the Dutch netcode and different dynamic models which can represent PV systems.

The literature research unveiled that the representation of PV systems can be split into two categories i.e. large-scale PV systems and aggregated PV systems. From TenneT's perspective, PV systems connected to the transmission domain are considered large-scale PV systems and PV systems connected to the distribution domain are considered aggregated PV systems. For large-scale PV systems the selection was made to model such systems with the *Large-scale PV model* or *Central Station PV System model* developed by WECC since this dynamic model is considered to be the standard for modelling large PV systems and has been thoroughly studied and verified. For aggregated PV systems the latest iteration to represent multiple PV systems has been selected which is the *DER_A model*. The parameter assignment of these models was done as follows, the parameters which align with the grid connection requirements such as reactive current gain and deadband of the voltage control are assigned the values required by the Dutch netcode. The reactive current gain for PV systems connected to the transmission domain was assigned a value of 5 while the PV systems present at distribution level were assigned a value of 2 as this is consistent with the Dutch netcode. Additionally, the deadband for reactive current injection was set to 5% for both case studies, however, this deadband yielded convergence problems in the TenneT network case study as the voltage was too tightly controlled and hence was modified to 10%. Furthermore, parameters which are highly dependent on the manufacturer have been assigned values of existing PV systems in the Netherlands. Such parameters refer to PI gains, which determine how assertively the PV systems respond to a contingency. Parameters which did not influence the dynamic behaviour are assigned typical values found in the literature. Lastly, the remaining parameters were assigned values with the combination of literature research and a sensitivity study. Two parameter sets were proposed for aggregated PV systems as the Dutch netcode makes a distinction between type A and type B, C ,D1 PV systems in terms of reactive current injection. This methodology led to the proposed parameter sets for large-scale PV systems and aggregation of PV systems adhering to the grid connection requirements of the Netherlands.

The transient- and voltage stability was firstly evaluated in an IEEE 9 bus network with different PV penetration levels. Modifications were made to the network to obtain cases with different PV penetration levels. The transient stability was analysed by introducing a three-phase fault in the network and evaluating the critical clearing time. The analysis indicated that the steady-state operating point of a synchronous generator has a significant influence on the transient stability. It was also shown that a reduction in short-circuit current in the network leads to more critical dynamic operating points of the synchronous generator leading to a decrease in transient stability. In such a small network it was also presented that the removal of the most critical synchronous generator for a specific fault leads to an increase in transient stability. Concerning the voltage stability, it was shown that for the networks with lower short-circuit current levels, the voltage drops were more severe. Additionally, the voltage drop near a generation unit is highly dependent on the type of generation unit as the voltage drops near a synchronous generator were less severe compared to a PV system of the same capacity due to the difference in their reactive current injection.

Following this, an extensive transmission network i.e. the TenneT network was used as a case study and was evaluated based on the transient- and voltage stability for different situations. Firstly, a selection of different hours was done,

where different hours were selected with varying corresponding short-circuit levels. Moreover, python scripts were used to implement the dynamic PV systems with a high level of detail in the TenneT dynamic grid model. In the transient stability analysis, three different buses of interest were selected close to synchronous generation units. Across all cases the operating point of the synchronous generator was set to a fixed value and the generator bus voltage was brought within 0.01 pu across the cases to isolate the impact of the short-circuit current on the transient stability. The analysis proved that the impact of PV systems on the transient stability (at a bus near a synchronous generator) is highly dependent on the amount of short-circuit current which is contributed by all the PV systems relative to the total short-circuit current at the bus — this relationship is defined as the SCC PV ratio. The higher the SCC PV ratio, entailing the higher the contribution of PV systems relative to the total short-circuit current at the faulted bus, the bigger the influence of PV systems on the transient stability. For low SCC PV ratios, it was shown that the PV systems had little to no influence on the transient stability. As synchronous generators are being decommissioned and new PV systems are added to the network more regions will shift towards high SCC PV ratios hence the influence of PV systems on the transient stability shall only increase. Methods to improve the transient stability were also analysed. The first proposed method was to limit the operating region of critical synchronous generators to improve transient stability as it was shown that the operating point of a synchronous generator significantly reduces the transient stability when close to it's active power limits and under-excited. The second proposed method was to increase the total short-circuit current at the faulted bus by adding a reactive compensation device such as a synchronous condenser or STATCOM. The third and final proposed method is the decrease of the reactance between synchronous generator and faulted HV bus as the losses of reactive power shall be reduced hence leading to an improvement in transient stability.

The voltage stability was assessed based on three different aspects i.e. voltage drop, voltage spread and voltage recovery. In the analysis, it was shown that the magnitude of the voltage drops at nearby buses increased as the short-circuit current levels decreased. Additionally, the voltage drop at a bus located electrically very far from the faulted bus also saw an increased voltage drop for the cases with lower short-circuit current levels. This led to the conclusion that scenarios with lower short-circuit levels yield a higher voltage drop at neighbouring buses and lead to a wider area of the network being affected by the fault. Furthermore, for voltage recovery the cases where PV systems were represented by dynamic models were compared to cases where PV systems were represented with negative load. These cases had similar network conditions only the dynamic response of the PV systems was excluded for the negative load cases. This analysis proved that the voltage recovery occurs at a quicker rate for the cases with dynamic models hence the added short-circuit contribution of the PV systems aided the voltage recovery. As synchronous generators are continually being phased out and PV systems are added to power system networks, the voltage stability shall be more vulnerable to deeper voltage drops, wider areas of the network being affected by a fault and longer voltage recovery times due to the decrease of short-circuit current levels. A proposal for improving voltage stability was the placement of reactive compensation devices such as a synchronous condenser or STATCOM to increase the short-circuit levels in the networks and hence improving the voltage drops, voltage spread and voltage recovery time.

Acknowledgements

Contents

List of Figures

List of Tables

List of Abbreviations

APRC   Active Power Reference Control

ARCC   Additional Reactive Current Control

AT   Alternative Transition

BRCC   Base Reactive Current Control

CA   Climate Agreement

CCT   Critical Clearing Time

DG   Distributed Generation

DM   Dynamic Model

DSO   Distribution System Operator

FAPI   Fast Active Power Injection

FCT   Fault Clearing Time

FRT   Fault-Ride-Through

FSI   Foundation for System Integration

GC   Grid Code

GCR   Grid Connection Requirements

GHG   Greenhouse Gas

HV   High Voltage

IBG   Inverter-Based Generation

IP   Investment Plan

IP2020   Investment Plan of 2020

LVPL   Low Voltage Power Logic

NC   Network Codes

NL   Negative Load

PGM   Power-Generating Module

PLL   Phase-Locked Loop

POI   Point of Interconnection

PPM   Power Park Module

PSS/E   Power System Simulator for Engineers

PV   Photo-Voltaic

REMTF   Renewable Energy Modeling Task Force

RES   Renewable Energy Sources

RfG   Requirements for Generators

ROCOF   Rate of Change of Frequency

RPRC   Reactive Power Reference Control

RQ   Research Questions

S-OB   Sub-Objectives

SCC   Short-Circuit Current

SCR   Short-Circuit Ratio

SG   Synchronous Generator

SPGM   Synchronous Power-Generating Module

TSO   Transmission System Operator

WECC   Western Electric Coordinating Council

1

Introduction

This chapter starts with the background and motivation of this master thesis project. Following this introduction, the problem is defined to provide the reader with a clear and concise explanation of the context of this research. This is followed up by an outline of the objectives to obtain a step-wise approach of providing a substantive answer to the defined research questions. Moreover, the main scientific contributions of this research shall be explored. Lastly, the outline of the report is discussed in a chapter-wise manner.

1.1. Background

Over the last couple of years the temperature of the surface of the earth has increased significantly. It is projected, if no additional measures are taken, an increase between 1.1°C and 6.4°C will take place of the global-mean surface temperature over the coming 100 years [1]. To put this into perspective, the increase of global temperature from 1880 to 1980 is equivalent to 0.28°C, while the last 20 years has seen an increase of 0.42°C [2]. The change of global temperature over the years is shown in Figure 1.1.
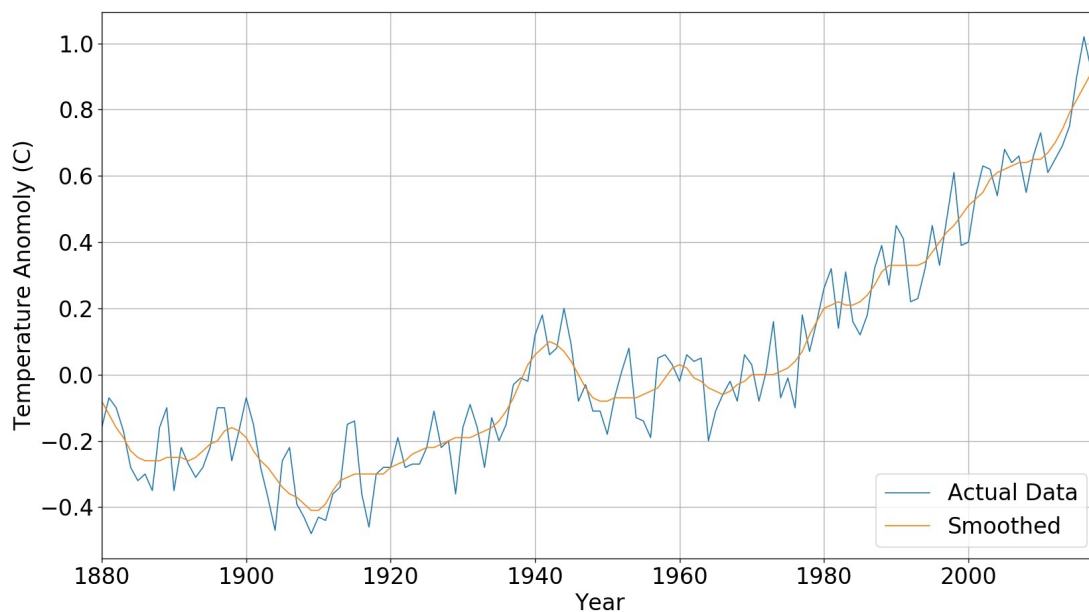
Figure 1.1: Change in global temperature [2]

This significant change in temperature has brought along with it higher temperatures, higher frequency of extreme weather events and has had a cascaded effect on all forms of life on earth [3]. The emission of greenhouse gases (GHGs) are the root cause for soaring temperatures on the surface of the earth. These earth-damaging gases come

from different sectors such as the energy sector, agriculture sector and waste sector, just to name a few. One of the biggest causes of emission of GHGs, and consequently climate change, is the energy sector, accounting for a whopping 82.7% of GHG emissions in 2017 in the Netherlands [4]. A huge part of the GHG emissions in the energy sector is due to the production of electrical energy with fossil fuels such as coal and gas.

Consequently, policies are now being introduced to reduce and eventually eliminate these earth-harming production units. The Paris agreement is a global warming change agreement implemented in November 2016 involving over 180 countries, striving mainly to restrict the increase of global temperature 'well below' 2°C compared to the pre-industrial time age [5]. To achieve this, the Netherlands has introduced a climate agreement which defines a certain set of measures to reduce the emission of GHGs by nearly half by 2030 compared to 1990 [6]. Due to establishment of these policies, thermal power plants consisting of synchronous generators are gradually being replaced by mostly inverter-based generation (IBG) such as solar PV parks and wind parks. Ensuingly, solar PV systems have seen an immense growth in the last couple of years in the Netherlands. The installed capacity of solar PV systems over the years in the Netherlands is provided in Figure 1.2.
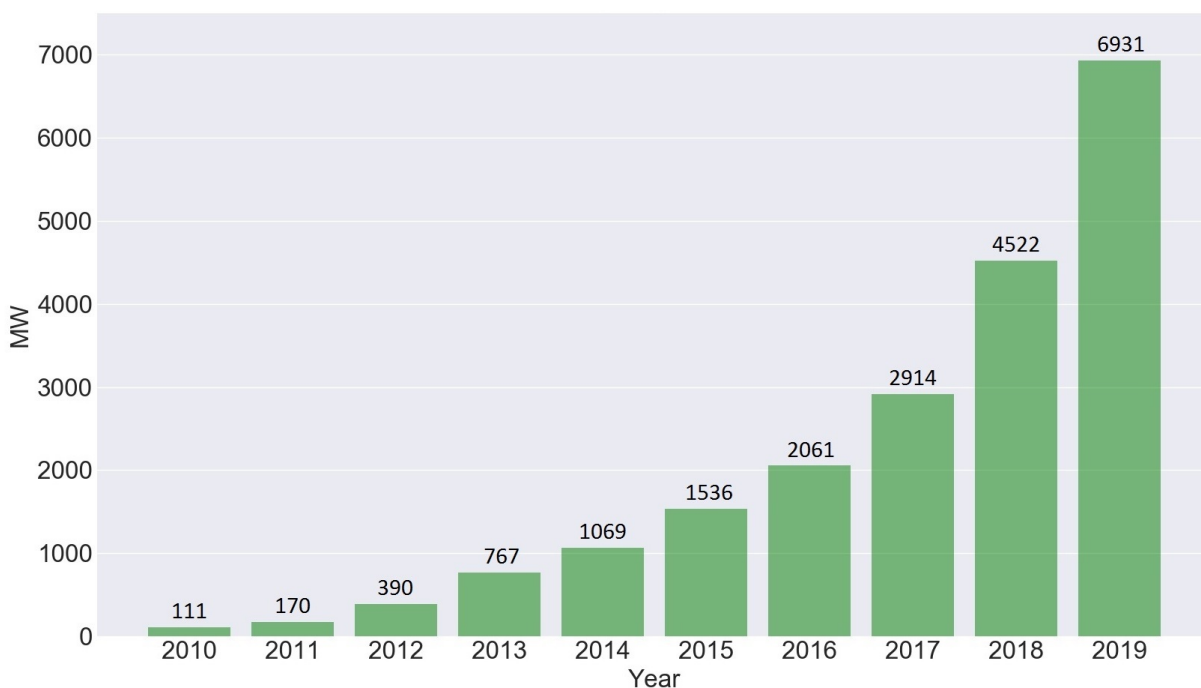
Figure 1.2: Installed PV capacity in the Netherlands [7]

The increase of IBG has brought along with it significant changes of the power system in structure and general behaviour. The structural changes in electrical power systems have been effectively encapsulated in [8], stating the following,

> *Power systems are being transformed from vertically-designed systems with unidirectional transmission to-distribution power flows to horizontally-designed systems with bidirectional power flows between all voltage levels.*

The above-mentioned statement looks at the changes in the electrical power system from a topological or structural point of view. Another important aspect of the changes is the technological transformation which is taking place in electrical power systems across the world. This transformation has carried with it challenges for power system stability such as decreased inertia levels, resonances due to cables and power electronics and reduction of transient stability margins [9].

1.2. Problem Definition

As discussed in Section 1.1, the last decade has seen an immense growth of solar PV systems, this includes both large-scale solar PV Power Park Modules (PPMs) and distributed solar PV, and it is projected that this growth will continue due to environmental concerns. Presently, solar PV systems are not modelled with dynamic models and with a low

level of detail in the current dynamic grid model of TenneT, the Transmission System Operator (TSO) of the Netherlands. On the contrary, PV systems are modelled as a negative load providing no dynamic characteristics. However, due to the flourishing of solar PV systems, lessening of synchronous generators and newly introduced grid connection requirements stating that PPMs (including PV systems) should be able to ride through faults, the influence of solar PV systems on the dynamic behaviour of the power system keeps increasing hence an increased need for detailed modelling is necessary.

From a technological perspective conventional synchronous generators are defined by their physics and control, and solar PV systems are defined solely by their control algorithms [10]. The reduction of synchronous generators and an increase of inverter-based generation has brought with it challenges for preservation of power system stability such as worsening of transient stability and higher susceptibility to voltage instability. Henceforth, it is also of interest to look ahead and evaluate a network with high penetration of PV systems with respect to power system stability.

In this research project, PV systems i.e. large-scale solar PV and aggregation of distributed solar PV, will be modelled according to the European Requirements for Generators (RfG) and the requirements of the Dutch netcode. Additionally, a standard modelling approach, including proper selection of models and a default parameter set, for future PV plants shall be developed. Moreover, several case studies will be carried out based on TenneT's investment plan scenarios to determine the impact of a high penetration of large-scale and aggregated solar PV on rotor angle (transient) stability and short-term voltage stability. For these scenarios several different hours will be studied, where the hours or snapshots are in direct relation to the power flow distribution and the number of synchronous generators connected. Additionally, the possible risks shall be identified in the regions of interest and mitigation measures shall be proposed. The above-mentioned approach will be discussed in a structural manner subsequently.

1.3. Objectives and Research Questions

The overall objective of this research project is to,

Assess the impact of increased penetration levels of solar PV systems on a transmission network with respect to transient- and short-term voltage stability and to identify the potential instability risks and provide measures to apply accordingly

To carry out this research project and eventually reach the overall objective, several steps (sub-objectives) are laid out. These serve as a guideline for obtaining the overall objective. The sub-objectives (S-OBs) are,

S-OB1 Development of methodology to assign proper dynamic solar PV models and a standard parameter set to represent (future) solar PV PPMs, deduced from existing PV plants and literature research, in accordance with the RfG and the Dutch netcode.

- Study the RfG and Dutch netcode.
- Research different PV models and propose the PV models to be used.
- Study the control algorithms and parameter sets of the proposed PV models.
- Development of methodology and standard parameter set for selected PV models.

S-OB2 Make use of the parameter set developed in S-OB1 and evaluate the transient- and short-term voltage stability in an IEEE 9 bus network with different levels of solar PV penetration.

- Develop different solar PV penetration level cases within the IEEE 9 bus network.
- Assess the behaviour on the transient- and short-term voltage stability for the different cases.

S-OB3 Properly model all solar PV systems in the TenneT dynamic grid model with the proposed parameter set developed in S-OB1.

- Create a methodology in terms of capacity to model PV systems based on the requirements provided in the RfG and Dutch netcode.
- Model large-scale solar PV systems connected at transmission level.
- Model aggregated solar PV systems.

S-OB4 Examine the transient stability in areas of interest in the Dutch high voltage network.

- Explanation of the assessment method for evaluating the transient stability.

- Explanation of the areas selected to evaluate the transient stability.
- Analysis of the transient stability in selected areas.
- Provision of mitigation measures or methods to improve the transient stability.

S-OB5   Examine the short-term voltage stability in areas of interest in the Dutch high voltage network.

- Explanation of the assessment method for evaluating short-term voltage stability.
- Explanation of the areas selected to evaluate short-term voltage stability.
- Analysis of short-term voltage stability in selected areas.
- Provision of mitigation measures or methods to improve short-term voltage stability.

After completing the defined objectives, the following research questions (RQs) can be answered:

RQ1   *How can a model structure and default parameter set be developed for individual (future) solar PV PPMs?*

RQ2   *How does the transient stability in the Dutch high voltage grid change with increased penetration levels of solar PV?*

RQ3   *What impact does increased penetration of solar PV have on the voltage stability of the Dutch high voltage grid?*

RQ4   *How can a rule of thumb be developed to determine at which penetration level mitigation measures are needed in the relevant areas?*

RQ5   *What type of mitigation measures can be introduced to reduce the potential consequences of high penetration solar PV?*

1.4. Thesis contributions

This section describes the scientific contributions of this thesis. The literature study and findings are discussed in Chapter 2, 3 and 4.

Modelling of PV systems:
Chapter 3 and 4 discuss the grid connection requirements and the generic dynamic models used to represent PV systems. It is provided that currently at TenneT TSO B.V., PV systems are modelled as negative load and with a low level of detail. Additionally, no standard parameter set has been developed to represent the dynamic behaviour of PV systems in particular in the Netherlands. A contribution of this thesis is,

- Selection and justification of generic PV models to represent both large-scale PV systems and aggregated PV systems from the perspective of a TSO.
- Development of a standard parameter set for large-scale PV systems with emphasis on grid connection requirements in the Netherlands.
- Development of a standard parameter set for aggregated PV systems with emphasis on grid connection requirements in the Netherlands.

Stability analysis:
Chapter 2 discusses the current state of the impact of inverter-based generation on transient- and short-term voltage stability. The impact on transient stability indicates that the transient stability shall reduce at high levels of inverter-based generation. For voltage stability this chapter shows that, the voltage stability shall decrease also. This thesis shall contribute to,

- Evaluating the impact of PV systems on the transient stability. To be more precise, under which conditions do PV systems have significant contribution to the transient stability and under which conditions is the contribution insignificant. Additionally, an equation shall be proposed to estimate the impact of PV systems on the transient stability.
- Evaluating the impact of PV systems on the short-term voltage stability in particular voltage dips, voltage spread and voltage recovery. This evaluation shall be done by evaluating cases in which PV systems are represented with and without their dynamic model. Additionally, cases with different short-circuit current levels shall be evaluated and compared.

1.5. Outline Report

Chapter 2 — This chapter provides the definition of stability for power systems used in this research project. Furthermore, a classification is provided of the different forms of power system stability and it is shown which forms of power system stability shall be looked at in this research project. Moreover, existing literature of the impact of inverter-based generation on the different forms of power system stability is discussed.

Chapter 3 — This chapter explores the grid connection requirements of the Dutch power system, which are derived from the European Requirements for Generators and the Dutch netcode. Additionally, a classification is given for the power-generating modules based on their voltage level and capacity. The relevant requirements are discussed based on the assigned classification of voltage level and capacity for synchronous units and power park modules.

Chapter 4 — This chapter starts of with the necessity of modelling inverter-based generation, in particular PV systems. Additionally, a classification of PV systems is made and the proposed models used to represent these systems in this research project is discussed in detail. Also, a standard parameter set is derived with elaboration on the determined values.

Chapter 5 — This chapter examines an IEEE 9 bus system. The network is modified such that different scenarios corresponding to different penetration levels are obtained. The different scenarios are studied with respect to transient- and short-term voltage stability and the findings are discussed.

Chapter 6 — This chapter starts of with elaboration on the Investment Plan 2020 and it's different scenarios are briefly explored and a comparison of the scenarios is provided with regards to their solar PV capacity. Following this, the scenario selected is discussed and the selection of the hours corresponding to this scenario. Additionally, the method used for modelling of PV systems is discussed. Lastly, the findings are discussed with regards to transient- and short-term voltage stability and mitigation measures are presented.

Chapter 7 — This chapter discusses the main findings of this research project by providing substantive answers to the research questions formulated. Lastly, a separate section is dedicated to discuss future work which can be carried out associated to this research project.

2

Definition and Classification of Power System Stability

In this chapter, a brief history of power system stability will be highlighted. Furthermore, the definition and classification of power system stability is discussed. Additionally, an elaboration is provided on the different types of stability phenomena and which of these shall be the focus of this research. Due to the rapid growth of IBG and relevancy to this research, a separate section is dedicated to review the impact of IBG sources on the different aspects of power system stability.

2.1. Power System Stability

2.1.1. Introduction to Power System Stability

Power system stability studies became relevant during the early part of the 20th century. Back then the gross of stability problems were related to transferring of electrical energy over long distances [11]. The analysis occurred graphically with methods such as power circle diagrams and the equal area criterion. Thanks to the growth and interconnection of electrical networks, power system stability problems became more complex and prevalent [11]. Around the year 1930, power system dynamics were still calculated by hand with the use of the swing equation. Eventually, in the mid to late 20th century, digital computers proved to be an immense simplification tool for carrying out stability studies. Consequently, more studies could be carried out to obtain knowledge of how different networks would react to certain contingencies and also to look into the future how expansion of the grid would impact power system stability.

The definition of power system stability in this research is synonymous with the definition provided in [12],

Power system stability is the ability of an electric power system, for a given initial operating condition, to regain a state of operating equilibrium after being subjected to a physical disturbance, with most system variables bounded so that practically the entire system remains intact.

Power system stability can be categorised in:

- Rotor Angle Stability
- Frequency Stability
- Voltage Stability

This categorisation and sub-categorisation is provided in Figure 2.1.
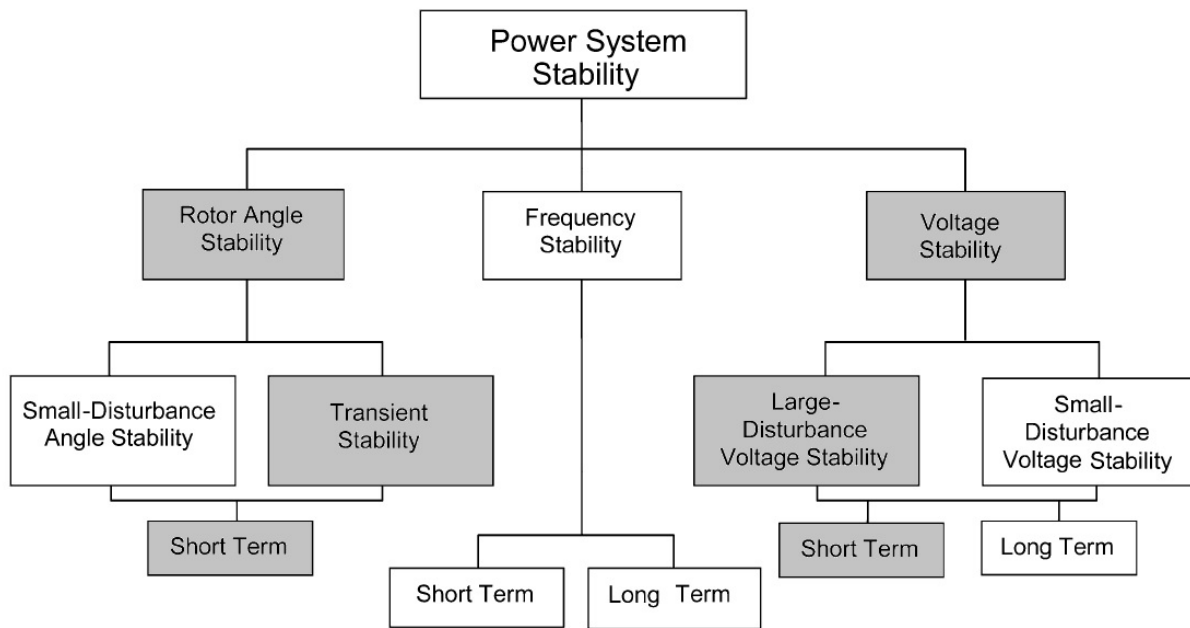
Figure 2.1: Categorisation of power system stability [12]

The focus of this research with regards to power system stability is highlighted in grey in Figure 2.1. In the subsequent sections, a more in-depth explanation of the three types of power system stability is provided.

2.1.2. Rotor Angle Stability

Rotor angle stability is related to the ability of the synchronous machines in interconnected power systems to remain in synchronism during normal conditions and contingencies [11],[13]. Rotor angle stability is dependent on the restoration ability of the balance between the electromagnetic torque and mechanical torque of every synchronous machine in the network [11]. Rotor angle stability can be divided in,

1. *Small-signal (or small-disturbance) stability* refers to the ability of the power system to remain in synchronism during the occurrence of small disturbances [11]. Such small disturbances occur in a continuous manner in the power system i.e. load variations and generation variations. In such studies the disturbances are deemed to be small enough to linearise the system for analysis [12]. Another method of analysis of small-signal stability is by way of signal based records, here an estimation is made of several parameters of sinusoidal components in signal records, this method of analysis is called *Prony Analysis*. Small-signal instability can arise due to two causes which are lack of synchronising torque (resulting in a aperiodic drift of the rotor angle) and lack of damping torque (resulting in an increase in the amplitude of rotor angle oscillations). Most small-signal stability problems nowadays are due to lack of damping torque [12]. Additionally, oscillations can occur locally or globally. Local oscillations refers to the oscillations of a single power plant (or a set of generators within a plant) oscillating against the rest of the power systems. Global oscillations are when a part of the system is oscillating against another part of the system [12].

2. *Transient (or large-disturbance) stability* is associated with the ability of the power system to remain in synchronism when subjected to a large disturbance e.g. short-circuit at a bus, transmission line or loss of generation [12]. The initial operating state of the network and the magnitude of the disturbance are two important factors for determining the transient stability [12]. Transient instability expresses itself in large swings of generator rotor angles and is determined/influenced by the non-linear power-angle relationship [12]. Transient instability occurs when not enough synchronising torque is present during a transient disturbance, this usually leads to *first swing instability*. However, in big interconnected networks, transient instability doesn't always result in first swing instability but could also express itself as large excursions after the first swing [13]. The period of interest for transient studies is 3 to 5 seconds — for large networks this can be extended to 20 seconds with dominant inter-area swing modes [12]. There are several methods to analyse transient stability such as Lyapunov's function, numerical time-domain analysis and calculation of the *critical clearing time* (CCT) [14].

2.1.3. Frequency Stability

Frequency stability is concerned with the ability of the power system to preserve steady frequency after the occurrence of a severe contingency with as consequence a large imbalance between production and consumption of electrical energy [12]. Frequency stability depends on the time period needed to restore equilibrium between load and generation and is expressed by way of large frequency excursions which can result in tripping of generation units and loads [12]. An indicator of the magnitude of imbalance between load and generation (if the total inertia of the interconnected network is known) is the rate of change of frequency (ROCOF), which represents the gradient of frequency with respect to time. This research shall not focus on frequency stability, however, the different classes of stability don't appear in their pure form hence an overlap is present between the different forms of stability [12]. If certains aspects of frequency stability become of importance for this research, this will be mentioned in the text.

2.1.4. Voltage Stability

Voltage stability is concerned with the ability of the power system to preserve steady voltages at all buses in the network after being subjected to a disturbance [12]. Voltage stability depends on the restoration ability of equilibrium from the power system between load demand and generation. As shown in Figure 2.1, disturbances can be large (loss of generation, short-circuit at bus or line) or small (load variations). To be able to preserve or restore steady voltages, the equilibrium between the demand and the supply should be restored in the power system [15]. Voltage instability expresses itself in the form of large voltage sags or spikes at different buses and can lead to tripping of devices in the network due to their protection. In worst cases, voltage instability can cause a cascading effect in the network and lead to local or a complete blackout [15].

2.2. State of the Art

2.2.1. Impact of IBG on Rotor Angle Stability

In this section, the impact which an increased amount of inverter-based generation has on the rotor angle stability in particular transient stability will be discussed. The influence of IBG on the transient stability can be divided mainly in [8],[15],

- *Technology-dependent impact*
  Due to newly introduced connection requirements, inverter-based generation have to ride through a fault and provide fast fault current. Because of their contribution to the short-circuit current, the transient stability improves from this aspect if the IBG units are able to remain connected and contribute to the total short-circuit current [15].

- *Penetration level-dependent impact*
  Initially, transient stability might improve with the addition of inverter-based generation due to mainly the reduced loading of synchronous generators. However, as synchronous generators are being phased out, the transient stability might decrease due to higher loading of remaining generators and lower total short-circuit current levels.

- *Location dependent impact*
  Inverter-based generation units which are located closely to synchronous generators can aid the transient stability due to their short-circuit contribution. For IBG units located electrically further from synchronous generators, their short-circuit contribution decreases and hence also their effect on the transient stability decreases [15].

The above stated categorisation are just a few aspects as to how IBG influences transient stability but are most important for this research. As also stated above, the overall transient stability based on a study conducted by EirGrid [16], shall initially improve as the addition of inverter-based generation units will lead to decreased loading of the synchronous generators and improvement of reactive current injection. At a certain point, as synchronous generators are being decommissioned, however, the loading of the remaining synchronous generators will increase and the reactive current injection will reduce hence causing the decrease of transient stability [15].

2.2.2. Impact of IBG on Frequency Stability

The biggest influence inverter-based generation units have on the frequency stability is due their lack of inherent inertia. The majority of the inertia present in a power system today is largely contributed by synchronous generators [15]. As synchronous generators are being replaced by inverter-based generation units, the total inertia in a power system network hence decreases. The rate of change of frequency is dependent on the imbalance between demand and production and the total system inertia. Henceforth, with the decrease of system inertia, power systems are more susceptible to higher ROCOFs and deeper frequency nadirs [15].

2.2.3. Impact of IBG on Voltage Stability

The increase of inverter-based generation units has had an influence on all the categories of power system stability including voltage stability. The most important aspect which shall be discussed is the reduction of reactive power. Increased level of inverter-based generation units and reduction of synchronous generators have caused a decrease in reactive power in the power system [15]. This is due to the fact that inverter-based generation do not provide the same capabilities compared to synchronous generators in terms of reactive power. In other words, synchronous generators contribute more towards maintaining and restoring voltage stability compared to IBG. Henceforth, the decrease in reactive power in the power system leads to a more vulnerable network in terms of voltage stability [15].

3

Grid Connection Requirements

In this chapter, the grid connection requirements of the Dutch power system are discussed. The connection requirements are derived from both the European Requirements for Generators and the Dutch netcode [17],[18]. The importance of the grid connection requirements with regards to security of supply and transitioning to renewable energy sources will be argued. It is highlighted for which power-generating modules the grid connection requirements are valid and a categorisation will be presented for power-generating modules based on voltage level and capacity range. The power-generating modules should comply to the requirements in accordance with their classification which shall be discussed in this chapter.

3.1. Introduction

Grid Connection Requirements (GCR) are a set of technical regulations which provide specific conditions for grid connected power-generating modules (PGMs) in order to maintain and preserve power system security, to smoothen the transition to renewable energy sources and to provide equitable conditions for competition on the electricity market [8],[17]. The first relevant document with regards to GCR is the European Requirements for Generators. This document lays out a framework for European TSOs and system operators for connection requirements of power-generating modules such as synchronous power-generating modules, power park modules and offshore power park modules, and leaves certain parameter settings up to the TSO and system operators of relevant areas to take into account structural- and technological differences in their respective regions and their own preferences usually based on operation prior to the RfG [17]. For the Dutch power system these parameter settings are documented in the Dutch netcode [18]. These two documents intertwine to form a complete view of the connection requirements of power-generating modules for the Dutch power system.

In [17] and [18], a distinction is made between power-generating modules based on their voltage level and capacity range. The distinction consists of five types i.e. type 0, A, B, C and D. The classification of these different types is provided in Table 3.1.

Generator type	Voltage level	Operator	Capacity range
Type 0	< 110 kV	and	0 – 0.0008 MW
Type A	< 110 kV	and	0.0008 MW – 1 MW
Type B	< 110 kV	and	1 MW – 50 MW
Type C	< 110 kV	and	50 MW – 60 MW
Type D1	< 110 kV	and	≥ 60 MW
Type D2	≥ 110 kV	and	all

Table 3.1: Definition of generator types [15],[17],[18]

In Table 3.1, the different types of generators are shown based on their voltage level and capacity range. The type 0 power-generating modules will not be considered in the simulations and will not be discussed further, as their capacity is negligible and there are no requirements for these type of power-generating modules to provide support in

case of contingencies [18]. An important note to highlight is that the classification provided in Table 3.1 has made a distinction between type D power-generating modules below 110 kV (type D1) and higher than or equal to 110 kV (type D2) since certain requirements provide different conditions for type D1 and type D2. Additionally, as stated, a generator is considered of Type D2[1] when the voltage level is equal or higher than 110 kV, irrelevant of the capacity of the generator. However, at these voltage levels it is expected that the capacity of the generators or set of generators are generally quite high. Moreover, when referring to type D in the text, this encompasses both type D1 and type D2.

The classification provided in Table 3.1 is of high importance to the requirements that will be discussed in the subsequent sections, because dissimilar generator types have to adhere to different requirements.

The GCR discussed in this chapter are aimed at connections of new power-generating modules with the exception of [17],

- Power-generating modules connected to islands of the Member states of the European Union at transmission and distribution levels which are operated asynchronously to the Continental European Grid.
- Power-generating modules installed as back-up power sources and operate for less than 5 minutes per month when the system is operating normally.
- Power-generating modules without a permanent connection point which are used in cases of imbalance to provide additional temporary power.
- Energy storage devices with exception of pump-storage power-generating modules.

The GCR discussed in this chapter does <u>not</u> apply to existing power-generating modules with the exception of [17],

- Big modifications to existing type C or type D power-generating modules [2].
- In case a regulatory authority or Member State determines that an existing connection should be terminated or altered to take into account the GCR.

In this research, however, the GCR will be taken into account for all power-generating modules. In other words, all the power-generating modules used for the simulations will be tuned to meet the requirements set by the GCR.

The classification made for power-generating modules regarding the requirements they have to comply with is twofold. The first classification is based on generator types as provided in Table 3.1. The second classification is made based on the type of generating unit and it's geographical location. This classification is provided below,

- Synchronous Power-Generating Modules (SPGMs) — refers to generation sources which are in constant direct relation, hence synchronism, in terms of the generator speed and the frequency of the network voltage during normal operation [17].
- Power Park Modules (PPMs) — refers to a set of generation sources which are not synchronously connected but connected by way of power electronics to the grid, and also have a single point of connection to the transmission or distribution network [17].
- Offshore Power Park Modules (OPPMs) — are similar to PPMs, however, the location of these set of generation sources is offshore.

The subsequent sections shall discuss the requirements which need to be obliged by all power-generating modules namely synchronous power-generating-, power park- and offshore power park modules for the different generator types. A separate section will discuss the requirements only valid for synchronous power-generating modules. The final section of this chapter discusses the requirements necessary for power park modules.

3.2. Requirements applicable to all power-generating modules

In this section selected requirements[3] relevant for this research project are discussed which are applicable to all power-generating modules, hence these connection requirements are applicable to synchronous power-generating-, power park- and offshore power park modules. The varying generator types should comply to different requirements.

---

[1]The Dutch TSO, TenneT TSO B.V., oversees areas which are equal and higher than 110 kV (with the exception of offshore regions), hence all generator types of the TenneT region are of Type D2

[2]Refer to Article 4(1) of [17]

[3]Refer to [17] and [18] for the full set of requirements

To encompass all forms of power system stability as defined in Chapter 2, requirements classified as frequency stability shall also be discussed, but will not be used in any other sense in this research unless specified otherwise. An overview of the relevant requirements is provided in Table 3.2.

Requirement	Classification	Type A	Type B	Type C	Type D
Frequency Ranges	Frequency Stability	x	x	x	x
Rate of Change of Frequency withstand capability	Frequency Stability	x	x	x	x
Maximum Active Power Reduction at underfrequency	Frequency Stability	x	x	x	x
Active Power Reduction	Frequency Stability		x		
Active Power Controllability and Control Range	Frequency Stability			x	x
Fault Ride Through Capability of Generators connected below 110 kV	Robustness of Generating Units		x	x	D1
Fault Ride Through Capability of Generator connected at 110 kV or above	Robustness of Generating Units				D2
Steady State Stability	Robustness of Generating Units			x	x
Loss of Stability	General system management			x	x
Rate of Change of Active Power	General system management			x	x
High/Low Voltage Disconnection	Voltage stability			x	
Voltage ranges	Voltage stability				x

Table 3.2: Requirements applicable to all PGMs

Extra emphasis will be put on the green-coloured requirements as these affect the voltage- and/or transient stability directly.

Frequency Ranges
The requirement for frequency ranges defines the time period for which a power-generating module should be capable of remaining connected to the grid and operating optimally in the provided frequency ranges [17]. The frequency ranges with their respective time periods which generator types A, B, C and D have to adhere to, is provided in Table 3.3.

Frequency Range	Time period for operation
47.5 - 48.5 Hz	30 minutes
48.5 - 49 Hz	30 minutes
49 - 51 Hz	Unlimited
51 - 51.5 Hz	30 minutes

Table 3.3: Requirements for frequency ranges [17],[18]

Rate of Change of Frequency withstand Capability
The Rate of Change of Frequency (ROCOF) is the change of frequency with respect to time. In other words, the ROCOF represents the gradient of the frequency in the power system. ROCOF is of importance for frequency stability since the value of the ROCOF provides an indication of the magnitude of the disturbance. This requirement provides a ROCOF range and time period in which the power-generating modules should remain connected. At the time of writing these parameters have the status of reserved [18].

Maximum Active Power Reduction at underfrequency

Certain power-generating modules cannot supply their full active power during underfrequency events because of technical reasons, and may be allowed by the TSO to decrease their active power production when a certain underfrequency threshold is reached starting at 49.5 Hz [15],[17]. Below 49.5 Hz, the power-generating modules in the Dutch power system are allowed to decrease their active power production with a gradient of 10% of their maximum capacity at 50 Hz, per frequency decrease of 1 Hz [18].

Active Power Reduction

Power-generating modules of type B should able to reduce their active power production within 5 seconds to zero if given the instruction. Moreover, the relevant system operator can demand certain requirements for equipment to allow for remote operation of active power production [15],[17],[18].

Active Power Controllability and Control Range

Power-generating modules of type C and type D should have the ability to modify active power production based on the instructions provided by the relevant system operator or the relevant TSO. This new instructed set point should be reached within a certain time period set by the relevant system operator or the relevant TSO [15],[17]. This time period differs per power-generating module and is written in the connection and transport agreement [18].

Fault-ride-through capability of power-generating modules connected below 110 kV

Fault-ride-through (FRT) is the ability of power-generating modules to remain connected (should the voltage of the generation unit remain above the given profile) to the network during voltage deviations due to occurrence of a fault. Power-generating modules of type B, type C and type D1 should adhere to the fault-ride-through profile established for power-generating modules connected below 110 kV. A voltage-against-time-profile is specified by Dutch netcode at the point of connection for contingencies.

The generic fault-ride-through profile is provided in Figure 3.1 and the voltage and time parameters for the FRT curve applicable to type B, type C and type D1 are provided in Table 3.4.
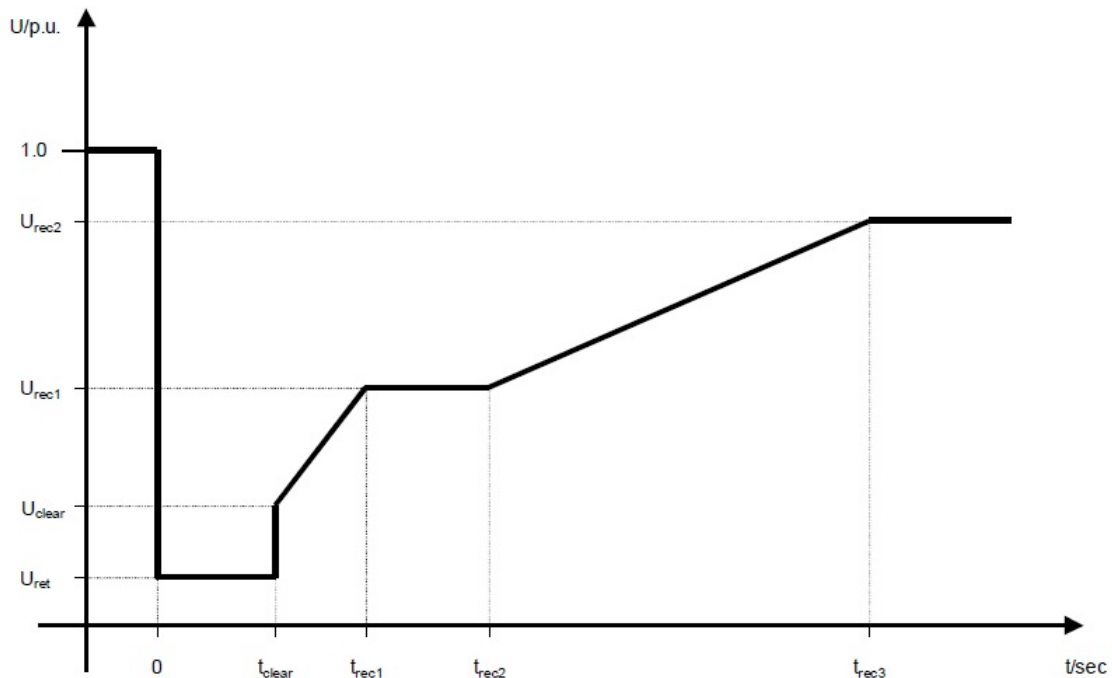
Figure 3.1: Generic fault-ride-through profile [17]

	Synchronous power-generating module	**Power park module**
U_{ret}	0.05 pu	0.05 pu
U_{clear}	0.70 pu	0.05 pu (= U_{ret})
U_{rec1}	0.70 pu (= U_{clear})	0.05 pu (= U_{clear})
U_{rec2}	0.85 pu	0.85 pu
t_{clear}	0.15 s	0.25 s
t_{rec1}	0.15 s (= t_{clear})	0.25 s (= t_{clear})
t_{rec2}	0.15 s (= t_{rec1})	0.25 s (= t_{rec1})
t_{rec3}	1.5 s	3.0 s

Table 3.4: Fault-ride-through voltage and time parameters for type B, C and D1 PGMs [17],[18]

In Table 3.4, it is shown that a distinction in fault-ride-through profile is made between the synchronous power-generating modules and power park modules. This distinction is due to the ability of synchronous power-generating modules to provide 5 to 6 times the short-circuit current compared to their rating, while power park modules can only provide approximately 1.2 times of short-circuit current of their rating. Consequently, synchronous-power generating modules have a quicker restoration of voltage. Sketching the FRT curves with the parameters shown in Table 3.4, yields the curves shown in Figure 3.2.
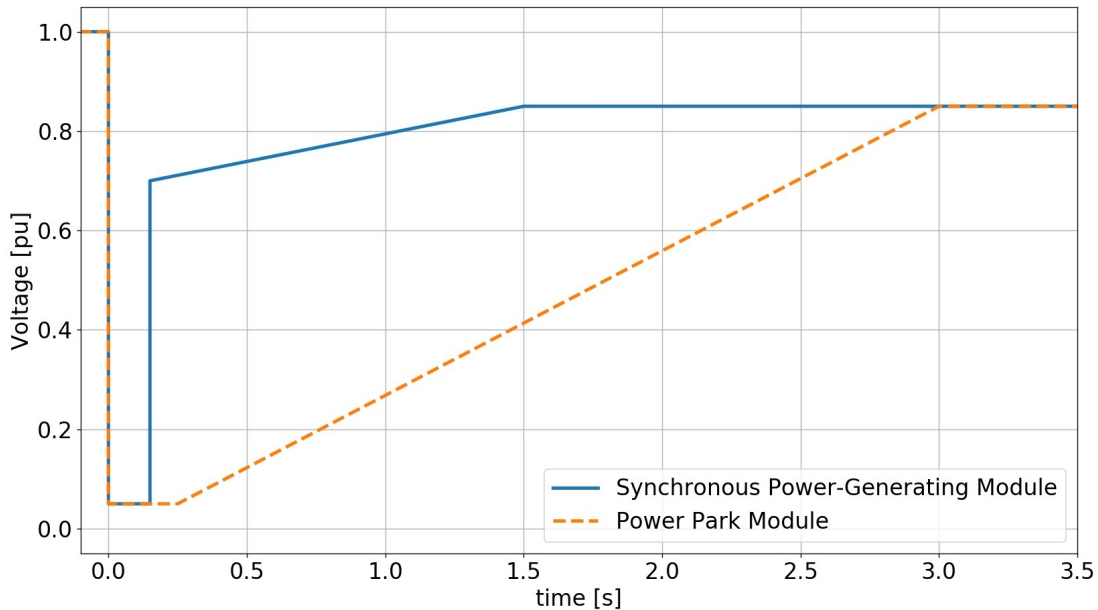
Figure 3.2: Fault-ride-through curve for PGMs below 110 kV [17],[18]

Fault-ride-through capability of power-generating modules connected at 110 kV or above

The fault-ride-through capability of power-generating modules connected at 110 kV or above is a requirement for type D2 generators. The voltage and time parameters for the FRT curve are provided in Table 3.5.

	Synchronous power-generating module	Power park module
U_{ret}	0 pu	0 pu
U_{clear}	0.25 pu	0 pu (= U_{ret})
U_{rec1}	0.70 pu	0 pu (= U_{clear})
U_{rec2}	0.85 pu	0.85 pu
t_{clear}	0.25 s	0.25 s
t_{rec1}	0.3 s	0.25 s (= t_{clear})
t_{rec2}	0.3 s (= t_{rec1})	0.25 s (= t_{rec1})
t_{rec3}	1.5 s	3 s

Table 3.5: Fault-ride-through voltage and time parameters for type D2 PGMs [17],[18]

Using the same profile provided in Figure 3.1, yields the sketched FRT curves for synchronous power-generating modules and power park modules of type D2 power-generating modules shown in Figure 3.3.
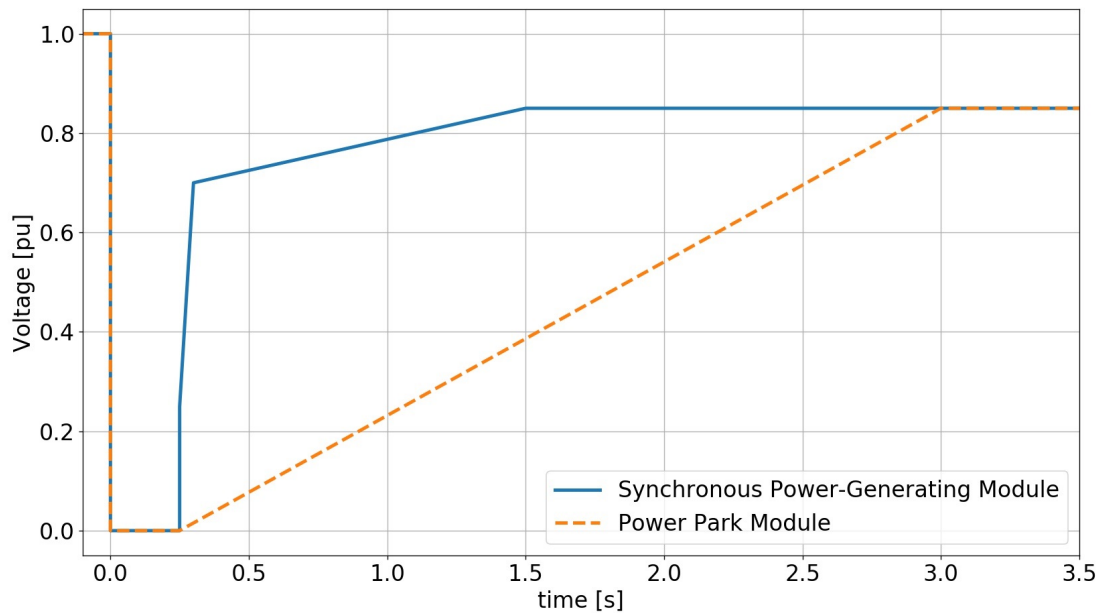
Figure 3.3: Fault-ride-through curve for PGMs at and above 110 kV [17],[18]

The requirements for type D2 power-generating modules are stricter compared to the power-generating modules below 110 kV, as these power-generating modules are usually of higher capacity hence providing more support during contingencies. In Figure 3.4, the FRT curves of the power park modules equal to and higher than 110 kV (type D2) and below 110 kV (type B, C, D1) are compared.
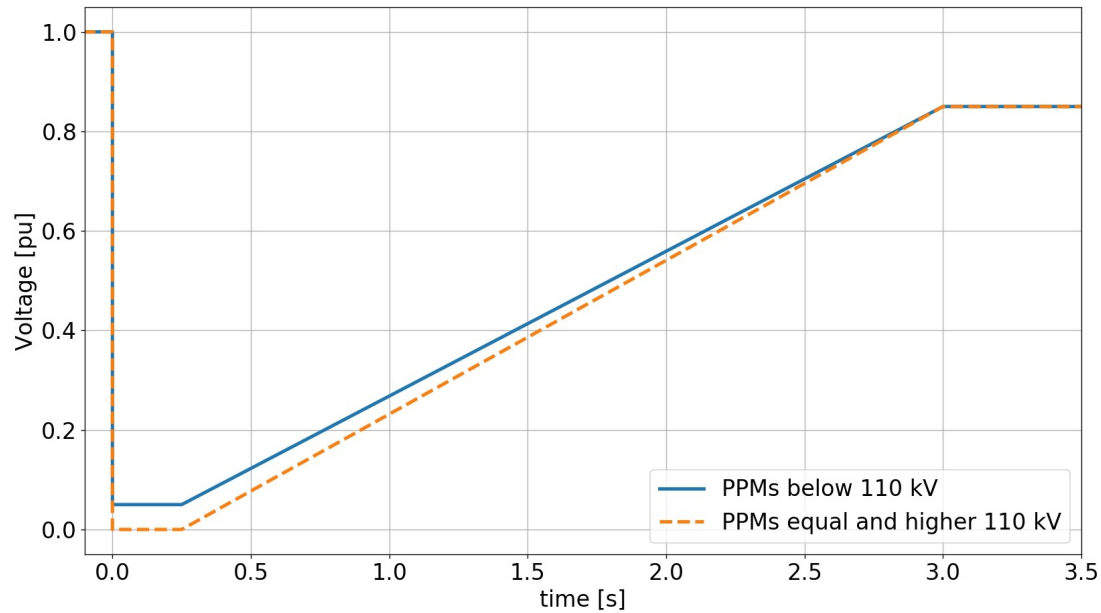
Figure 3.4: Comparison of fault-ride-through curves for PPMs [17],[18]

It can be seen in Figure 3.4, that indeed the FRT curve for PPMs connected at 110 kV or higher (type D2 PGMs) is more rigorous compared to the FRT curve for PPMs connected below 110 kV. In other words, type D2 power-generating modules should stay connected for scenarios where the voltage dips are lower. This is to be expected, since type D2 units are generally large power-generating modules which can provide significant support during contingencies compared to other power-generating module types.

Steady-state stability
In the case of occurrence of power oscillations, power-generating modules of type C and type D should be able to preserve steady-state stability when operating within the P-Q capability diagram [17].

Loss of Stability
Automatic disconnection should occur from the power system for power-generating modules of type C and type D when angular instability or loss of control occurs in order to maintain power system security or to avoid damaging the power-generating module [15],[17]. This criteria is written in the connection and transport agreement [18].

Rate of Change of Active Power
Type C and type D power-generating modules have to adhere to minimum and maximum limits of the rate of change of active power specified by the relevant TSO. This specification is made by taking into account the characteristic of prime mover technology [15],[17].

High/Low Voltage Disconnection
Power-generating modules of type C should be able to automatically disconnect from the network in case voltage thresholds are exceeded, with voltage thresholds below 0.85pu and above 1.15pu. These settings are determined by the connected party, but shouldn't interfere with fault-ride-through parameters [17],[18].

Voltage ranges
This requirements obliges type D2 power-generating modules to remain connected to the power system for the voltage ranges with their time periods of operation indicated in Tables 3.6 and 3.7, where the connection point of the power-generating module is used as 1 pu voltage reference point.

Voltage range	Time period for operation
0.85 - 0.90 pu	60 minutes
0.90 - 1.118 pu	Unlimited
1.118 - 1.15 pu	20 minutes

Table 3.6: Voltage ranges for Type D2 PGMs 110 kV to 300 kV [17],[18]

Voltage range	Time period for operation
0.85 - 0.90 pu	60 minutes
0.90 - 1.05 pu	Unlimited
1.05 - 1.10 pu	20 minutes

Table 3.7: Voltage ranges for Type D2 PGMs 300 kV to 400 kV [17],[18]

3.3. Requirements applicable to synchronous power-generating modules

The requirements discussed in this section are exclusively valid for synchronous power-generating modules. These requirements are provided in Table 3.8.

Requirement	Classification	Type A	Type B	Type C	Type D
Post Fault Active Power Recovery	Robustness of Generating Units		x	x	x
Reactive power capability at maximum active power	Voltage stability			x	x
Reactive power capability below maximum active power	Voltage stability			x	x
Voltage control system	Voltage stability				x

Table 3.8: Requirements applicable to SPGMs [17],[18]

Post Fault Active Power Recovery

This requirement indicates the amount of time after the clearance of a fault that the active power in-feed needs to be restored. The goal of this requirement is to quickly restore active power generation so that frequency deviations can be halted and kept to a minimum. The conditions for the recovery after the fault is dependant on the area. Certain synchronous areas, which possess a low total system inertia, are more susceptible to frequency deviations, hence fast/rapid post fault active power recovery is required, while other synchronous areas are not as sensitive to frequency swings [19].

Reactive power capability at maximum active power

This requirement indicates that type C and type D synchronous power-generating modules should be able to supply reactive power within the limits of U-Q/Pmax-profile established by the relevant system operator [15],[19]. At the time of writing, this article has the status of reserved in the Netcode [18]. A proposal has been handed in by *Netbeheer Nederland* [20], which will be discussed in this report. The U-Q/Pmax-profile proposed in [20] is shown in Figure 3.5.
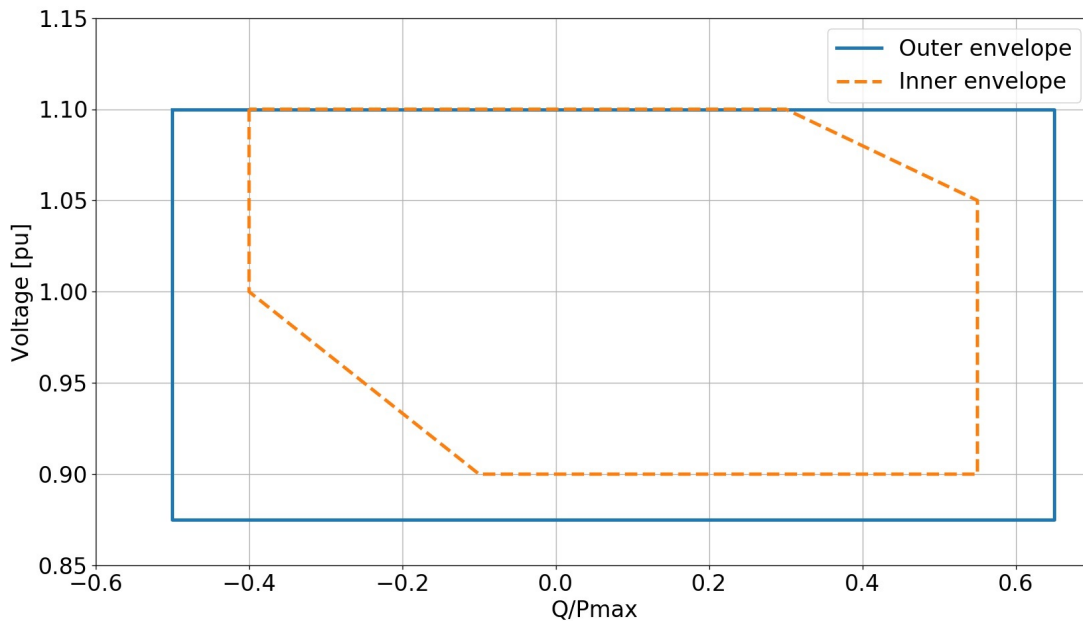
Figure 3.5: U-Q/Pmax-profile for SPGMs [17],[18]

Synchronous power-generating modules of type C and type D operating at maximum capacity in the Dutch power system should be able to provide reactive power within the boundaries provided by the inner envelope (dotted orange line) of Figure 3.5.

Reactive power capability below maximum active power
The synchronous power-generating module should posses the ability to operate within the region of the provided P-Q capability diagram in the case of operation below the maximum active power [15].

Voltage control system
Synchronous power-generating modules of type D should have a voltage control system, where the parameters and components should be commonly agreed to by the facility owner, relevant system operator and the relevant TSO. Apart from the requirements for the Automatic Voltage Regulator, the excitation control system shall consist of the following specific characteristics [15],

- Bandwidth limitation of output signal

- Under-excitation limiter

- Over-excitation limiter

- Stator current limiter

- Power System Stabiliser (PSS) function

3.4. Requirements applicable to power park modules
The additional requirements applicable to power park modules are shown in Table 3.9.

Requirement	Classification	Type A	Type B	Type C	Type D
Synthetic Inertia Capability	Frequency stability			x	x
Post-fault active power Recovery	Robustness of Generating Units		x	x	x
Provision of fast fault current	Voltage Stability		x	x	x
Priority to Active or Reactive Power Contribution	Voltage Stability			x	x
Reactive Power Capability at Maximum Active Power	Voltage Stability			x	x
Reactive Power Capability Below Maximum Active Power	Voltage Stability			x	x
Reactive Power Control Modes	Voltage Stability			x	x
Power Oscillations Damping Control	Voltage Stability			x	x

Table 3.9: Requirements applicable to PPMs [17],[18]

Synthetic Inertia Capability
In contrast to synchronous generators, power park modules inherently don't contribute to the inertia of the power system. Power systems with high penetration of power park modules without the added feature of synthetic inertia, are susceptible to large frequency excursions and large ROCOFs due to it's inability to contribute to the total inertia of the network. To avoid this, this requirement has been introduced for larger capacity PPMs to provide synthetic inertia or emulated inertia to mimic the (inherent) inertia from synchronous generators. Power-generating modules of type C and type D should have the added control algorithm to provide (synthetic) inertia, essentially equating to fast control algorithms to obtain a similar reaction to the inherent inertia provided by synchronous generators. At the time of writing, there is no requirement for synthetic inertia capability in the Dutch netcode [18].

A method of synthetic inertia has been introduced in [21] defined as Fast Active Power Injection (FAPI). FAPI is defined as the application of a control action to power electronic converters by continuously monitoring the frequency and active power balance in small time frames and accordingly injecting or absorbing active power dependent on the imbalance [21].

Post-fault active power recovery
Similar to the requirements for synchronous-power generating modules, the post-fault active power recovery requirement puts a condition for the time period in which power park modules of type B, type C and type D provide the active power needed for recovery after clearance of the fault to avoid large frequency excursions [15]. This time period and also a magnitude and accuracy for active power recover is determined by the relevant TSO.
The minimal requirements from proposed by *Netbeheer Nederland* in [20] are,

- The recovery of active power starts from 90% of the voltage before the fault.

- The maximum allowed time for recovery of active power is between 0.5 and 10 seconds.

- The magnitude of the recovery of active power is at least 90% of the active power prior to the fault.

- The accuracy of the recovery of active power is within 10% of the active power prior to the fault.

Provision of fast fault current
This requirement states that power park modules of type B, type C and type D should be able to provide fast fault current when a symmetric (three-phase) fault occurs. Furthermore, if applicable, the relevant system operator in collaboration with the relevant TSO can specify the asymmetrical fast fault current requirements in the case of asymmetrical faults. At the time of writing, this requirement has the status of reserved — the proposal[4] on 23 January 2020 of *Netbeheer Nederland* as documented in [22] will be discussed. Fast fault current should be provided for symmetrical faults (three-phase faults) at the connection point under the following conditions,

- Additional reactive current is provided when the voltage deviation at the terminals of the individual power-generating modules is either larger than 10% of the effective value or when a sudden change in the instantaneous voltage occurs of at least 5% of the peak value of the nominal voltage.

- The voltage control system provides additional reactive current injection at the terminals of the individual power-generating modules with a minimum 2% and maximum 6% of the nominal current per percent voltage deviation.

---

[4]Note that these requirements are proposed by *Netbeheer Nederland* and still await approval hence the requirements are not adopted (yet)

- The rise time (which refers to the time necessary after fault occurrence for the additional reactive current injection to reach a value of 90% of the stable end value) shall not exceed 30 ms and the settling time (which refers to the time necessary after fault occurrence for the additional reactive current injection to remain permanently in the range of 90% and 110% of the stable end value) shall not exceed 60 ms.

- The additional injected reactive current ΔIb is the difference of the reactive current during the fault and the reactive current before the fault and is proportional to the voltage deviation as indicated in Equation 3.1.

$$\Delta Ib = \frac{(U - U_0)}{U_N} \times I_N \times k \tag{3.1}$$

where,

ΔIb	=	additional reactive current injection
$\frac{U - U_0}{U_N}$	=	relative voltage deviation in pu
U	=	voltage during fault
U_0	=	voltage before the fault
U_N	=	nominal voltage
I_N	=	nominal current
k	=	slope for additional reactive current injection

- The range of k shall be between 2 and 6, where the value of 2 is assigned for power park modules connected to a network with a nominal voltage lower than 66 kV and the value of 5 is assigned for power park modules connected to a network with a nominal voltage of 66 kV and higher.

The proposal document [20] states that the same conditions hold for fast fault current for Power Park Modules in the case of asymmetric faults as for symmetrical faults.

Priority to Active or Reactive Power Contribution
Type C and type D power-generating modules should prioritise either active power contribution or reactive power contribution during faults. The setting for which contribution is of higher importance is determined by the relevant TSO. For active power contribution priority, the active power needs to be provided earlier than 150 ms after the fault occurs to maintain the frequency within certain boundaries [17].

Reactive Power Capability at Maximum Active Power
Similar to the requirements discussed for synchronous generating-power modules, power park modules of type C and type D should also be able to provide reactive power within the limits specified for the U-Q/Pmax-profile for PPMs. The provided U-Q/Pmax-profile is also taken from the proposed profile by Netbeheer Nederland [20] and currently has the status of reserved in the current Netcode. The proposed profile is shown in Figure 3.6.
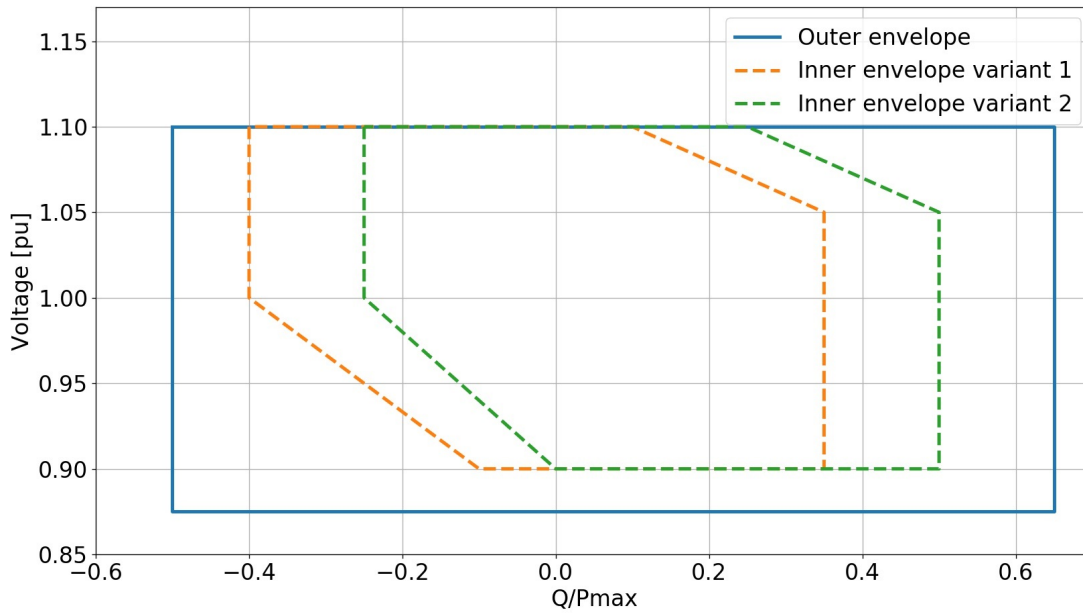
Figure 3.6: U-Q/Pmax-profile for PPMs [15],[17],[18]

In Figure 3.6, 2 variants of the inner envelope are provided (the dotted orange- and dotted green line). The choice of variant 1 or 2 is made on individual basis (between connected party and network operator) dependent on the reactive power needs in that particular area [20].

Reactive Power Capability below Maximum Active Power
Tthis requirement is valid for operation of the power park modules type C and type D below it's maximum active power capacity and states that the ability of reactive power provision requirements is determined by the relevant system operator in collaboration with the relevant TSO. Additionally, a P-Q/Pmax-profile is determined for which the power park modules shall provide reactive power below maximum capacity. Within this specified P-Q/Pmax-profile, the power-generating module shall be able to operate at any point [17].

Reactive Power Control Modes
The reactive power control modes for power park modules of type C and type D consist of voltage control mode, reactive power control mode and power factor control mode. The selection of the mode is a collaborative decision between relevant system operator, relevant TSO and power park module owner [17].

Power Oscillations Damping Control
Power-generating modules of type C and type D should have the ability to contribute to damp out power oscillations. The control modes voltage and reactive power control characteristics of power park modules should not negatively affect power oscillation damping and, if necessary, supplementary control loops should be added to aid this [15],[17].

4

Modelling & Control of PV Systems

This chapter introduces the models used to represent the dynamic behaviour of solar PV systems. A distinction is made between models representing large-scale PV systems and aggregated distribution PV systems. The association of large-scale PV systems and aggregated distribution PV systems with the generator types discussed in Chapter 3 is provided. Separate sections are used to discuss the two models used to represent these PV systems. Additionally, a detailed explanation regarding the models and the inner-workings of the control algorithms is provided. The limitations of the PV models are also discussed briefly. Ultimately, a standard parameter set is proposed to be used towards the representation of a wide array of PV systems in the Dutch high voltage network.

4.1. Introduction

As elaborated in Chapter 1, the power system is shifting from a largely synchronous generator dominated grid to a hybrid grid consisting of a mixture of primarily synchronous generators and inverter-based generation. This transformation of the power system will bring (and has partially already brought) with it numerous challenges such as larger frequency deviations and lower short-circuit current in certain areas resulting in deeper voltage sags during disturbances in such areas. Another challenge which is brought upon by this ongoing change is the representation of the dynamic behaviour of inverter-based generation in simulation studies. Proper representation of inverter-based generation is becoming more important than ever because of the rapid growth of these energy sources. Consequently, inverter-based generation such as PV systems can no longer be ignored and have to be modelled adequately when carrying out dynamic studies. Conventional generation sources such as synchronous generators have well-defined models to perform stability studies [14]. This, however, is not the case (yet) for inverter-based generation, since the development is still ongoing for generic models and typical parametristation [14]. Instead manufactures have the task of creating detailed and specific models for their PV systems. In recent times, a lot of energy and resources has gone towards the development of generic inverter-based generation models. In other words, research is being done on developing generic models to represent a broad spectrum of inverter-based generation models. Generic models for wind power plants are currently more widely accepted compared to generic models for PV systems [23]. However, in recent years, several generic PV models have been proposed, especially by the Western Electricity Coordinating Council (WECC), alongside extensive validation studies.

When modelling solar PV systems, two distinct types of PV systems shall be looked at i.e.,

- Large-scale PV systems
- (Aggregation of) Distributed PV systems

Large-scale PV systems refers to single large solar PV parks which are usually connected at transmission level. Large-scale PV systems are defined in [24] as solar PV parks which have a minimum capacity of 10 MW. The large-scale PV systems are modelled in power system stability studies by the *large-scale PV model*, which will be discussed subsequently, as this has been the standard for modelling large-scale PV systems in recent years. An alternative is the IEC 61400-27-1 which is used to represent wind turbines, however, this model has not been officially released at the time of writing and the models are not present in current software, thus it will not be taken into account.

Distributed PV Systems are solar PV parks which are connected at distribution level, usually implying smaller capacity ranges. In this research project, the aggregation of distributed PV systems shall be looked at, which offer an approximate representation of the accumulated behaviour of smaller distribution-connected PV units that are modelled at

a transmission bus [24]. The representation of aggregated distribution-connected PV systems will be achieved with the use of the *DER_A model*, as this model is the latest published model for representing aggregation of distributed PV systems with ample flexibility to take into grid connection requirements and potential changes [25]. As this model represents the aggregation of multiple distribution PV systems, validation with measured data is not possible, however, in [26] validation has been conducted based on the expected knowledge of the dynamic behaviour.

TenneT TSO B.V. is the sole TSO of the Netherlands and oversees the transmission regions in the Dutch power system with voltage levels of 110 kV, 150 kV, 220 kV and 380 kV. To this end, as also stated in Chapter 3, all PV Power Park Modules connected to the TenneT region are considered of type D2. Such transmission connected PV systems shall be modelled by the *large-scale PV model*. Consequently, all PV Power Park Modules connected at distribution level (below 110 kV) fall under type B, C and D1 PGMs. The aggregation of these distribution connected PV systems shall be modelled by the *DER_A model*. The implementation of the models and all simulations are conducted in the software PSS/E version 34.7.

4.2. Large-scale PV Model

4.2.1. Introduction

The *Large-scale PV model* (also referred to as *Central Station PV Plant Model* or *WECC Generic PV Model*) is a positive-sequence model that represents the important dynamic behaviour of large-scale PV systems with a single connection point at transmission level. This model has been developed by the WECC Renewable Energy Modeling Task Force (REMTF) and has been largely based on the Type 4 Wind Turbine Model (also developed by WECC REMTF) due to the characteristic that both types are connected to the grid by a power electronics interface [27]. The large-scale PV Model consists of 3 modules i.e. [27],

- REGC_A – Renewable Energy Generator/Converter Module
- REEC_B – Renewable Energy Electrical Control Module
- REPC_A – Renewable Electrical Plant Level Control Module

The three modules inherently do not possess protection systems [14], however, voltage- or frequency protection modules can be added in PSS/E with the modules VRGTPA and FRQTPA, respectively [27].

The interconnection between the 3 modules is provided in Figure 4.1.
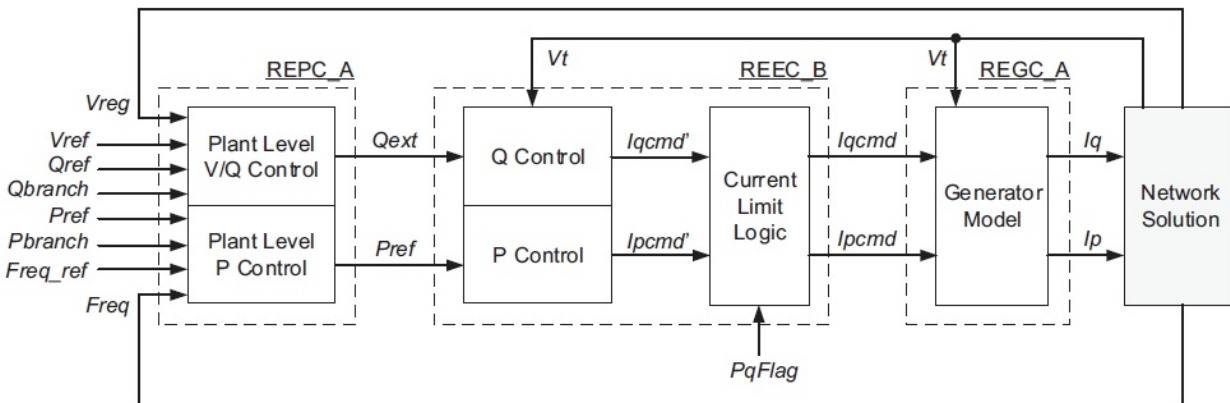
Figure 4.1: Interconnection of large-scale PV modules [24]

The definitions of all variables in Figure 4.1 are provided in Table 4.1.

Parameter	Description
Vreg	Regulated bus voltage
Vref	Regulated bus initial voltage
Qref	Regulated branch initial reactive power flow
Qbranch	Branch reactive power flow for plant Q regulation
Pref	Active power command from plant controller
Freq_ref	Initial frequency deviation
Freq	Frequency deviation
Qext	Reactive power command from plant controller
Vt	Terminal voltage
Iqcmd'	Desired reactive current command
Ipcmd'	Desired active current command
Pqflag	Active or reactive current priority flag
Iqcmd	Actual reactive current command
Ipcmd	Actual active current command
Iq	Reactive terminal current
Ip	Active terminal current

Table 4.1: Definition of parameters shown in Figure 4.1 [24]

The Plant Level Control (REPC_A), which is an optional module, uses the values provided by the network solution to generate active- and reactive power references for the electrical control module. If the plant level controller is excluded, the active- and reactive power references are provided directly by the network solution [28]. The electrical control module receives the power references from the plant level controller and converts these into current commands for the generator/converter module. The produced current commands are received by the generator/converter module which is responsible for the injection of currents [27]. The REGC_A module has the fastest controls, followed by the REEC_B module and lastly the relatively slow plant controller module REPC_A [14], this is shown in Figure 4.2.
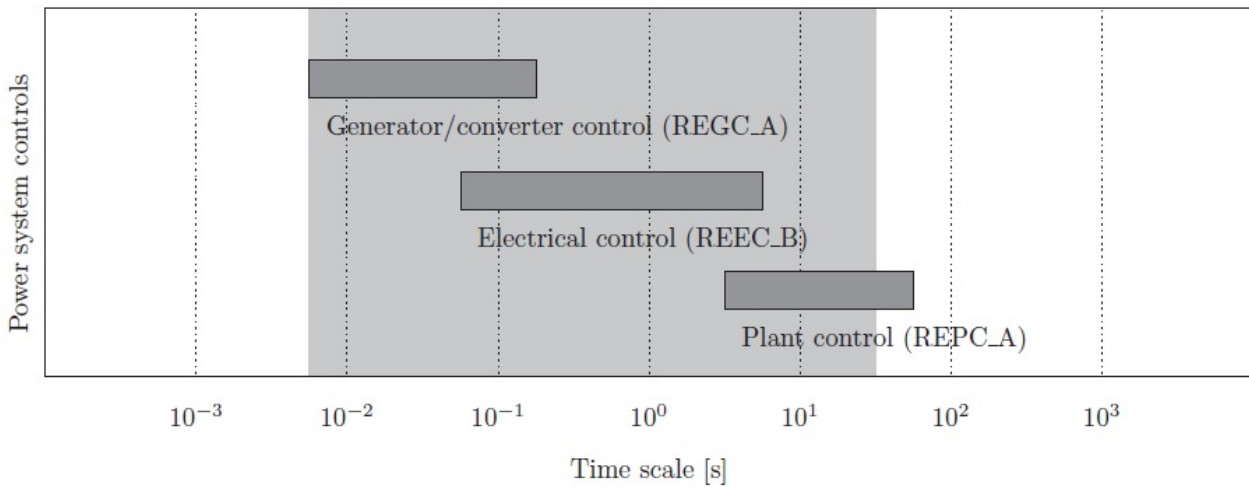
Figure 4.2: Speed of the controls of the large-scale PV modules [14]

In the subsequent sections, an in-depth examination will be provided of the three modules of the large-scale PV model

by exploring the control algorithms of the modules. The large-scale PV model will be used in the simulation software PSS/E 34.7 for this research project to model large-scale PV systems in congruence with the definition provided in Section 4.1.

4.2.2. Renewable Energy Generator/Converter Module (REGC_A)

The block diagram of the REGC_A module is provided in Figure 4.3. A description of the parameters shown in Figure 4.3 is provided in both Appendix A and B.
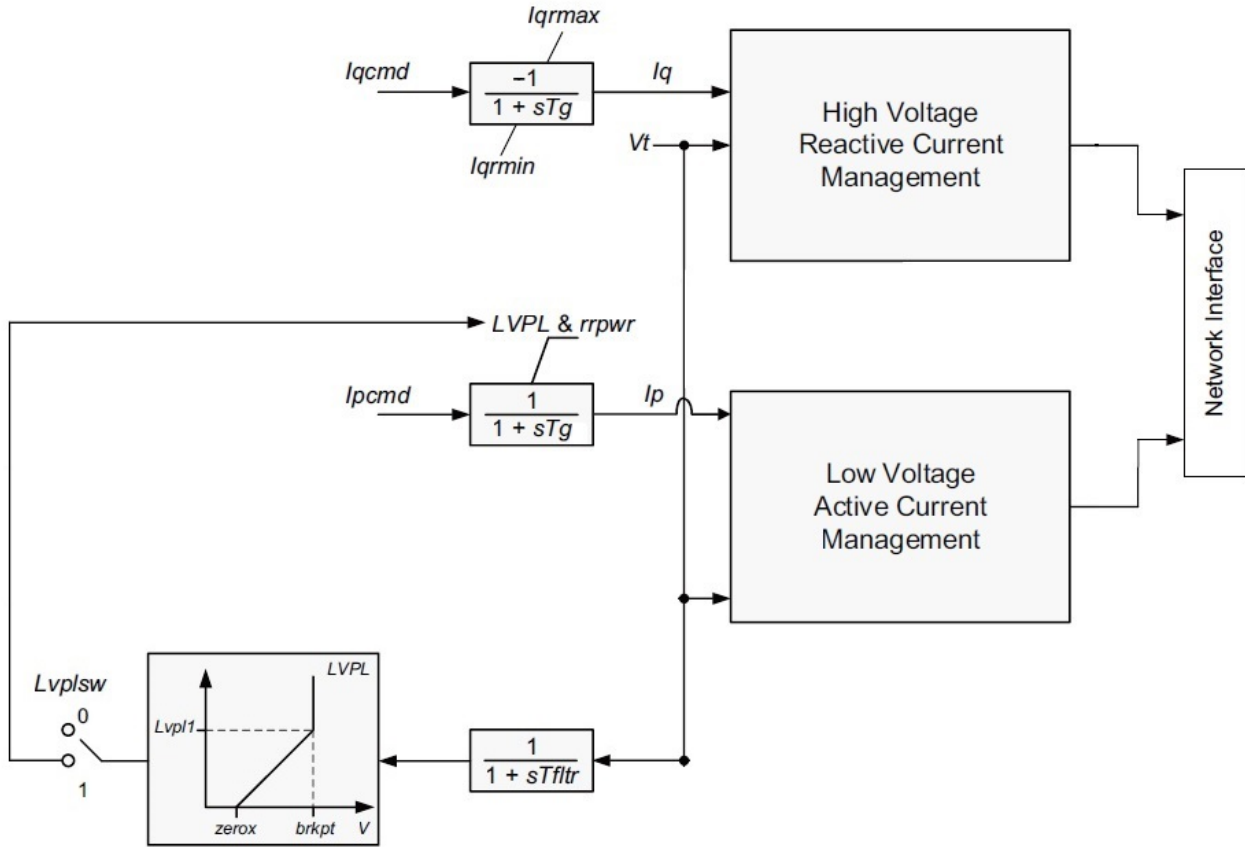
Figure 4.3: Block diagram of REGC_A module [14]

The REGC_A module receives the reactive- and active current commands *Iqcmd* and *Ipcmd* from the electrical control module REEC_B. These commands are passed through the current regulator. The delay (lag time constant) of the current regulator is taken into account by *Tg*. The output yields the actual reactive and active currents *Iq* and *Ip*. The reactive current *Iq* and the terminal voltage *Vt* are passed through the *High Voltage Reactive Current Management Module*. This module has the function of limiting the reactive current injection so that the terminal voltage does not exceed the limit set by the user [27]. The control within this module is provided in Figure 4.4.
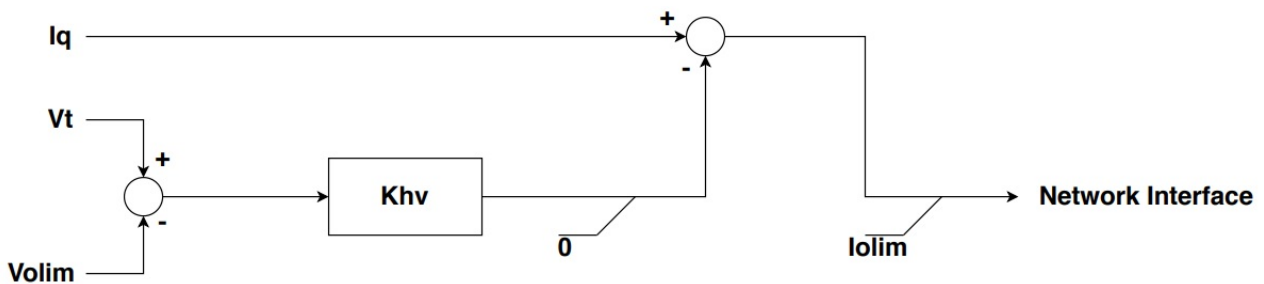
Figure 4.4: High voltage reactive current management module [29]

The terminal voltage *Vt* is subtracted from the voltage limit *Volim*. This difference is multiplied by high voltage clamp logic acceleration factor *Khv*, which in it's turn is subtracted from the reactive current command to obtain a reduced

reactive current injection. Please note that if $Vt \leq Volim$, the High Voltage Reactive Current Module will not be activated as this will result in a negative value while the output of Khv has a lower bound of zero. To summarise the workings of the High Voltage Reactive Current Management, should the terminal voltage Vt of the generator exceed the user-set voltage limit $Volim$, which is set higher than Vt, the module will reduce the reactive current injection dependent on the difference between Vt and $Volim$, and the assigned value to Khv.

The active current command *Ipcmd* is also passed through a current regulator to obtain the actual active current *Ip*. There are two upper limits set which are the active current limit which is determined by the Low Voltage Power Logic (LVPL), and the ramp-rate of active power *Rrpwr* which provides a limit for the increase of the active power with respect to time. The active current *Ip* and the terminal voltage *Vt* are passed through the *Low Voltage Active Current Management Module*. This module has been implemented to emulate changes in active power with voltage variation due to the Phase Locked Loop (PLL) controls [27], as it has been discussed in [30] that the PLL controls react to changes in terminal voltage. The block diagram of this module is provided in Figure 4.5.
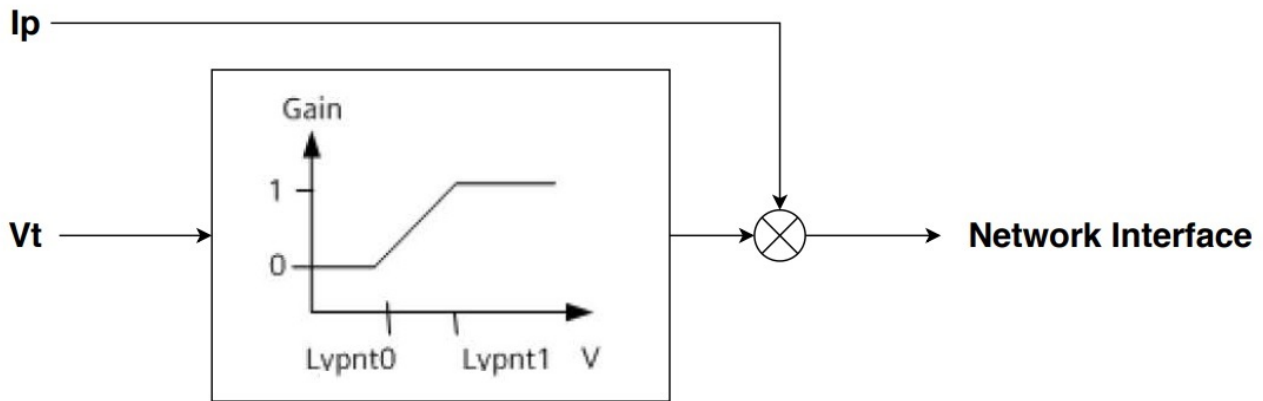
Figure 4.5: Low voltage active current management module [29]

The terminal voltage is passed through the piecewise linear function shown in Figure 4.5. If the voltage is within the user-settable limits *Lvpnt0* and *Lvpnt1*, the active current is multiplied by the numerical value between 0 and 1 dependent on the position of the terminal voltage *Vt* on the graph. Consequently, this causes a reduced active current injection. Moreover, if the terminal voltage *Vt* is higher than *Lvpnt1* then the Low Voltage Active Current Management Module will not be activated. Additionally, if the terminal voltage *Vt* is below *Lvpnt0* then there will be no active current injection. To recap the function of the *Low Voltage Active Current Management Module*, it is implemented to represent the active power output behaviour during low voltage events.

4.2.3. Renewable Energy Electrical Control Module (REEC_B)
The block diagram of the electrical control module (REEC_B) is provided in Figure 4.6. A description of the parameters shown in Figure 4.6 is provided in both Appendix A and B.
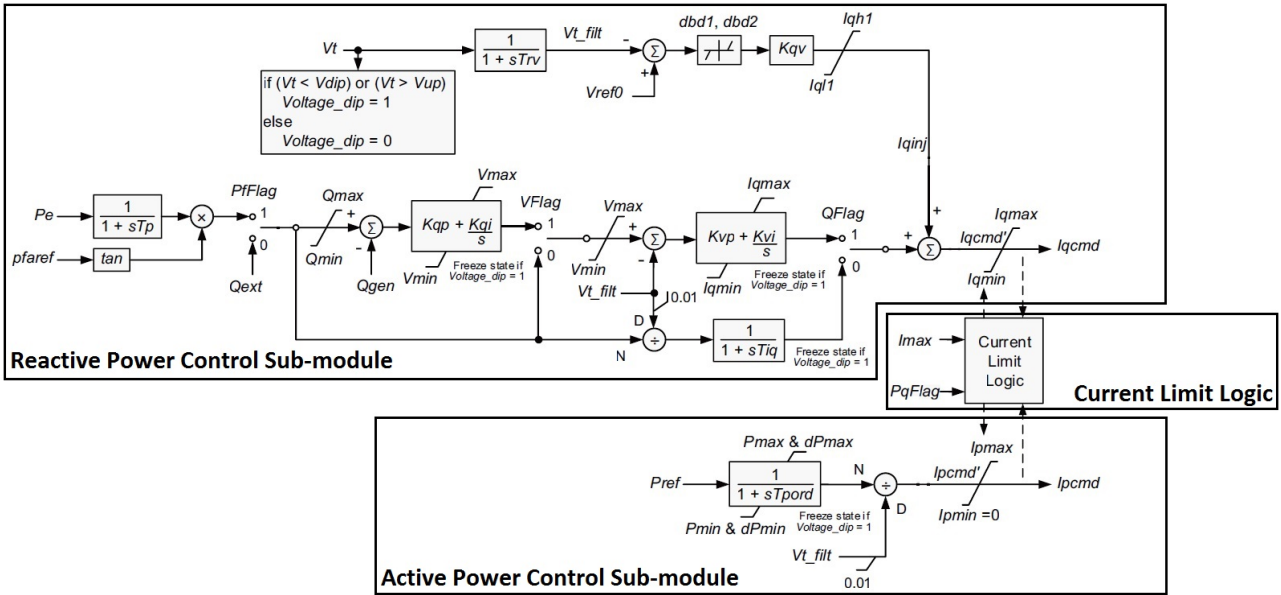
Figure 4.6: Block diagram of REEC_B module [14]

The main goal of the electrical control module is to convert the active- and reactive power references into inverter current commands [27]. The REEC_B module consists of three main sub-modules which are,

- Active Power Control Sub-module
- Reactive Power Control Sub-module
- Current Limit Logic

Active Power Control Sub-module
The active power control sub-module is shown in Figure 4.7.
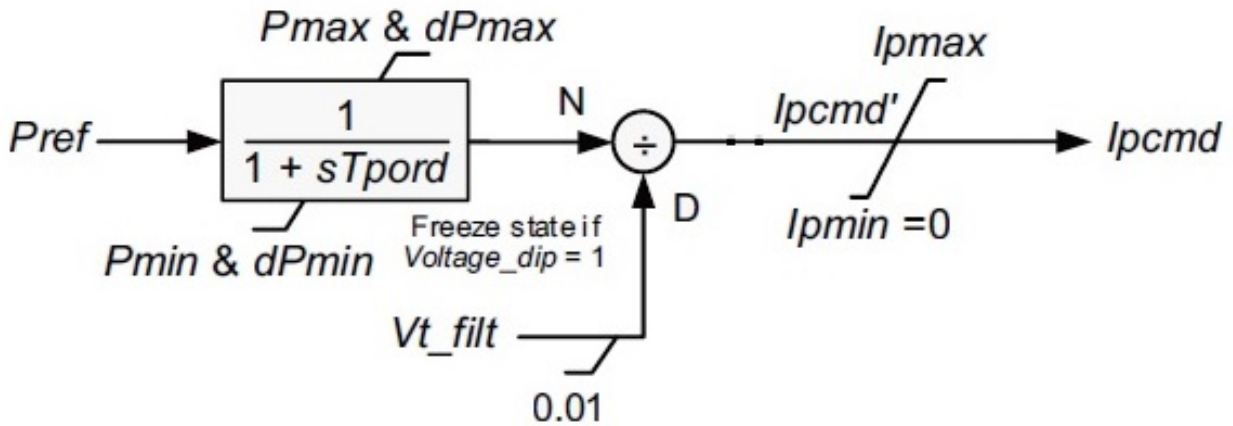
Figure 4.7: Active Power Control Sub-Module of REEC_B [29]

The active power control sub-module has the function of converting the active power reference *Pref* to an active current command *Ipcmd*. This is achieved by passing the active power reference *Pref*, which is provided by the plant controller model REPC_A or by the solved power flow case when no plant controller model is present, through a first-order low pass filter with a time constant *Tpord* with upper and lower limits for active power and ramp rates. The output of the first-order low pass filter is then divided by the terminal voltage *Vt* to produce the initial active current command *Ipcmd'*, which is limited by *Ipmin* and *Ipmax* to obtain the active current command *Ipcmd* in per unit. The method of determining *Ipmin* and *Ipmax* will be provided during the discussion of the current limit logic [27].

Reactive Power Control Sub-module
The reactive power control sub-module is shown in Figure 4.8.
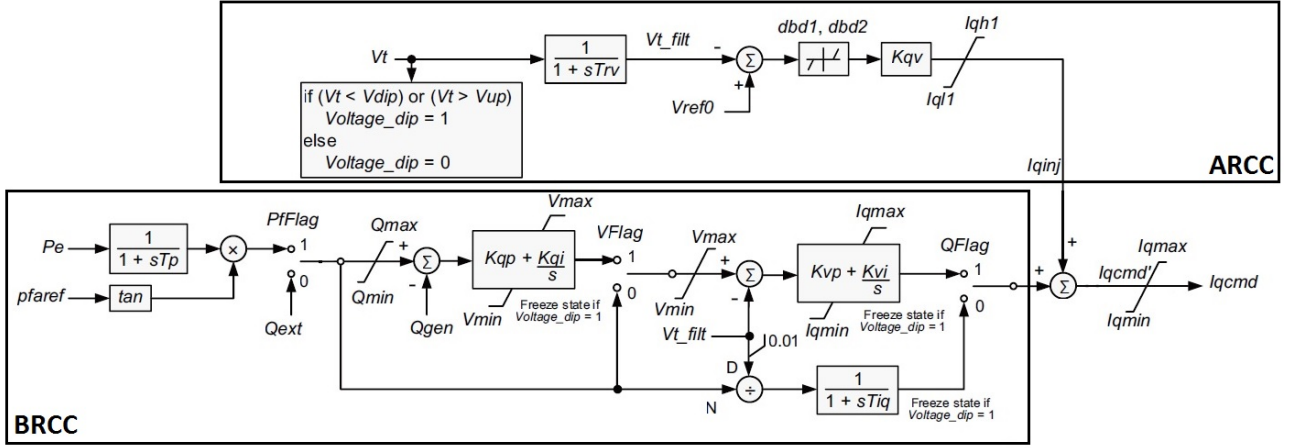
Figure 4.8: Reactive Power Control Sub-Module of REEC_B [29]

The reactive power control sub-module can also be divided into two main parts i.e.,

- Additional Reactive Current Control (ARCC)
- Base Reactive Current Control (BRCC)

The additional reactive current control has the function of providing additional reactive current (i.e. fast fault current injection as denoted in Chapter 3) during under-voltage events or reducing the reactive current injection in cases of over-voltage, essentially providing proportional control of the terminal voltage [27]. The terminal voltage Vt is passed through a transducer, with a time constant Trv to yield the filtered terminal voltage Vt_filt which is compared to the reference voltage $Vref0$. This *error* is passed through a user-settable deadband, if the value of the error is within this deadband, no action will be taken from the additional reactive current control module. If the error is outside of the deadband, this value is multiplied by the reactive current injection gain Kqv and passed through upper $Iqh1$ and lower $Iql1$ boundary limits to yield the supplementary reactive current injection $Iqinj$. Additionally, an added variable has been added to denote the status of the PV System, which is *Voltage_dip*. This variable works as demonstrated in Equation 4.1 [14].

$$\text{Voltage\_dip} = \left\{ \begin{array}{ll} 1 & \text{if } Vt < Vdip \text{ or } Vt > Vup \text{ (fault condition)} \\ 0 & \text{otherwise (normal operating condition)} \end{array} \right. \tag{4.1}$$

The lower- and upper voltage limit $Vdip$ and Vup, respectively, are user-settable parameters. Hence, if the terminal voltage is higher than Vup or lower than $Vdip$, the PV system is said to be in fault condition. An additional consequence which the fault condition has on the controls of the PV system model is that the state variables of the control blocks are frozen. A demonstration of the freeze function is provided in Appendix C. Finally, the name of the variable might be confusing to the reader, as the variable *Voltage_dip* not only provides the status of fault condition in the case of a decrease of voltage below the user-settable limit $Vdip$ but also when the voltage increases beyond Vup.

The base reactive current control has two modes of operation i.e. [28],

- Constant Power Factor Control
- Constant Reactive Power Control

The constant power factor control is activated by setting *PfFlag* to 1. In this mode of operation, the power factor is taken from the solved power flow case. The reactive power is calculated as shown in Equation 4.2 to maintain a constant power factor,

$$Q_e = P_e \times tan(pfa) \tag{4.2}$$

The constant reactive power control is activated by setting *PfFlag* to 0. For this mode of operation the reactive power reference *Qext* is taken from the power flow solution or from the plant controller module REPC_A, if connected. This signal is then passed through 0, 1 or 2 PI controllers dependent on the settings assigned to the different flags and ultimately the reactive current command of the base reactive current control is determined — the settings assigned to the different flags determine the control mode. The different reactive control modes[1] are provided in Table 4.2 [2].

---

[1] *Local* refers to the regulation on converter level

[2] *N/A* means that the setting of that flag has no impact on the control mode

Control Mode	PfFlag	VFlag	QFlag
Local constant Q control	0	N/A	0
Local constant power factor control	1	N/A	0
Local voltage control	0	0	1
Local coordinated Q/V control	0	1	1

Table 4.2: Reactive control modes of REEC_B module [31]

The output of the base reactive current control added to the output of the additional reactive current control form the initial reactive current command *Iqcmd'*. This signal is then passed through the reactive current limits (which are determined by the current limit logic — discussed subsequently), which then produces the reactive current command *Iqcmd.*

Current Limit Logic
The current limit logic of the REEC_B module is provided in Figure 4.9.
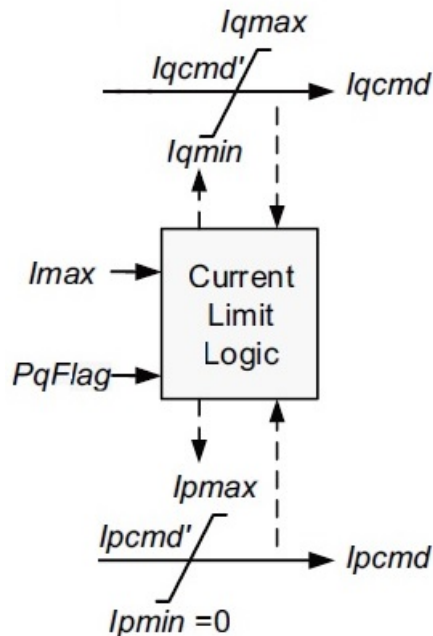
Figure 4.9: Current Limit Logic of REEC_B [29]

The converters have a rated capacity (usually in the order of 1.1 pu of their nominal rating) and in certain situations they will not be able to satisfy both the active- and reactive power commands. The current limit logic prioritises the active- or reactive current dependent on the value assigned to *PqFlag*. The priority established for selecting either binary value for *PqFlag* is shown in Table 4.3.

PqFlag	Priority
1	P-priority
0	Q-priority

Table 4.3: Current Limit Logic Priorities

The Equations 4.3 and 4.4 are used to determine the maximum and minimum active- and reactive current limits,

$$\text{P-Priority} = \begin{cases} \text{Ipmax = Imax} \\ \text{Ipmin = 0} \\ \text{Iqmax} = \sqrt{Imax^2 - Iqcmd^2} \\ \text{Iqmin = -Iqmax} \end{cases} \tag{4.3}$$

$$\text{Q-Priority} = \begin{cases} \text{Ipmax} = \sqrt{Imax^2 - Iqcmd^2} \\ \text{Ipmin = 0} \\ \text{Iqmax = Imax} \\ \text{Iqmin = -Iqmax} \end{cases} \tag{4.4}$$

4.2.4. Renewable Energy Plant Level Control Module (REPC_A)

The block diagram of the REPC_A module is provided in Figure 4.10. A description of the parameters shown in Figure 4.10 is provided in both Appendix A and B.
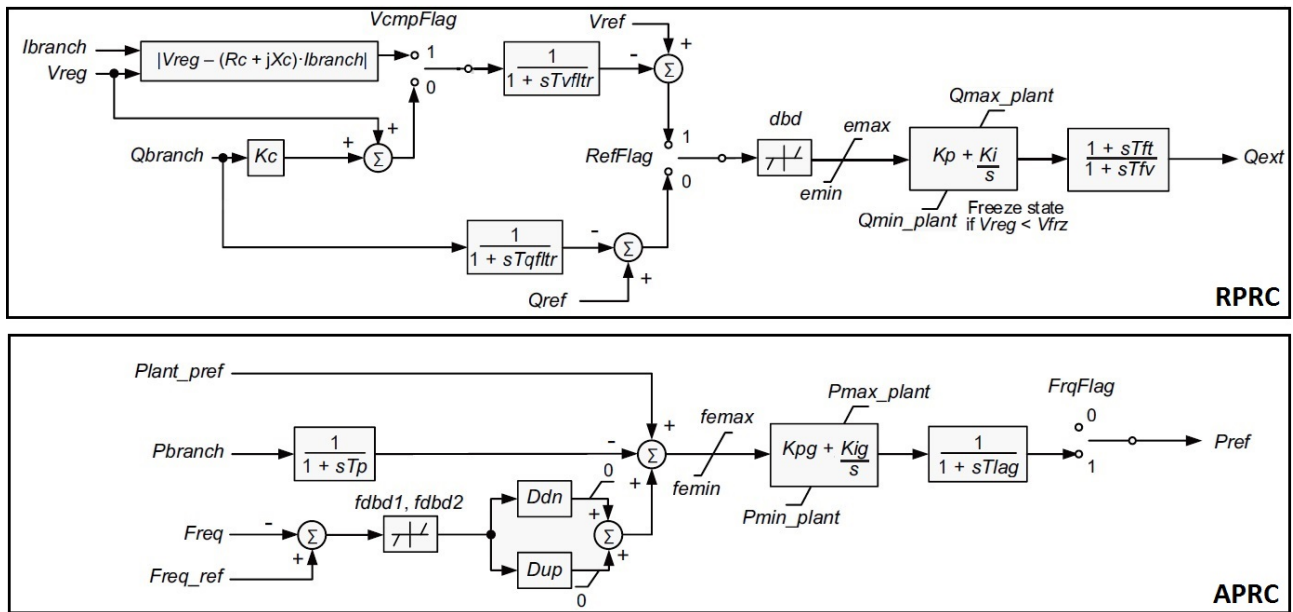
Figure 4.10: Block diagram of REPC_A module [14]

The REPC_A Module is an optional module and has the function of generating active- and reactive power references for the electrical control module [27]. If this model is not present, the active- and reactive power references are taken from the network solution. The generation of the active- and reactive power references in the REPC_A module occurs separately as shown in Figure 4.10. Hence the REPC_A Module can be categorised in,

- Reactive Power Reference Control (RPRC)
- Active Power Reference Control (APRC)

Reactive Power Reference Control

The reactive power reference control has the ability to be set to plant level voltage control or plant level reactive power control with the parameter *RefFlag* — Table 4.4 provides the control modes which are associated with the assigned binary value for this parameter.

RefFlag	Control Mode
1	Plant-level Voltage Control
0	Plant-level Reactive Power Control

Table 4.4: *RefFlag* settings

If plant-level voltage control mode is selected, there is an ability to also take into account line drop compensation or voltage droop with the parameter *VcompFlag*. Line drop compensation refers to the addition of an impedance to take into account the voltage drop due to the line/cable from the terminal of the plant to the bus to be controlled — usually the point of interconnection. The binary values associated with the operating mode for parameter *VcompFlag* are shown in Table 4.5.

VcompFlag	Control Mode
1	Line Drop Compensation
0	Voltage Droop Control

Table 4.5: *VcompFlag* settings

The line drop compensation can be neglected by adjusting the dynamic data file so that the branch flows to the plant controller are zero [27]. The attained error is passed through a deadband and limiter and then passed through a PI controller and first-order lead-lag compensator to obtain the reactive power reference which is sent to the electrical control module REEC_B [27].

The reactive power control options of the REPC_A module with the REGC_A and REEC_B modules are provided in Table 4.6.

Functionality	PfFlag	Vflag	Qflag	RefFlag
Plant level Q control	0	N/A	0	0
Plant level V control	0	N/A	0	1
Plant level Q control + local coordinated V/Q control	0	1	1	0
Plant level V control + local coordinated V/Q control	0	1	1	1

Table 4.6: Reactive power control options of REPC_A module (in combination with REGC_A and REEC_B)

If the plant controller module REPC_A is left out when modelling a PV system, the reactive power control options shown in Table 4.2 are possible.

Active Power Reference Control
The Active power reference control is implemented to emulate the frequency response. This control mode can be activated by setting *Freq_Flag* to 1 and setting it to 0 for deactivation. If the active power control is activated, the frequency is compared to the reference frequency. This error is then passed through a deadband and then through up- and down regulation gains *Dup* and *Ddn*, respectively. These gains represent up and down regulation droops. Since PV systems usually operate at their maximum capability, responding to under-frequency events will not be possible, hence *Dup* is usually set to 0. The output of these signals are summed and this yields the additional or reduced active power to obtain the active power reference, which is summed up with the plant active power reference *Plant_pref* and subtracted from the branch active power *Pbranch*. This summation is passed through a frequency limiter followed by a PI Controller eventually yielding the active power reference *Pref* which is sent to the electrical control module REEC_B.

The active power control options of the REPC_A Module are provided in Table 4.7.

Functionality	Freq_Flag	Ddn	Dup
No governor response	0	N/A	N/A
Governor response with down regulation only	1	>0	0
Governor response with up and down regulation	1	>0	>0

Table 4.7: Active power control options of REPC_A module

4.3. Distributed PV Model

4.3.1. Introduction

Distributed PV Systems, as discussed in the Introduction of Chapter 4, are connected at distribution level. Besides the rapid increase of inverter-based generation at transmission level, PV systems connected at distribution level have also seen an immense growth [32]. The requirements that these PV systems should adhere to, depends where they fall in the classification of PGMs discussed in Chapter 3. To represent distributed PV systems in dynamic case studies, distributed PV models are used. Additionally, these models are also used to represent the aggregation of distributed PV systems by using aggregation techniques and modelling the aggregated system at transmission level to obtain an acceptable representation of the gross distributed PV systems [33]. In the last decade several distributed PV Models have been proposed such as the PVD1 model and the DER_A model. The DER_A model is the latest iteration of distributed PV model and is the successor to the PVD1 model [32]. The DER_A model stands for the Distributed Energy Resource Model Version A, and is a model used for modelling the positive-sequence dynamic behaviour of aggregated distributed solar PV. This aggregation provides a representation of all the small- and medium solar PV systems scattered at lower- to medium voltage levels [32]. This model is derived from the large-scale PV model, discussed in the previous section, which includes the models REPC_A, REEC_B and REGC_A [25]. The large-scale PV model contains 121 parameters and 16 states, thus is too complex for representation of aggregated solar PV. Moreover, this model was developed to depict the behaviour of a single large renewable plant and thus may not be easily adaptable to incorporate the aggregation of distributed generators [34]. Therefore, the DER_A model was developed to provide a straightforward approach to modelling the aggregation of distributed PV systems, and also a reduction in parameters and states was established without diminishing the core functionalities to adequately represent the dynamic behaviour. Lastly, the DER_A model can be used as a standalone model but can also be implemented in the composite load model.

4.3.2. Overview Control Module

The block diagram of the DER_A model is shown in Figure 4.11. A description of the parameters shown in Figure 4.11 is provided in Appendix B.
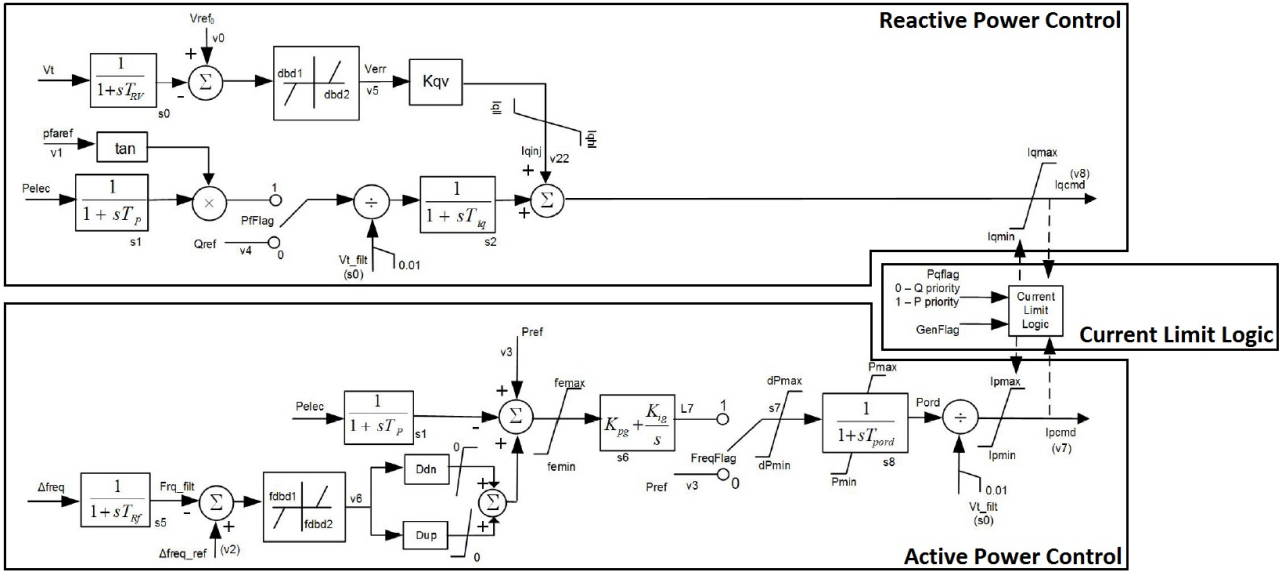
(a) Electrical control module
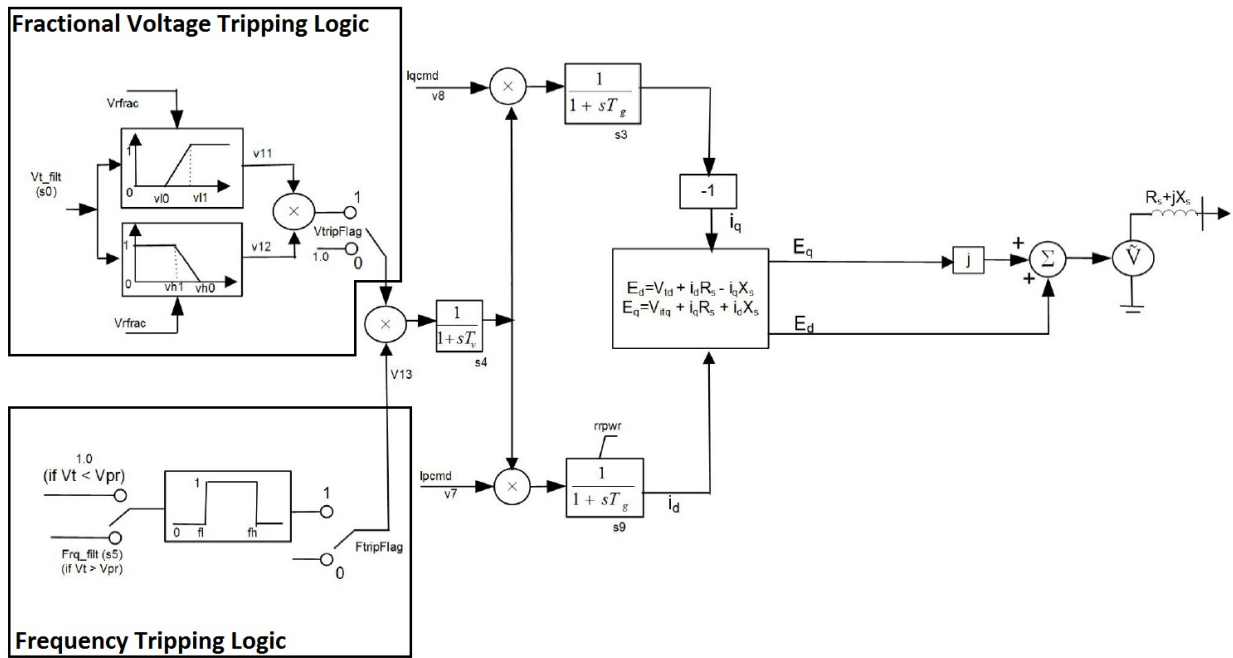
(b) Generator module

Figure 4.11: Block diagram of DER_A model [29]

The DER_A model can be subdivided in numerous sub-modules based on their functionality,

- Reactive Power Control
- Active Power Control
- Current Limit Logic
- Fractional Voltage Tripping Logic
- Frequency Tripping Logic

Reactive Power Control
The reactive power control of the DER_A model is shown in Figure 4.12.
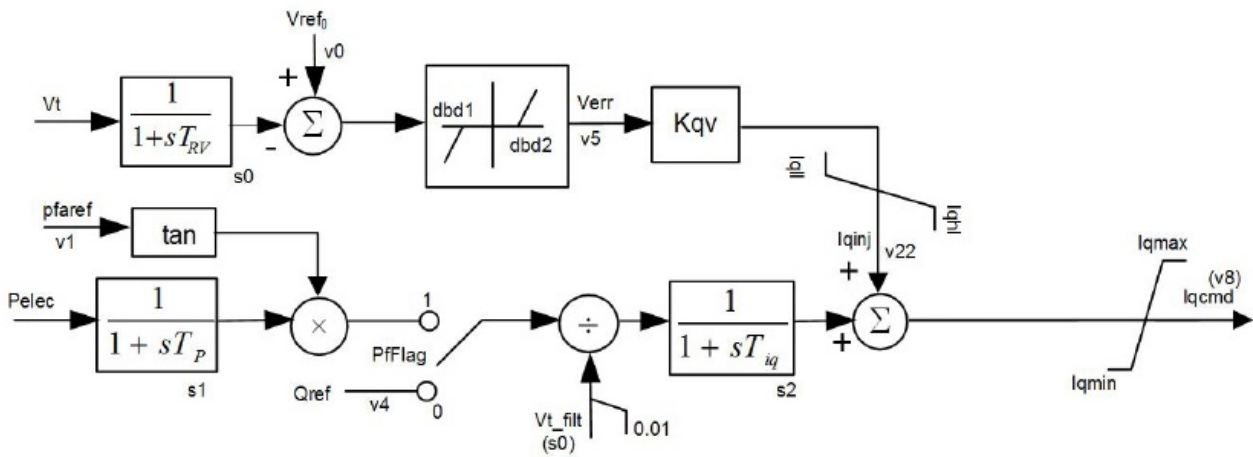
Figure 4.12: Reactive Power Control of DER_A model [29]

For reactive power control, the terminal voltage *Vt* is firstly filtered to obtain the filtered terminal voltage *Vt_filt* and is then compared to the reference voltage *Vref.* This error is then passed through a deadband with deadband limits set by the user. The deadband has the function of disabling voltage control when the voltage error is within the deadband limits. However, if the voltage error is outside of the deadband, the voltage control is activated. After passing the deadband, the output of the deadband is multiplied by a proportional control gain *Kqv*, which yields the current *Iqinj* that needs to be injected to maintain the voltage. This current is also compared to maximum and minimum current limits for voltage control. If the aggregation of PV systems does not provide reactive current injection during disturbances, this part of the control module can be disabled by setting *Kqv* equal to zero.

Similarly as the large-scale PV model, the reactive power control of the DER_A model has the ability to operate in either constant power factor mode and constant reactive power mode. This mode is determined by the binary value assigned to *PfFlag*. If *PfFlag* is equal to 1, then the same method as described by Equation 4.2 is used. Following this, the calculated reactive power is divided by the terminal voltage *Vt* to obtain the reactive current needed to achieve a constant power factor angle. On condition that *PfFlag* is equal to 0, the reference reactive power is used and then also divided by the terminal voltage to obtain the reactive current. Lastly, the two calculated reactive currents are summed and the reactive current command is established, which is compared to the maximum and minimum reactive current limits [26].

Active Power Control
The active power control of the DER_A model is shown in Figure 4.13.
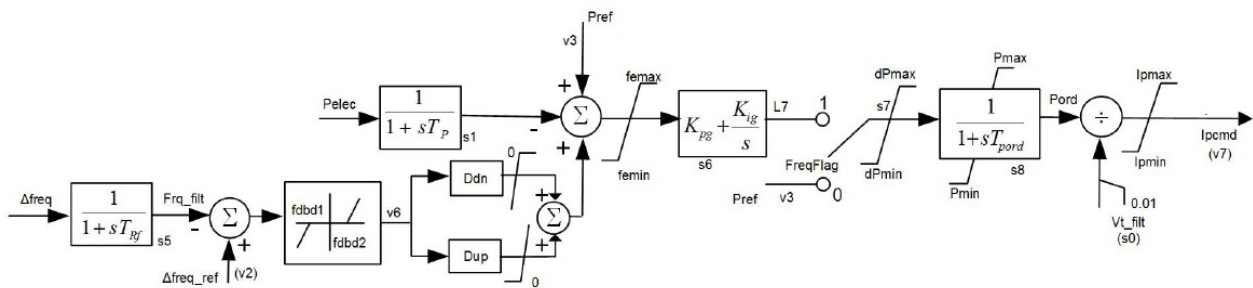
Figure 4.13: Active Power Control of DER_A Model [29]

In this part of the controls the user has the ability to enable or disable frequency support. This can be done by setting *FreqFlag* either to 0 or 1, where 0 indicates that frequency support is disabled while 1 indicates that it is enabled. If frequency support is enabled then the frequency deviation is compared to a reference frequency deviation. This signal is then passed through a deadband (similar to what was discussed in reactive power control), thus if the error lies within the deadband limits no frequency control will occur. The parameters *Ddn* and *Dup* represent the droop gains

for over- and under-frequency, respectively [26]. As also indicated in the large-scale PV model, PV systems usually operate at their maximum capability thus *Dup* is usually set to 0. The output of *Ddn* and *Dup* is then summed, this value is fed through a comparator with the reference active power and the actual active power. The result is fed through a PI controller, which eventually yields the active power command. This command is divided by the terminal voltage to achieve the active current command whilst also taking into account the active current limits (defined by current limit logic). For the condition that the frequency support is disabled, the reference active power is divided by the terminal voltage to attain the active current command.

The Active Power Control of the DER_A model has combined the functionalities of Active Power Control of the Plant controller REPC_A and the electrical control module REEC_B. The frequency control is taken from the REPC_A module, while the translation to the active current command *Ipcmd* is taken from the REEC_B module.

Current Limit Logic
The current limit logic is shown in Figure 4.14.
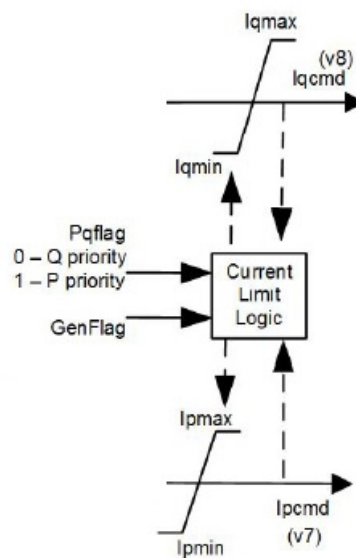
Figure 4.14: Current Limit Logic of DER_A model [29]

The current limit logic has the same function as the current limit logic described for the electrical control module REEC_B of the large-scale PV model. It prioritises the active- or reactive current command depending on the value assigned to *Pqflag*. The same value definition holds as provided in Table 4.3. The current limits are determined in the same manner shown in Equations 4.3 and 4.4. Moreover, the DER_A model also has the ability to function as an energy storage device, this can be achieved by setting *GenFlag* equal to 0. However, since the main interest of this research is to model renewable energy sources which produce electrical energy, the value of *GenFlag* will be kept equal to 1.

Fractional Voltage Tripping Logic
The DER_A model has the ability to emulate fractional tripping when the voltage goes below or above certain assigned values. The fractional tripping logic is shown in Figure 4.15.
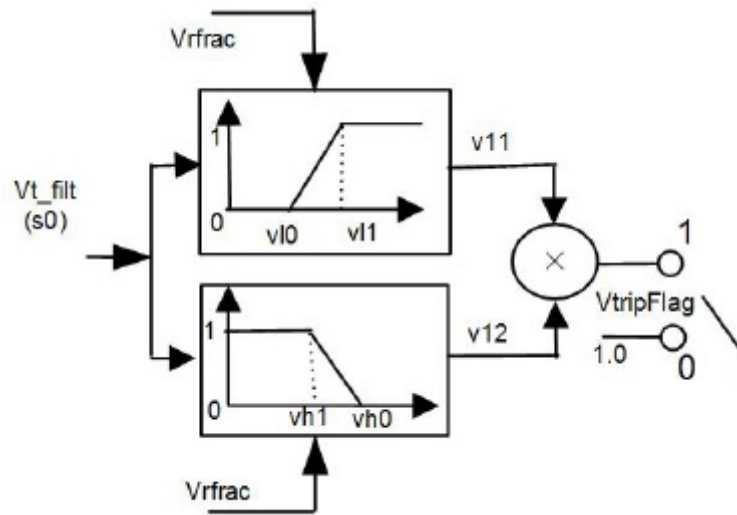
Figure 4.15: Fractional Voltage Tripping of DER_A model [29]

If the voltage goes above or below the thresholds *vh1* or *vl1*, respectively, then the aggregated PV systems will trip in a linear manner, eventually leading to all aggregated PV systems tripping at thresholds *vh0* or *vl0*. *Vrfrac* establishes the fraction of aggregated PV systems which recover after the voltage returns within the interval of *vl1* and *vh1*. This logic has been implemented to mimic partial tripping of Distributed Energy Resources (DERs) in the aggregated model [32].

Frequency Tripping Logic
The frequency tripping logic is shown in Figure 4.16.
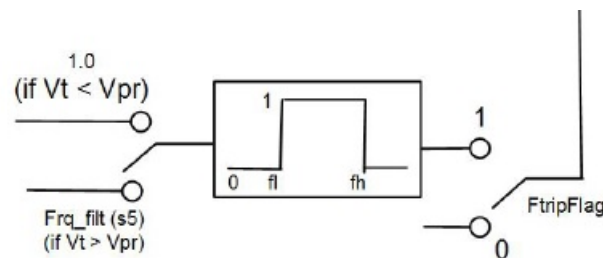
Figure 4.16: Frequency Tripping Logic of DER_A model [29]

The frequency tripping logic is enabled when *FtripFlag* is set to 1. If the voltage is below a certain threshold *Vpr* then the frequency tripping logic is disabled. If the terminal voltage is larger than *Vpr* then the frequency will be compared to the under-frequency and over-frequency thresholds. Both under-frequency *fl* and over-frequency thresholds *fh* have a cut-out timer assigned to them *tfl* and *tfh*, respectively. Should the frequency be below or above the frequency thresholds longer than the assigned delay then the solar PV system will trip. Unlike the voltage tripping logic, no fractional tripping is present for frequency. Thus, if the frequency is surpassed for the duration of time the whole unit/aggregated model will trip.

4.4. Shortcomings of Models

The PV dynamic models discussed in Section 4.2 and 4.3 are very closely related to one another, as the DER_A model is derived from the large-scale PV model. These models try to emulate the behaviour of real PV systems with emphasis on the most important characteristics, however, an exact depiction of real PV systems cannot be achieved because of certain limitations of these models. The shortcomings of the PV models will be discussed next, and the minor differences of the discussed PV models with respect to their limitations.

The main shortcomings of the PV models are [35],

1. The study of contingencies in power system networks consists of balanced and unbalanced faults, where the

analysis of unbalanced faults requires the use of sequence networks. Both the PV models are developed as positive-sequence models and hence are not developed for analysis of unbalanced faults.

2. The large-scale PV model is represented in commercial software as a current source model which can result in numerical instability under high RES penetration levels [26]. Whereas, the DER_A model has been updated by making use of a voltage source representation.

3. There is no explicit representation of the converter PLL and it's dynamics in either of the PV Models, however, an emulation of the behaviour of the PLL at decreased voltage levels has been implemented in the large-scale PV model. Additionally, the PV models simulate a limited frequency bandwidth and hence do not include the inner-current control loops and other detailed characteristics of the controls of the converter.

4. As discussed in Chapter 3, FRT profiles are of great importance to determine if a PV system should ride through a fault. The PV models, however, do not have the ability to assign a FRT profile to the model and to disconnect accordingly.

5. Over the time interval of dynamic simulations (3 – 20 seconds) it is possible that solar irradiance varies in actual scenarios, however, the PV models do not provide the option to add a solar irradiation profile therefore the solar irradiation is assumed constant during simulations.

6. The DER_A model does not take into account the controllable elements present in the distribution network such as controllable reactive power compensation devices and tap changers.

7. Small-signal stability as highlighted in Chapter 2, is the ability of the power system to remain in synchronism during the occurrence of small disturbances. The validity of the PV models with respect to these stability studies is yet to be investigated since it has yet to be determined if linearisation of the system yields reliable state-space models. This topic is outside of the scope of this thesis.

4.5. Parameters

4.5.1. Introduction

For PV generic models, the parameter set is essential to (satisfactorily) represent the dynamic behaviour of specific PV systems. For models which represent specific PV systems, a very detailed parameter set can be assigned based on most significantly the converter/inverter specifications [14]. However, when developing a PV generic model with a parameter set to portray a wide array of PV systems, the goal is to capture important behaviour of these systems and not necessarily the minute details. Accordingly, this thesis shall contribute to the development of a generic parameter set to represent PV systems based on the current grid connection requirements in the Dutch grid, typical specification of state of the art PV inverters, ordinary converter and filter time constants in combination with sensitivity studies for relevant parameters. In the sensitivity study, the network provided in Appendix A is used and a three-phase bolted fault is introduced at bus 5 (POI) at time instance t=2s and cleared after 6 cycles at time instance t=2.12s. The time step used for the simulations is 0.004s.

4.5.2. Large-Scale PV Model

The large-scale PV model consists of three separate modules with a total of 75 parameters. The assignment of important parameters shall be discussed next for the three modules. The remaining parameters have been assigned based on the values discussed in [14] and [24]. The assigned values to the parameters have been determined as shown in Figure 4.17.
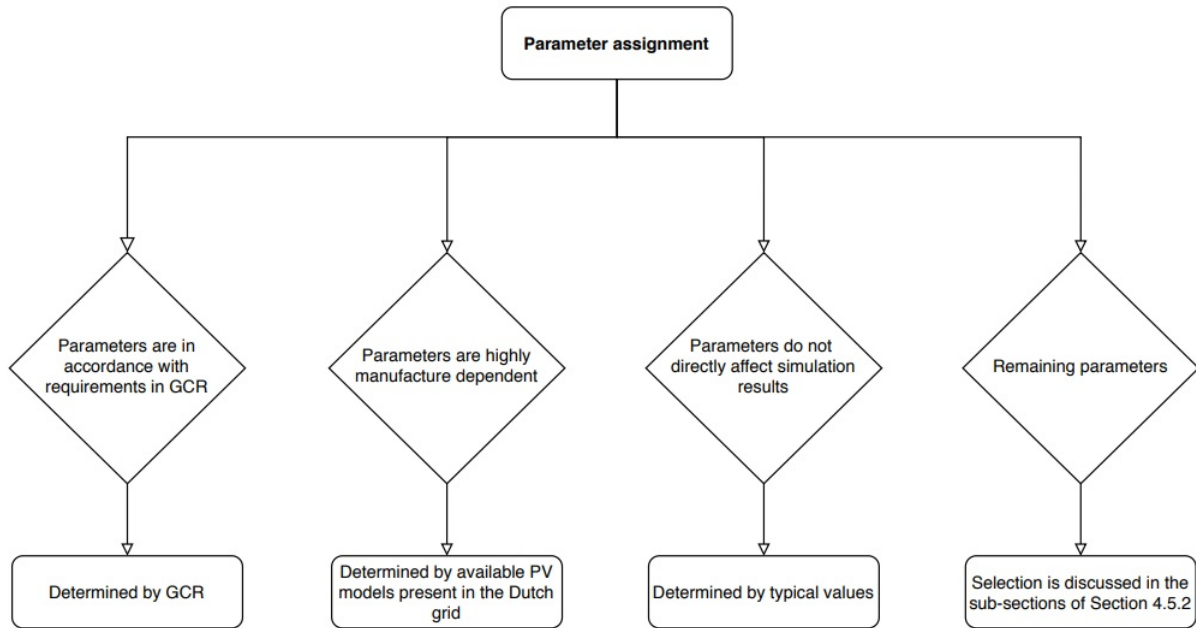
Figure 4.17: Flowchart assignment parameters of proposed parameter set

REGC_A Module

The REGC_A Module consists of 15 parameters [29]. The *High Voltage Reactive Current Management Module*, which serves to reduce reactive power above a certain voltage threshold, has been deactivated by setting *Khv* equal to zero since there is no requirement in the Dutch netcode for PPMs to reduce their reactive power output if the voltage exceeds a certain threshold. The surrounding parameters of this module have been assigned typical values as they do not influence the simulation results. Additionally, the parameter *Iolim*[3] has been set equal to *Imax*, which is the maximum current of the converter, so that the maximum permissible reactive current injection is equal to the maximum current capability of the converter. Moreover, the parameter *Tg* is of importance for processing and injecting the provided active- and reactive current commands. This can be seen in Figure 4.18.

---

[3]The value assigned to *Iolim* is a negative because of the negative sign assigned to $\frac{1}{1+sTg}$
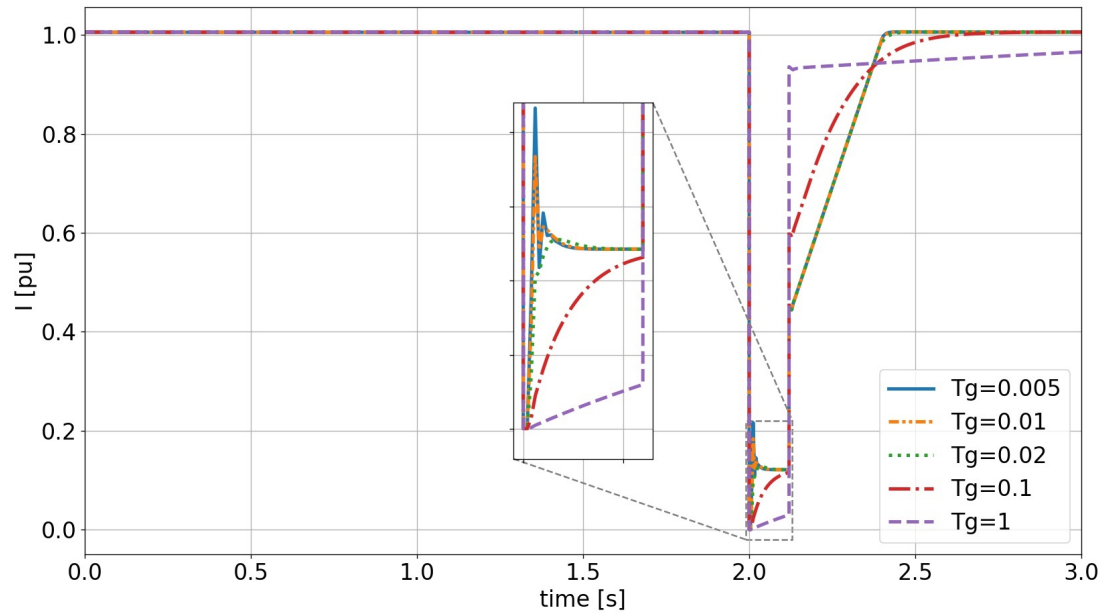
(a) Active current injection
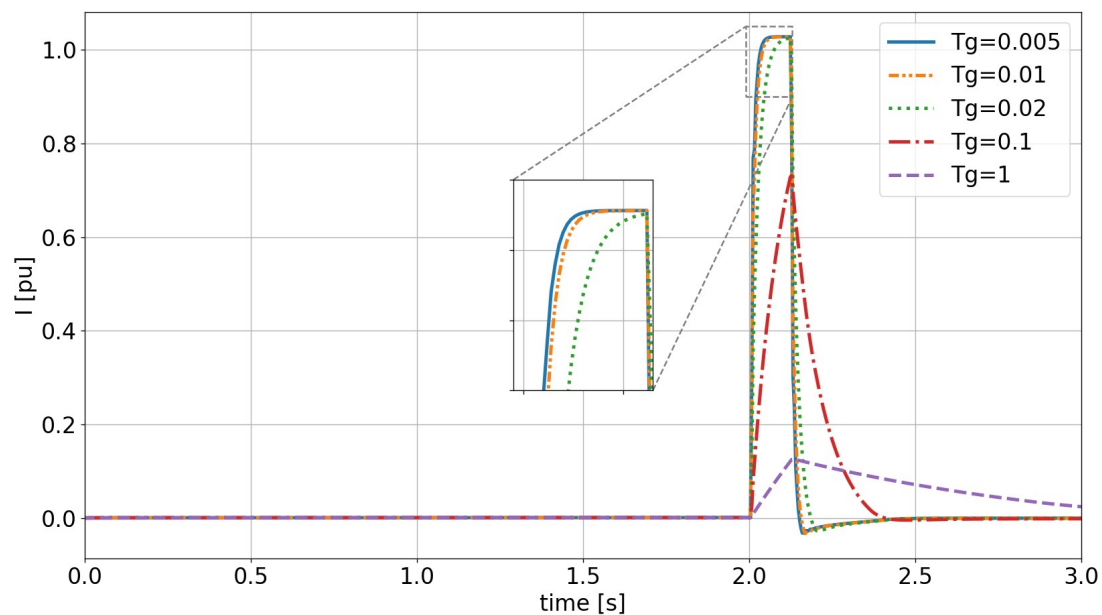
(b) Reactive current injection

Figure 4.18: Current injection of PV system with varying values of *Tg*

In Figure 4.18, it is shown that the parameter *Tg* plays an important role in the speed of the active- and reactive cur-
rent injection. The typical value of *Tg* provided in [24] is 0.02s, however, this document dates back to 2012. In the
latest parameter sets of individual PV systems, the value 0.005s is assigned to *Tg*. As shown in Figure 4.18, the lower
the value assigned to *Tg*, the faster the active- and reactive current injection occurs. In contrast, when the value of
Tg is high, the active- and reactive current injection occurs with a significant delay resulting in little to no active- and
reactive current injection for faults which occur and are cleared on a very short time interval. Additionally, for high
values of *Tg* the settling time is of longer duration. It should be noted that the active current injection after clearance

of the fault, is similar for the values 0.005s, 0.01s and 0.02s of *Tg* since the active current injection change is limited by *Rrpwr*, which will be discussed next. For the proposed standard parameter set the value of 0.005s will be used for *Tg*.

The parameter *Rrpwr* provides an upper limitation for the active current ramp-up rate after fault clearance, essentially limiting the increase of active power per time unit. The behaviour of different values of *Rrpwr* is provided in Figure 4.19.
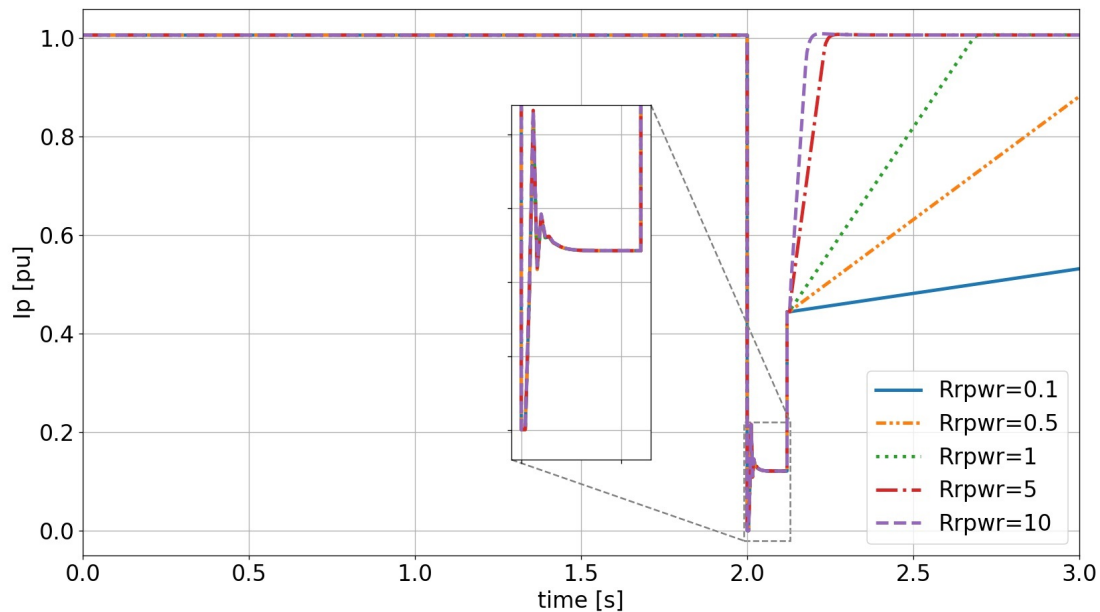
Figure 4.19: Active current injection of PV system for varying values of *Rrpwr*

As shown in Figure 4.19, the speed of the active current injection after fault clearance is strongly determined by the parameter *Rrpwr*. Additionally, it can also be seen that the ramp rate limit does not apply to instantaneous and very sudden changes — this explains the behaviour right after the occurrence of the fault and the sudden increase in active current injection the moment the fault is cleared. According to [14], higher ramp rates increase the speed of voltage recovery. Using low values for *Rrpwr* instigates slow voltage recovery and could result into decrease of voltage beyond FRT profile as illustrated in [14]. In contrast, too high of a value for *Rrpwr* could potentially result in frequency problems due to high frequency sensitivity [14]. Another important aspect which the value *Rrpwr* influences is the Critical Clearing Time (CCT), larger values of *Rrpwr* increase the CCT [14]. In [14] and [24], the value of 10 pu/s is used for *Rrpwr*, this is seen as a typical value to represent PV systems. Additionally, the Netcode proposal handed in by *Netbeheer Nederland* states that the maximum permissible recovery of active power should be between 0.5 and 10 seconds, translating to a minimum value for *Rrpwr* between 2 pu/s and 0.1 pu/s [20], however this does not provide the whole picture, since this wide range takes into account all PPMs including wind turbines not fully connected via power electronics, which need additional time to provide active current recovery. To this end, the value of 10 pu/s shall be assigned to *Rrpwr* as this is consistent with literature and falls well within the limits set by the proposed requirements.

The *Low Voltage Power Logic* switch has been turned off by setting the value *lvplsw* equal to zero. This has been done since this characteristic is highly dependent on the manufacturer and the deactivation of the module does not influence the reactive current injection during contingencies [36].

REEC_B Module
The REEC_B Module consists of 30 parameters [29]. The parameters of the ARCC control sub-module provided in Figure 4.8 have been aligned to the fast fault current provision requirement provided in Chapter 3, which states that fast fault current needs to be provided with either a 5% instantaneous change of voltage or a 10% gradual change. Since, the behaviour during faults is mainly looked at, the parameters shall be attuned to the 5% instantaneous change case. This value has been used for the IEEE 9 Bus network study discussed in Chapter 5. However, for the TenneT

network study using this value led to convergence problems as the voltage is controlled very narrowly and a lot of PV systems are present in the model. To this end, the assigned values for the TenneT network study have been modified to eradicate the convergence problems. A deadband has been placed of 10% voltage deviation on the PV systems as shown in Table 4.8. Additionally, the reactive current injection gain (denoted as k in the GCR and as Kqv in REEC_B module) has been assigned the value 5 as the PV systems modelled by the large-scale PV model are all above 110 kV, which is the value assigned to k at this voltage level in the proposed provision of fast fault current injection [22]. Also, the fast fault current injection by the ARCC sub-module is limited to 1 pu by setting $Iqhl$ equal to 1. The assigned values to the parameters of this sub-module are shown in Table 4.8.

Parameter	Description	Value IEEE 9 Bus Network	Value TenneT Network
Vdip (pu)	Lower voltage threshold to activate additional reactive current injection logic	0.95	0.9
Vup (pu)	Upper voltage threshold to activate additional reactive current injection logic	1.05	1.1
dbd1 (pu)	Lower threshold voltage error deadband	-0.05	-0.1
dbd2 (pu)	Upper threshold voltage error deadband	0.05	0.1
Kqv	Reactive current injection gain of additional reactive current injection logic	5	
Iqhl (pu)	Upper limit on additional reactive current injection	1	
Iqll (pu)	Lower limit on additional reactive current injection	-1	

Table 4.8: Additional reactive current control parameters of REEC_B module

Additionally, the parameter Trv, which represents the terminal voltage bus filter time constant, is of high importance for fast fault current injection. Essentially, representing the measurement delay of the terminal voltage to the electrical control module due to the measurement device. The behaviour of the reactive current injection of the PV system is provided in Figure 4.20 for different values of Trv.
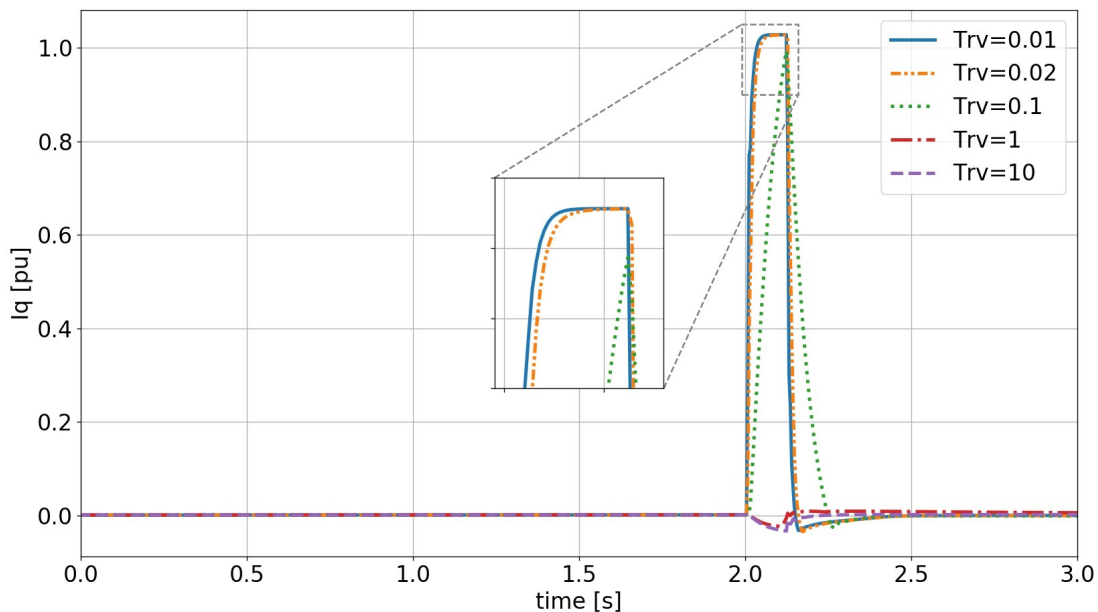
Figure 4.20: Reactive power response for varying values of Trv

As is provided in Figure 4.20, the speed of reactive current provision is highly dependent on the value of Trv. The typical values of this filter time constant are between 0.01s and 0.02s [24]. It is shown in Figure 4.20 that the reactive

current provision is fastest for the time constant 0.01s. Furthermore, once the fault is cleared the value of 0.01s also decreases it's reactive current injection the fastest. Consequently, the value 0.01s shall be selected for *Trv* in the proposed parameter set as this provides a proper representation for current and future PV systems. Furthermore, the maximum limit on total converter current *Imax* has been set to 1.1 as this provides a realistic approximation for inverter-based devices.

The values assigned to the gains of the two PI controllers *Kqi, Kqp, Kvi* and *Kvp* are strongly dependent on the manufacturer, hence the assigned values have been derived from the latest parameter sets provided by manufacturers for existing PV systems in the Dutch grid.

REPC_A Module
The plant controller (REPC_A) module generally has a slower response compared to the generator/converter and electrical control module as indicated in Figure 4.2. To see if the REPC_A module affects the dynamic response of the PV system during short-term contingencies, a test was conducted to examine the response with and without REPC_A module. The results of this study are provided in Section A.4 of Appendix A. It is shown that during a dynamic simulation of 3 seconds the plant controller does in fact, albeit limited, impact the behaviour of the PV system, in consequence the REPC_A module shall be included in the proposed parameter set.

The final proposed standard parameter set to represent individual (future) PV systems is provided in Tables B.1, B.2 and B.3 of Appendix B.

4.5.3. Distributed PV Model
As discussed in Section 4.3, the DER_A model is largely derived from the large-scale PV model discussed in Section 4.2, therefore there are a group of overlapping parameters in these two models — these parameters will be not be discussed again in this section unless stated otherwise. The important parameters assigned to the DER_A model will be discussed next.

The ARCC sub-module of the large-scale PV model shown in Figure 4.8 is also present in the DER_A model. It should be noted that there are different requirements for the reactive current injection gain (denoted as *k* in GCR) at distribution level, where a distinction is made for PPMs connected below and above 66 kV, however, as there are no distribution networks in the Netherlands above 66 kV, the reactive current injection gain of PPMs below 66 kV is used. Simirarly, as discussed for the large-scale PV model, the deadband for the TenneT network case study was modified due to convergence problems as shown in Table 4.9.

Parameter	Description	Value IEEE 9 Bus Network	Value TenneT Network
dbd1 (pu)	Lower threshold voltage error deadband	-0.05	-0.1
dbd2 (pu)	Upper threshold voltage error deadband	0.05	0.1
Kqv	Reactive current injection gain of additional reactive current injection logic	2	
Iqhl (pu)	Upper limit on additional reactive current injection	1	
Iqll (pu)	Lower limit on additional reactive current injection	-1	

Table 4.9: Additional reactive current control parameters of DER_A module

With regards to the fractional voltage tripping logic, the DER_A model will be used to represent PV systems of type A, B, C and D1 because these types of PPMs are present at distribution level in the Dutch grid. Type A PPMs have clearly defined requirements with regards to voltage tripping as shown in Table 4.10.

Parameter	Value	Response speed
Undervoltage protection 1 (pu)	0.8	2s
Undervoltage protection 2 (pu)	0.7	0.2s
Overvoltage protection (pu)	1.1	2s

Table 4.10: Voltage protection Type A PGMs [18]

To this end the parameters as shown in Table 4.11 are assigned to represent type A PPMs. Please note that the parameter *VtripFlag* should be set to 1 when modelling type A PPMs.

Parameter	Description	Value
vl0 (pu)	inverter voltage break-point for low voltage cut-out	0.7
vl1 (pu)	inverter voltage break-point for low voltage cut-out 2	0.7
vh0 (pu)	inverter voltage break-point for high voltage cut-out	1.1
vh1 (pu)	inverter voltage break-point for high voltage cut-out 2	1.1
tvl0 (s)	low voltage cut-out timer corresponding to voltage vl0	0.2
tvl1 (s)	low voltage cut-out timer corresponding to voltage vl1	0.2
tvh0 (s)	high voltage cut-out timer corresponding to voltage vh0	2
tvh1 (s)	high voltage cut-out timer corresponding to voltage vh1	2

Table 4.11: Fractional voltage tripping logic parameters to represent Type A PPMs

Type B, C and D1 PPMs have a similar FRT profile and have no explicit requirements with regards to voltage disconnection besides the FRT profile. Due to this, the voltage tripping logic is turned off to represent these types of PPMs by setting *VtripFlag* equal to 0.

Type A PPMs also have a requirement with regards to frequency disconnection. This requirement is provided in Table 4.12.

Parameter	Value	Response speed
Underfrequency protection (Hz)	47.5	2s
Overfrequency protection (Hz)	51.5	2s

Table 4.12: Frequency protection Type A PGMs [18]

The parameters assigned for type A representation with regards to frequency disconnection is provided in Table 4.13. Additionally, the parameter *FtripFlag* should be set to 1 to activate frequency tripping when representing type A PPMs.

Parameter	Description	Value
fl (Hz)	inverter frequency break-point for low frequency cut-out	47.5
fh (Hz)	inverter frequency break-point for high frequency cut-out	51.5
tfl (s)	low frequency cut-out timer corresponding to frequency fl	2
tfh (s)	high frequency cut-out timer corresponding to frequency fh	2

Table 4.13: Frequency tripping logic Parameters to represent Type A PPMs

Type B, C and D1 PPMs have no clear frequency disconnection requirement and hence for these types of PPMs the frequency tripping logic is deactivated by setting *FtripFlag* equal to 0.

The final proposed standard parameter set to represent the aggregation of distributed PV systems is provided in Table B.4 of Appendix B.

IEEE 9 Bus Network Case Study

This chapter shall make use of the proposed parameter set of the large-scale PV model discussed in Chapter 4 by analysing the transient- and short-term voltage stability of the IEEE 9 bus network and various modified IEEE 9 bus networks. Different penetration levels of solar PV systems i.e. 0% (also referred to as the base case), 27%, 51% and 77% shall be studied and a comparison of these different levels of solar PV networks shall be made with regards to transient- and short-term voltage stability. The goal of this study is to analyse if and how an increase in solar PV penetration level impacts the transient- and short-term voltage stability.

5.1. Studied Cases

The network which is studied in this chapter is the IEEE 9 bus system. The original network consists of 3 synchronous generators, 3 loads and 3 transformers interconnected through 9 buses and is denoted as the *Base case* with 0% solar PV penetration level. The single-line diagram of this network is provided in Figure 5.1. All pu values in this chapter are in terms of the system base of 100 MVA unless stated otherwise.
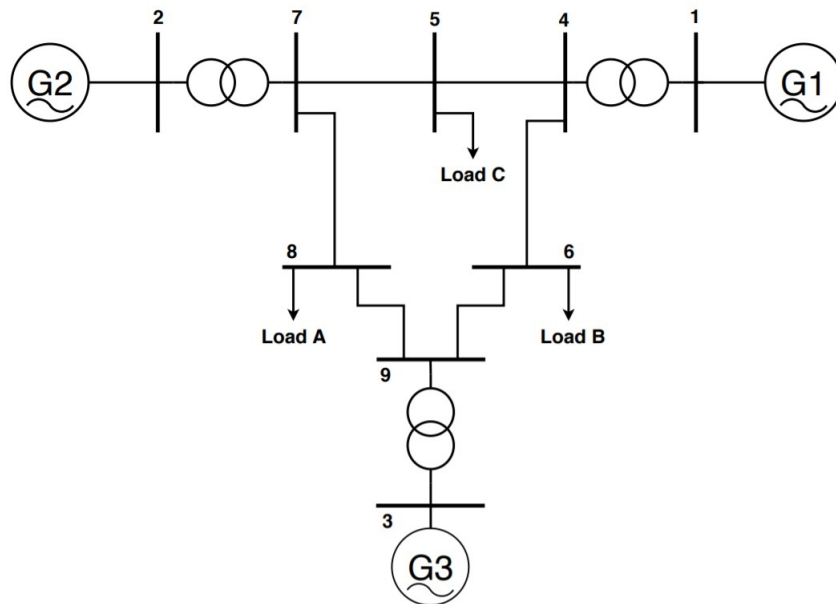
Figure 5.1: Base case of IEEE 9 bus system

To obtain different levels of PV penetration, the generators are replaced by PV systems with the same active power production operating at unity power factor. It should also be noted that synchronous generators provide significantly more short-circuit contribution during a contingency compared to a PV system of the same capacity. The method used to determine the level of PV penetration in a network is shown in Equation 5.1 provided below.

$$\% \text{ PV Penetration} = \frac{\text{Total PV Generation (MW)}}{\text{Total Generation (MW)}} \qquad (5.1)$$

The single-line diagrams of the networks at different PV penetration levels are provided in Figure 5.2.

(a) 27% PV penetration level

(b) 51% PV penetration level

(c) 77% PV penetration level
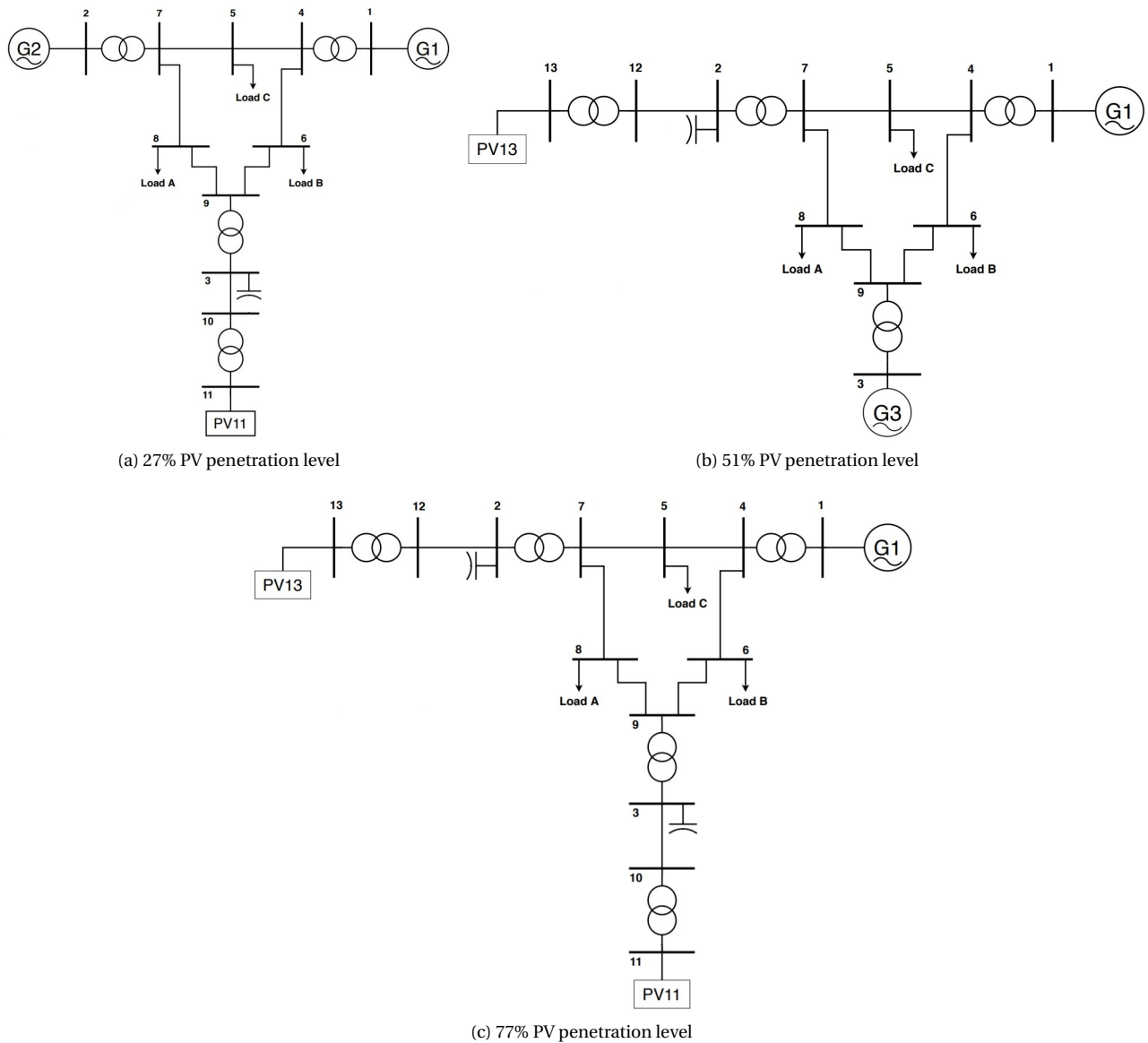
Figure 5.2: Modified IEEE 9 bus cases

In the sub-figures of Figure 5.2, it is shown that additional elements are added for the PV systems such as the LV/MV transformer and the line which represents the aggregation of internal/array cables — these additions are of great importance as it takes into account the collector system equivalent and the LV/MV equivalent transformer [37]. It is to be noted that the interconnection transmission line as discussed in [28] has been omitted to provide a fair comparison to the networks with synchronous generators since the synchronous generators are not connected to the rest of the network with an interconnection transmission line. Additionally, a plant-level reactive compensation is applied to achieve zero reactive power exchange at the point of interconnection as required by the Dutch netcode [18]. The parameters of all networks are provided in Appendix D. The power flow results of the different networks are provided in Table 5.1.

Case	Base Case		27% PV		51% PV		77% PV	
	P (MW)	Q (Mvar)	P (MW)	Q (Mvar)	P (MW)	Q (Mvar)	P (MW)	Q (Mvar)
G1	71.7	26.9	72.2	19.9	73.9	29.1	72.3	31.0
G2	163	4.6	163	-4.6	-	-	-	-
G3	85	-9.1	-	-	85	-6.1	-	-
PV11	-	-	85	0	-	-	85	0
PV13	-	-	-	-	163	0	163	0
Load A	100	35	100	35	100	35	100	35
Load B	90	30	90	30	90	30	90	30
Load C	125	50	125	50	125	50	125	50

Table 5.1: Power flow results of various cases

The added PV systems have been assigned the parameter set proposed in Chapter 4 and the mode assigned to the PV systems is the *Plant level Q control + local coordinated V/Q control* as provided in Table 4.6 with *Q-Priority*. This mode makes use of fast local control to instigate a quick voltage recovery, followed by the plant controller which restores, at a slower rate compared to the local control, the pre-fault reactive power [14]. This mode has been selected to achieve quick voltage support during contingencies and to eventually bring the reactive power exchange of the PV system to it's pre-fault value since the requirement of Dutch netcode states that the reactive power at the point of interconnection (POI) should be equal to zero[1] [18]. The transient- and short-term voltage stability are discussed in the subsequent sections.

5.2. Transient Stability

The transient stability of the networks provided in Figures 5.1 and 5.2 has been analysed with key performance indicator the *critical clearing time* (CCT) obtained with an iterative process[2]. The method to obtain the CCT is shown in the flowchart provided in Figure 5.3. For the analysis of transient stability, generator 1 (swing or slack bus) is used as the relative machine for rotor angles. Moreover, the network with 77% PV is not examined in the transient stability analysis due to the lack of availability of a reference generator as there is only one generator in this system.

---

[1]Article 3.17-5
[2]This iterative process has been aided by Python 2.7
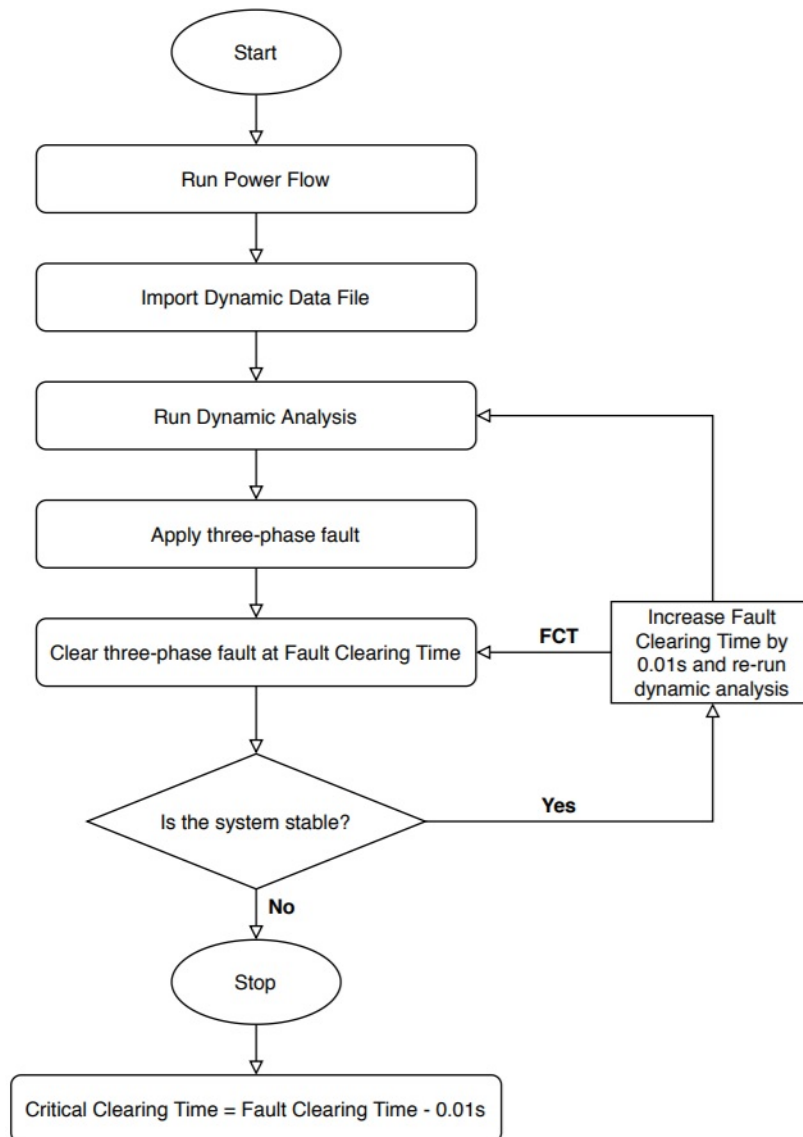
Figure 5.3: Flowchart for iterative process to obtain critical clearing time

When adding the PV systems in the IEEE 9 bus system as shown in Figure 5.2, two representations are explored for the PV systems. Firstly, the PV systems are represented by the *large-scale PV model* with the proposed parameter set discussed in Chapter 4. Secondly, the PV systems are represented by a negative load. This is done to clearly distinct if the transient stability is affected by the addition of the PV system and also to provide insight into how the landscape of the dynamic response changes when comparing the PV model case and negative load case at various penetration levels.

The critical clearing time is obtained with the iteration process shown in Figure 5.3. The dynamic simulation is conducted by introducing a three-phase fault at bus 8 at time t=1s. The obtained critical clearing times for the various networks and configurations are provided in Table 5.2, where *DM* refers to dynamic model entailing that PV systems are represented with their dynamic models while *NL* refers to negative load meaning PV systems are represented as negative load.

	Critical Clearing Time (ms)
Base Case	530
27% PV Level (with DM)	440
27% PV Level (with NL)	400
51% PV Level (with DM)	910
51% PV Level (with NL)	820

Table 5.2: Critical clearing time of IEEE 9 bus networks with three-phase fault at bus 8

Base Case and 27% Level PV Penetration

As shown in Table 5.2, it is seen that the critical clearing time decreases by approximately 100 ms with the replacement of generator 3 with a PV system. It is also clear from Table 5.2, that the two networks of 27% PV do not differ as considerably as the change from base case to 27% PV. From the latter it can be concluded that the transient stability is affected primarily because of the removal of the synchronous generator rather than the addition of the PV system. In Figure 5.4 the behaviour of the relative rotor angle of generator 2 is presented when a fault is introduced at bus 8 (at t=1s) with a fault clearing time (FCT) of 380 ms.
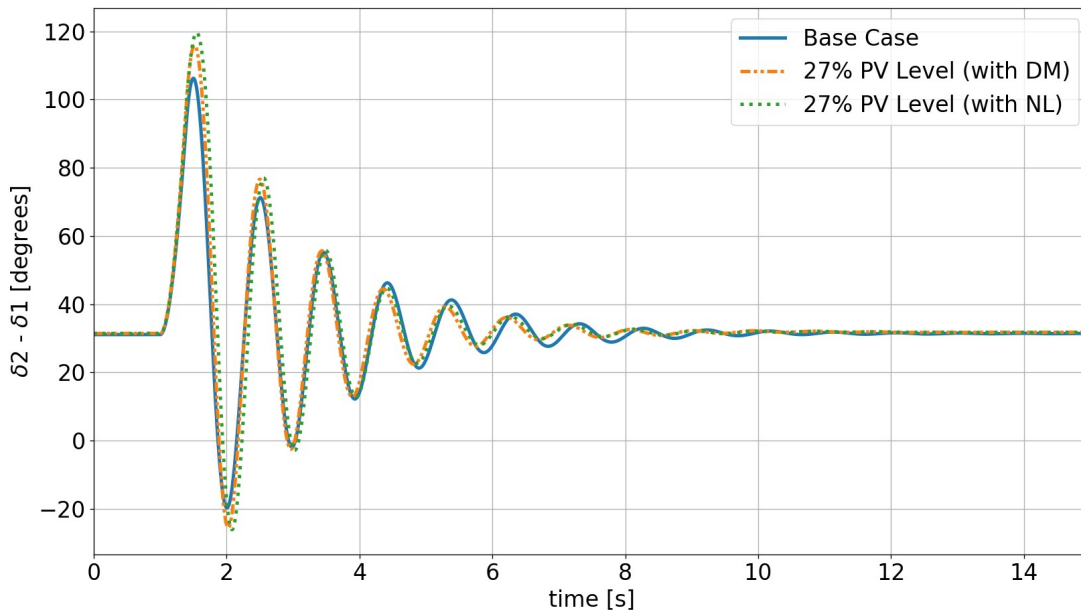
Figure 5.4: Relative rotor angle of generator 2

The results shown in Figure 5.4 are supportive of the numbers provided in Table 5.2. In this example, generator 2 is considered transiently stable for all cases since the oscillations are being damped. The amplitude of the rotor angle swings for the networks with 27% PV are higher compared to the base case. This is consistent with the critical clearing times provided in Table 5.2 since the amplitude of the rotor angle swings is highest for the case with negative load while the lowest amplitude rotor angle swings is seen for the base case. In consequence, the network with negative load 27% PV reaches instability first.

But why does the critical clearing time change when replacing generator 3 with a PV system or a negative load of the same active power output? First of all, it's important to identify the generator which loses synchronism and causes the system to become transiently unstable in the base case for a fault at bus 8. The behaviour of the relative rotor angles of generator 2 and 3 are shown in Figure 5.5.
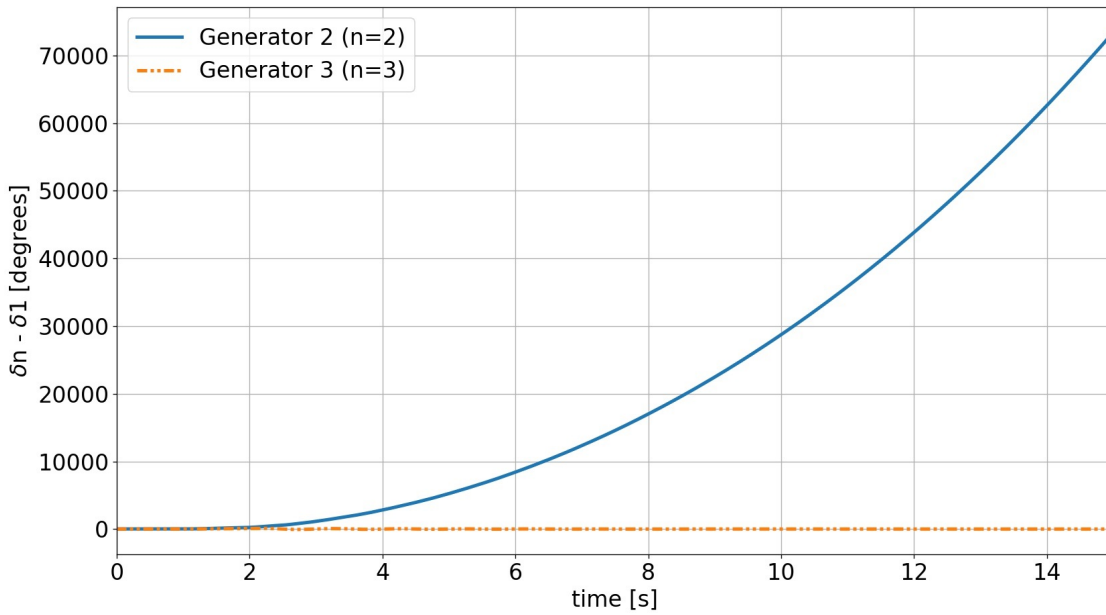
Figure 5.5: Relative rotor angle of generators in base case with FCT=550 ms
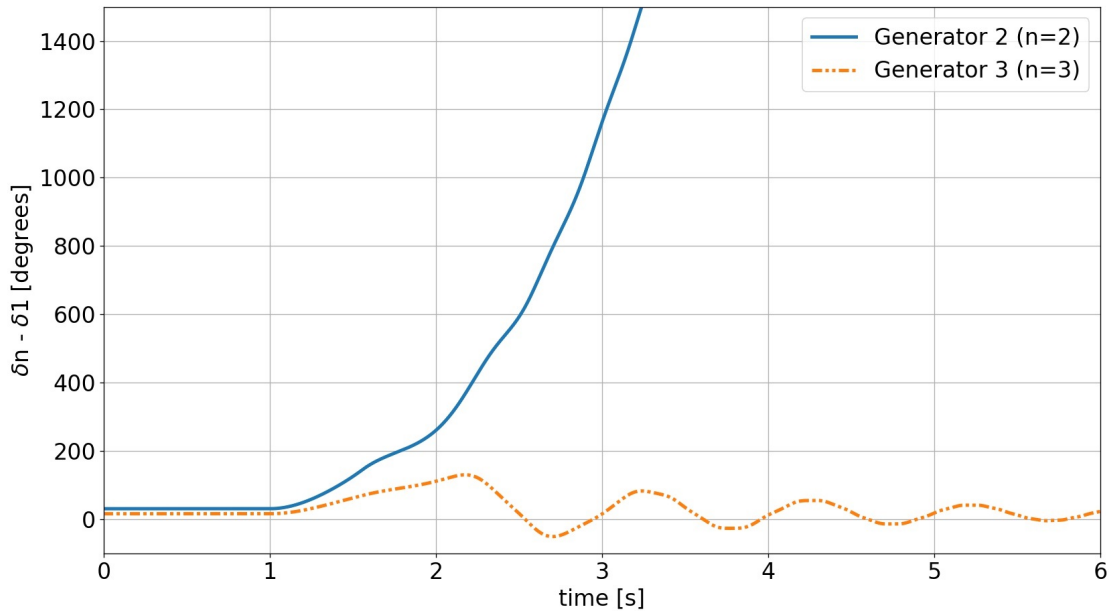
Figure 5.6: Zoomed relative rotor angle of generators in base case with FCT=550 ms

The rotor angle of generator 2 increases indefinitely with a fault clearing time of 550 ms, while the rotor angle of generator 3 contains damped oscillations — this is shown in Figure 5.6. Hence, generator 2 is the cause of the transient instability in the base case. Generator 2 is also the cause of transient instability in the networks with 27% PV as generator 3 has been replaced with it's active power equivalent PV system in these cases. Now that the source of instability has been identified, the focus shall be turned to generator 2.

Transitioning from the base case to the networks with 27% PV, causes the power flow distribution in the network to

change as shown in Table 5.1. This is caused due to the fact that the PV system replacing generator 3 operates at unity power factor and hence does not provide or absorb reactive power during steady-state conditions. In Table 5.1, it can be seen that generator 2 is loaded differently for the base case and the network with 27% PV. These values are once more provided in Table 5.3.

Case	Base Case		27% PV Level	
	P (MW)	Q (Mvar)	P (MW)	Q (Mvar)
G2	163	4.6	163	-4.6

Table 5.3: Power flow results of generator 2

The difference in loading as shown in Table 5.3 has an impact on the transient stability margin (the distance to transient instability [15]). The steady-state rotor angle of generator 2 is determined by it's steady-state active- and reactive power set points, this is also referred to as the *operating point* of the synchronous generator. The operating points of generator 2 for the base case and the 27% PV case are shown in Figure 5.7.
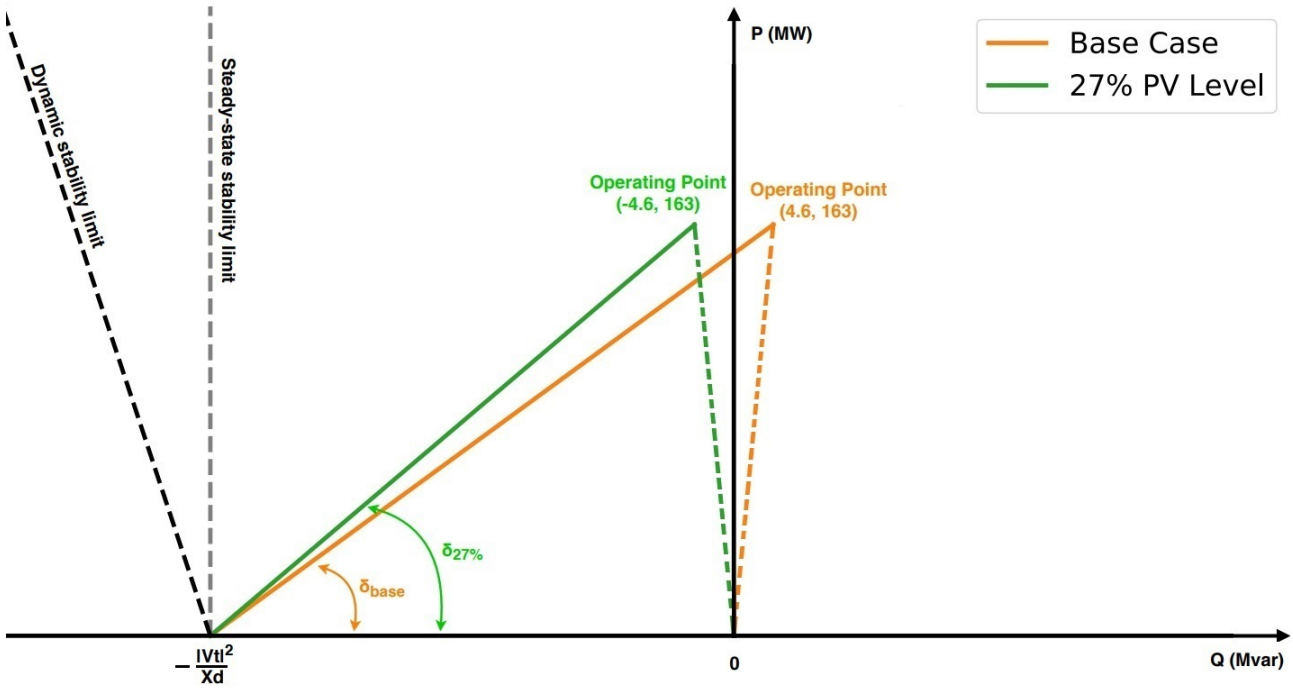
Figure 5.7: Rotor angle of generator 2 for base case and 27% PV level

In Figure 5.7, it can be seen that the steady-state operating point determines the steady-state rotor angle of the generator. Consequently, the transient stability margin is also partially determined by the steady-state operating point of the synchronous generator. It can be seen that the cases with 27% PV possess a slightly smaller steady-state stability margin compared to the base case. In other words, the distance to transient instability in terms of steady-state operating point of the synchronous generator is shorter for the cases with 27% PV.

To gain better insight into the behaviour of the synchronous generator and it's operating points, all *dynamic operating points*[3] are provided in Figure 5.8 and 5.9. The points have been obtained by running the simulation over a time span of 15 seconds so that the values reach their initial state after the fault.

---

[3]Dynamic operating points are defined as all operating points which the synchronous generator reaches during and after the disturbance
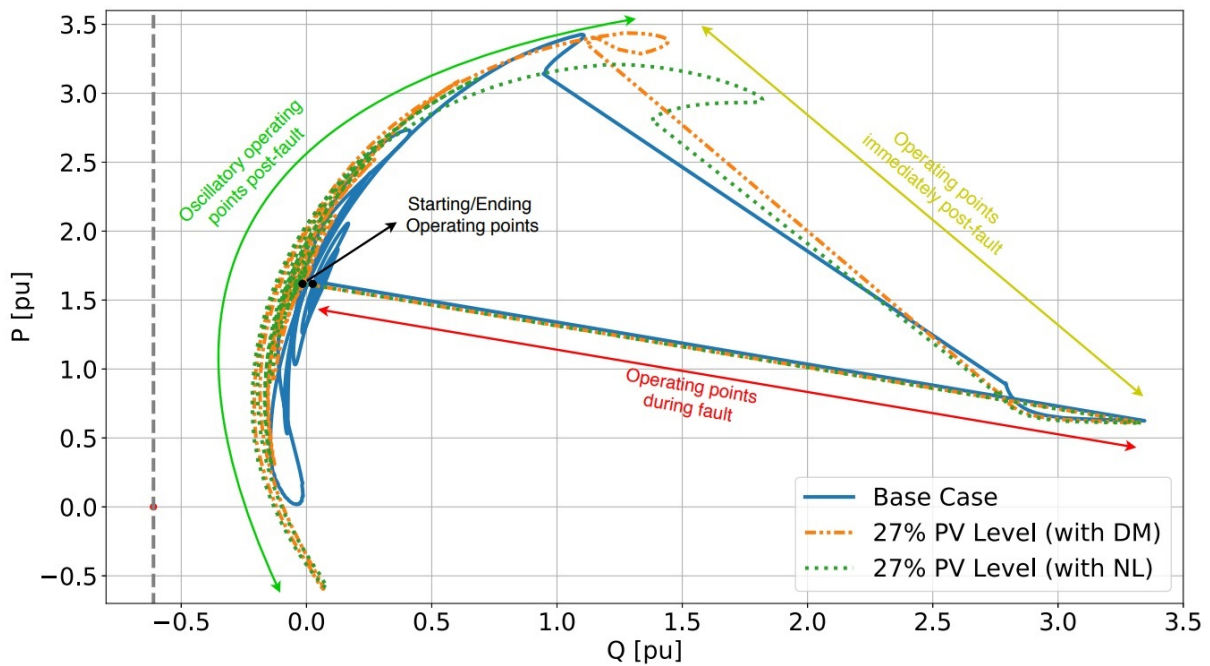
Figure 5.8: Operating points of synchronous generator 2 before, during and after fault
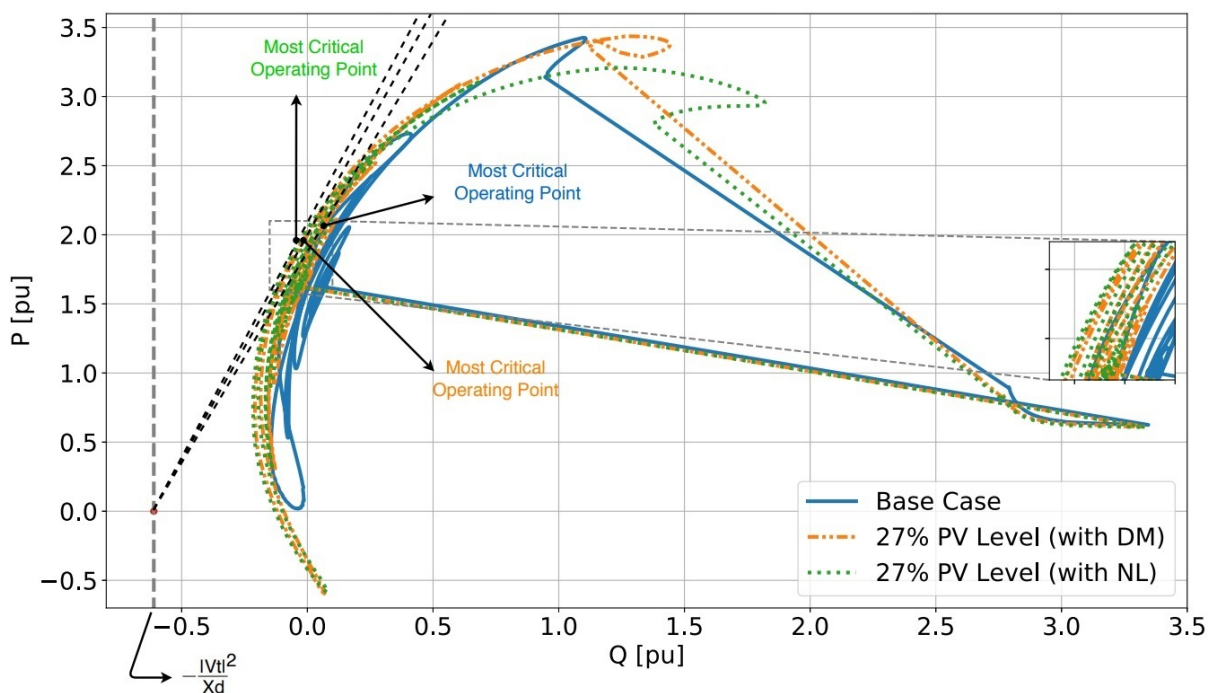
Figure 5.9: Operating points of synchronous generator 2

The operating point of synchronous generator 2 before the fault is the point (0.046, 1.63) for the base case and (-0.046, 1.63) for the cases with 27% PV. When the fault occurs the reactive power output of the generator significantly increases while the active power output gradually decreases — this response is denoted by the red line in Figure 5.8. The fault is then cleared at t=1.38s and reactive power output decreases while the active power output increases — the response immediately after the fault is shown by the yellow line in Figure 5.8. Lastly, generator 2 wants to return to it's initial operating point following the fault. The end operating point, which corresponds to the initial operating point, is achieved after oscillatory behaviour of the active and reactive power — the oscillatory response and corresponding

operating points are presented by the green line in Figure 5.8. Additionally, it is also seen that the synchronous machine goes into motor operation for a short duration for the cases with 27% PV.

In Figure 5.9, it is seen that the most critical point of the synchronous generator 2 for the base case is less critical compared to both 27% PV level cases. Therefore, due to the fact that the steady-state operating condition and dynamic operating conditions of the base case is lower compared to the cases with 27% PV, the transient stability margin of the base case is larger compared to the two other cases hence resulting in a higher critical clearing time for the base case.

Looking at the two cases with 27% PV, a slight difference is seen in the critical clearing time for these two cases. From Figure 5.9, it is seen that the case with negative load has an operating point at one point in time which has a slightly higher absorption of reactive power compared to the case with the dynamic model. This operating point causes the transient stability margin to decrease slightly, hence resulting in the smaller critical clearing time for the case with negative load compared to the case with the dynamic model. The synchronous generator reaches a more critical operating point due to the fact that the reactive power oscillations are higher at this particular generator which is caused by the reduced amount of total short-circuit current present during the fault. This phenomena shall be discussed later on in the analysis as it is more clearly seen in another case.

Base Case and 51% Level PV Penetration
As shown in Table 5.2, it is seen that the critical clearing time has increased for the cases with 51% PV. The extent to which the critical clearing time has increased has been magnified due to the small network and is due to the replacement of the most critical generator in the base case i.e. generator 2. Generator 2 is a critical generator in this network mainly due to the high loading (high operating point) of generator 2 compared to the other remaining generators and location of the fault. This results in a smaller transient stability margin of generator 2.

By replacing generator 2 in the network, the most critical generator in the case of a fault at bus 8 is essentially being removed from the network — this 'shifts' the critical clearing time to the following critical generator. The following critical generator in the network with a fault at bus 8 is generator 3 and has a larger transient stability margin hence causing the increased critical clearing time for this case.

Additionally, it is also seen that the 51% PV case with dynamic model and with negative load do differ notably in terms of critical clearing time compared to the same two cases for 27% PV. For the comparison between the case with dynamic model and the case with negative load all network conditions are similar aside from the fact that the PV system has a dynamic response for the case with dynamic model. In Figure 5.10, the operating points of the generator 3 are provided with a fault clearing time of 800 ms.
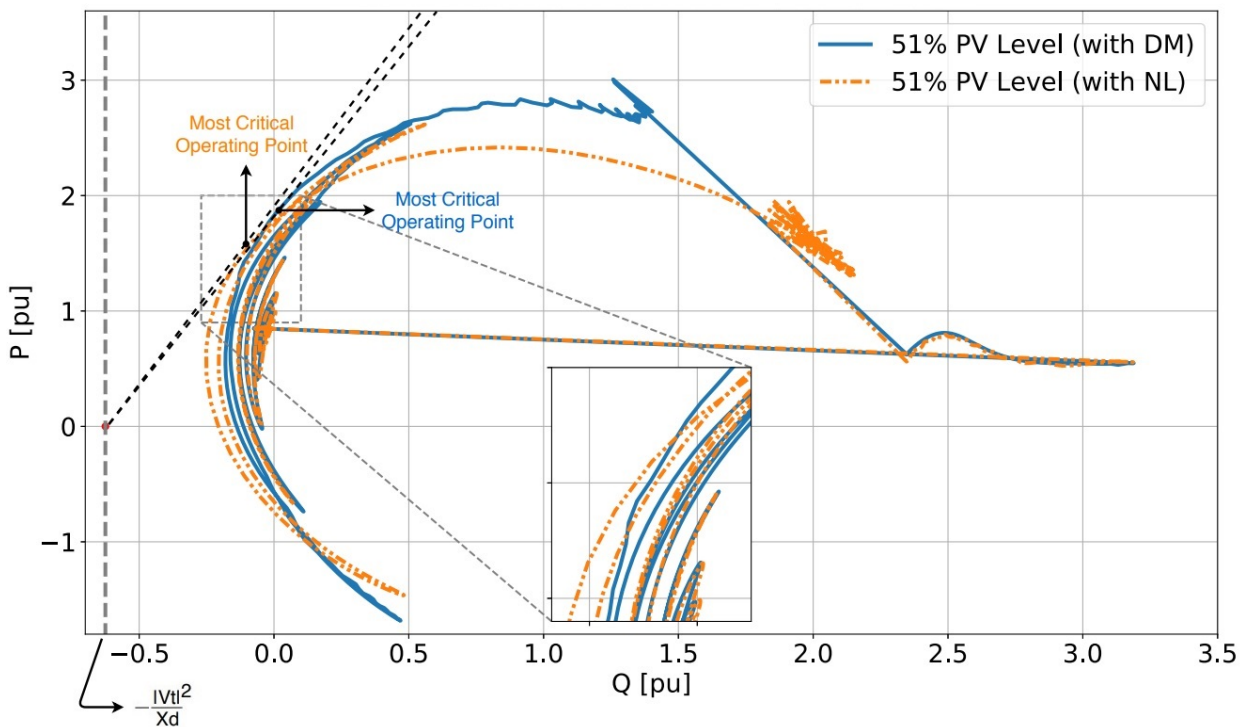
Figure 5.10: Operating points of synchronous generator 3

Looking at the operating points provided in Figure 5.10 (the sudden oscillatory behaviour right after the fault could be due to a mathematical error during the simulation), it can be seen that the 51% PV case with negative load obtains a dynamic operating point during the oscillatory behaviour after the fault which differs slightly from the dynamic model case. This part of the figure is zoomed in. This operating point causes the case with negative load to be more vulnerable to transient instability. In other words, transient instability shall occur earlier for the case with negative load due to a more critical operating point.

This can be further examined by looking at the reactive power output response of the synchronous generator 3 shown in Figure 5.11.
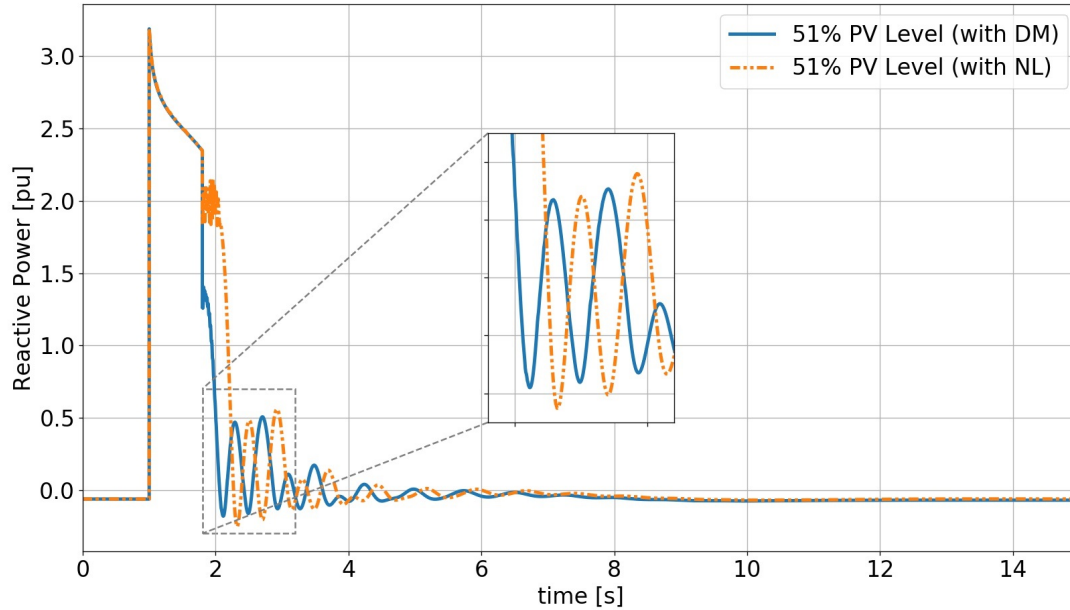
Figure 5.11: Reactive power output of synchronous generator 3

In Figure 5.11, it is seen that the reactive power output of synchronous generator 3 is quite oscillatory following the fault — which is also shown in Figure 5.10. This oscillatory behaviour is more pronounced in the case with negative load due to the *non-dynamic* negative load and hence the reduced amount of total short-circuit current present in the network. The oscillations of higher amplitude in the case with negative load causes the synchronous generator to reach an operating point which has a smaller stability margin compared to the case with the dynamic model — the difference in operating point is shown in Figure 5.10. Henceforth, it is seen that the reduction of total short-circuit current (as the only difference between the dynamic model case and negative load case is the additional injection of reactive current during the fault for the dynamic model case) in the network expresses itself in a more critical dynamic operating point of the synchronous generator hence leading to reduction of the critical clearing time.

Location of the fault near generators
In this section the fault has been introduced at a bus near the synchronous generator for the various cases. For the cases with 27% PV, the fault has been introduced at the bus 7. Similarly for the cases with 51% PV, the fault has been introduced at bus 9. The results are shown in Table 5.4.

CCT with fault at:	Bus 7 (ms)	Bus 8 (ms)	Bus 9 (ms)
Base Case	300	530	430
27% PV Case (with DM)	270	440	-
27% PV Case (with NL)	260	400	-
51% PV Case (with DM)	-	910	380
51% PV Case (with NL)	-	820	340

Table 5.4: Critical clearing time for faults at different buses

Looking at Table 5.4, it is shown that the critical clearing times are smallest for the faults that occur nearby generators i.e. bus 7 and 9. Additionally, it is shown that the critical clearing times are lower for cases with high PV penetration levels. Bus 9 shall be evaluated by comparing the base case and the case with 51% PV as this provides an interesting insight.

The behaviour of the synchronous generator 3 shall be looked at because the fault at bus 9 is closest to this generator. The initial operating point of generator 3 in both cases is provided in Table 5.5.

Case	Base Case		51% PV Level	
	P (MW)	Q (Mvar)	P (MW)	Q (Mvar)
G2	85	-9.1	85	-6.1

Table 5.5: Power flow results of generator 3

Figure 5.12 provides the rotor angle position of the synchronous generator for the base case and for the 51% PV case.
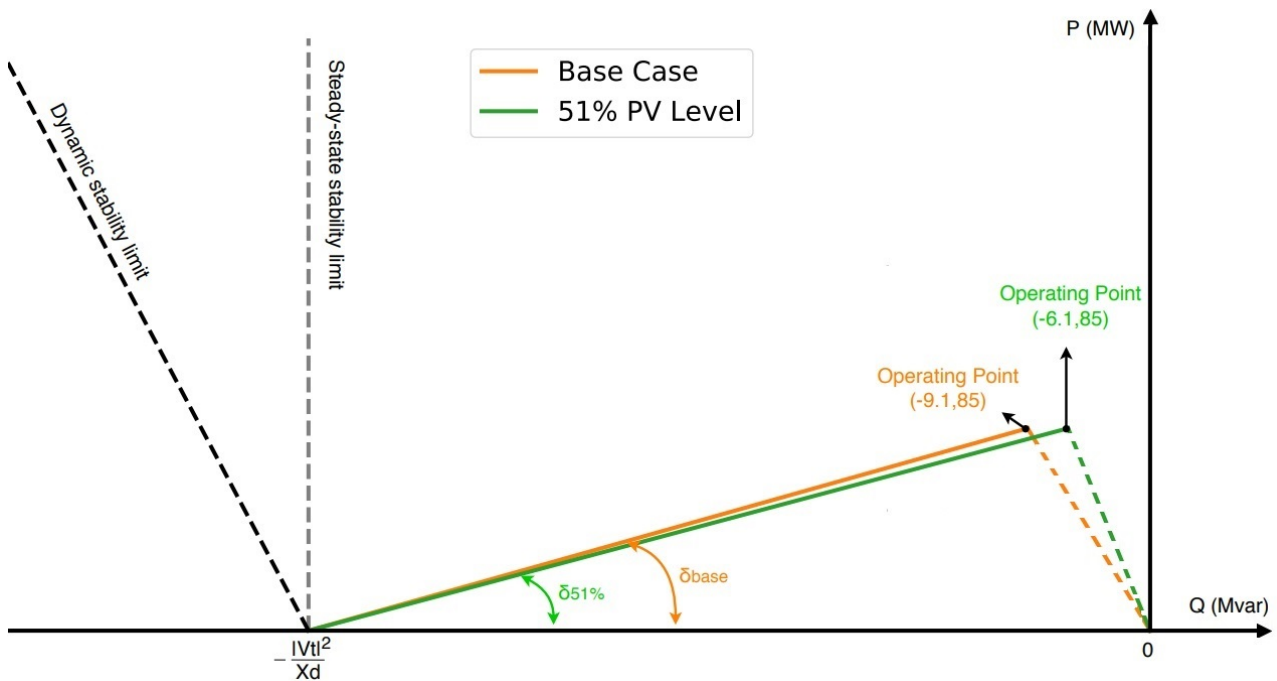
Figure 5.12: Rotor angle of generator 3 for base case and 51% PV level

In Figure 5.12, it is shown that the rotor angle of the base case is slightly higher compared to that of the case with 51% PV. In other words, the steady-state operating point shows that the steady-state transient stability margin of the base case is slightly smaller compared to the case with 51% PV but the critical clearing time of the former is still higher compared to the latter, which seems counter-intuitive.

Figure 5.13 provides the behaviour of the rotor angles of these cases when bus 9 is subjected to a three-phase fault with a fault clearing time of 370 ms.
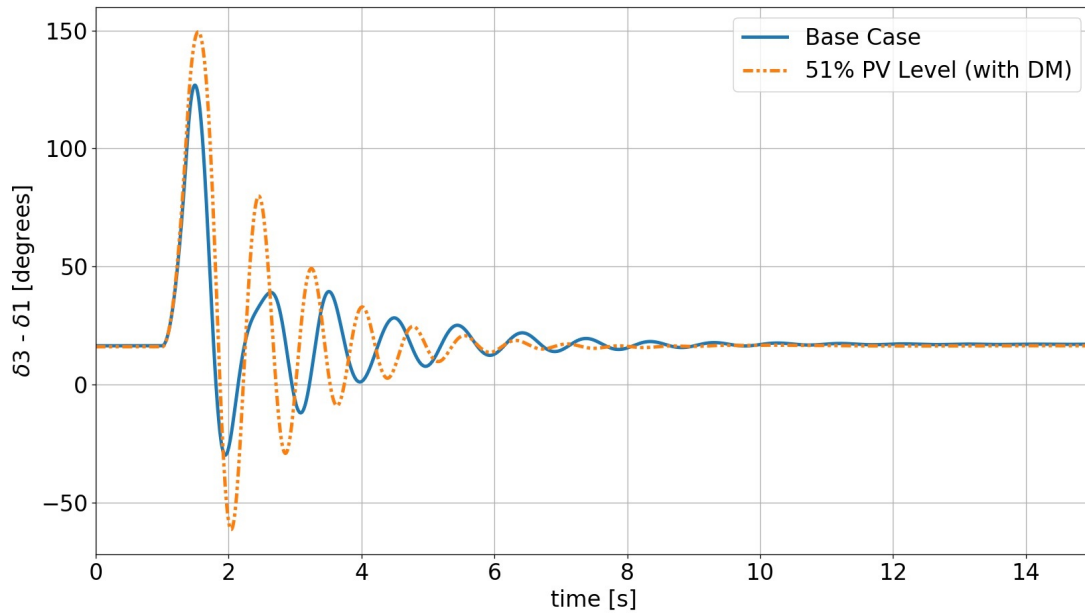
Figure 5.13: Relative rotor angle of generators with fault at bus 9 FCT=370ms

In Figure 5.13, it is shown that the rotor angle swings of the case with 51% PV are higher compared to the base case — this is consistent with the critical clearing times provided in Table 5.4. In Figure 5.14, the dynamic operating points of synchronous generator 3 are provided.
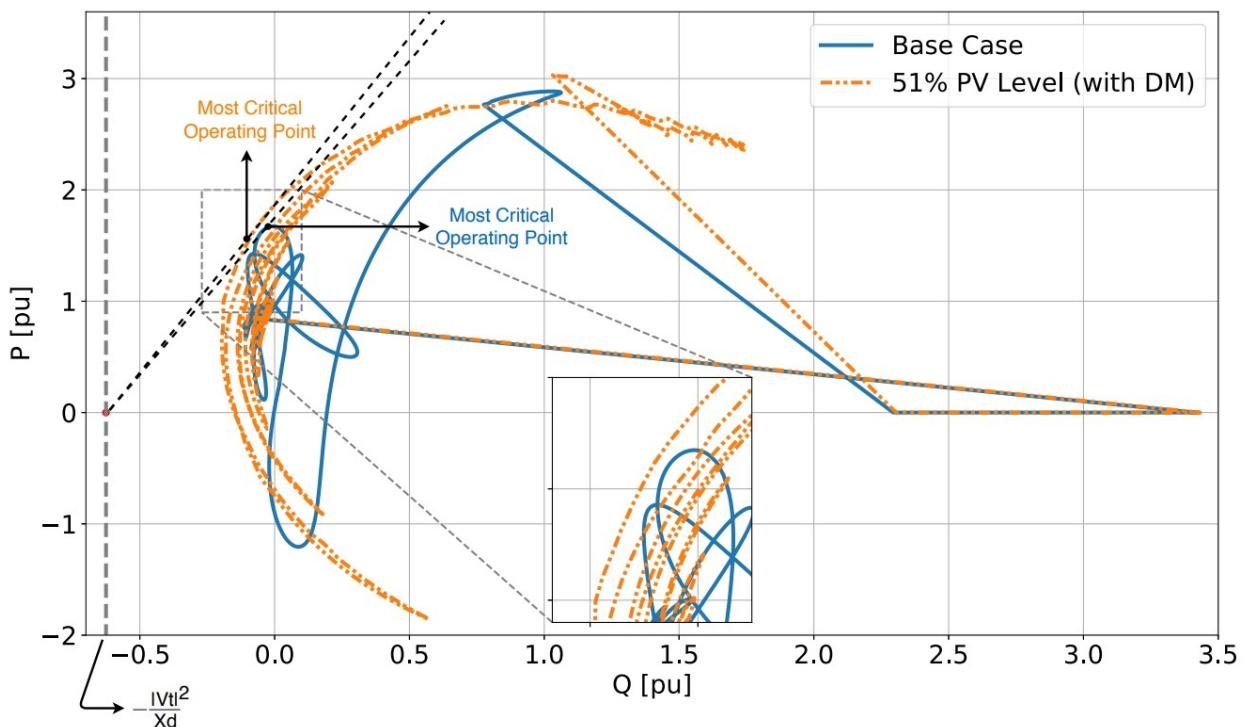
Figure 5.14: Operating points of synchronous generator 3 with fault at bus 9

In Figure 5.14, it is shown that despite the steady-state operating point shown in Figure 5.12, the dynamic operating points of the 51% PV case become more critical after the fault. As previously demonstrated, this is due to the fact that

the total short-circuit current in the network has reduced. This can also be viewed from the perspective of the reactive power of the synchronous generator 3 provided in Figure 5.15.
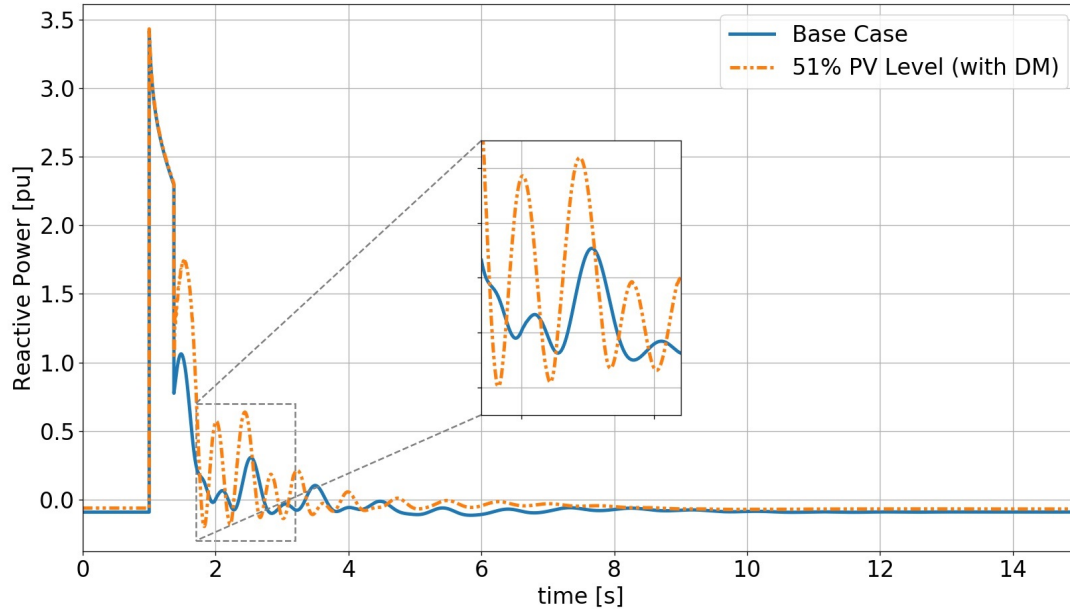
Figure 5.15: Reactive power output of synchronous generator 3 with fault at bus 9

In Figure 5.15, as also discussed in the comparison between the base case and the 51% PV case for a fault at bus 8, the oscillations of the reactive power output of the synchronous generator are of higher amplitude due to the reduced total short-circuit current in the network and hence causes the synchronous generator to operate at an operating point which is more critical and ultimately causing a lower transient stability margin for the 51% PV case.

Changing Inertia of generator 2 in Base Case
In this section the inertia of generator 2 has been increased in the base case to see how the inertia affects the transient stability. The differences are evaluated with an introduction of a fault at bus 8. The change of the inertia of generator 2 is shown in Table 5.6.

Generator 2	H (s)
Initial Inertia	3.33
Lower Inertia	1.33
Higher Inertia	8.33

Table 5.6: Inertia changes to generator 2

The rotor angle of synchronous generator 2 is shown in Figure 5.16 for varying values of the inertia. Additionally, the critical clearing time of the three cases is provided in Table 5.7.
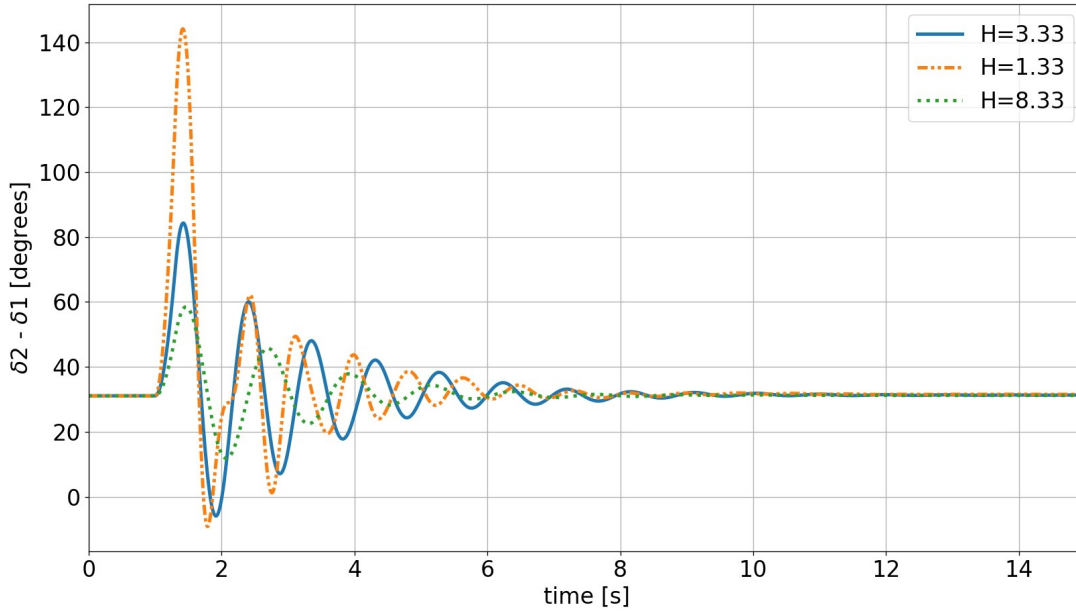
Figure 5.16: Relative rotor angle of generator 2 with different inertia FCT=300 ms

H (s)	CCT (ms)
3.33	530
1.33	320
8.33	970

Table 5.7: Critical clearing time with varying inertia of synchronous generator 2

The swing equation is provided in Equation 5.2.

$$\frac{d\delta^2}{dt^2} = \frac{P_m - P_e}{2H \cdot \omega_s} \tag{5.2}$$

The swing equation shown above, provides the relationship between the acceleration of the rotor angle and the inertia of the generator, synchronous speed and active power imbalance. The relationship states that the acceleration of the rotor angle is inversely proportional to the inertia of the synchronous generator. This is in consonance with the results provided in Figure 5.16 and Table 5.7 since it is shown that the lower the inertia of the generator, the higher the rotor angle swings and vice versa.

In the analysis it was demonstrated that the *critical clearing time* is dependent on several factors such as,

- The operating point of the synchronous generator before, during and after the fault. The operating point or also referred to as the *loading* of a synchronous generator determines the position of the rotor angle and hence yields information regarding the transient stability margin. In this analysis it was found that the transition from the base case to the case with 27% PV changed both the steady-state and dynamic operating points of the most critical generator in the network to a point where the transient stability margin decreased as shown in Figure 5.7. This could, however, be very different in larger networks, where initially PV systems are added to the network (rather than directly replacing synchronous generators). To this end, the loading of the existing synchronous generators could decrease and provide for an initial increase in transient stability as discussed in [15]. As synchronous generators are phased out, however, the loading of remaining synchronous generators could increase beyond the initial loading while the total short-circuit current decreases and hence leading to disadvantageous consequences for the transient stability.

- It was also evident from the analysis that the distinction in transient stability between the representation of PV systems with a dynamic PV model and negative load became more prominent as the capacity of PV systems in the network grew. The growth in difference between the case with dynamic model and the case with negative load is due to the difference between total short-circuit current injection into the network. It was shown that for the negative load representation, the decrease in total short-circuit current was expressed in terms of higher oscillations in the reactive power output hence leading to more critical dynamic operating points of the synchronous generator. This only serves as additional proof that PV systems (and all power electronic interfaced generation units for that matter) should be modelled with dynamic models to increase the accuracy of stability studies.

- Replacement of the most critical generator for a specific fault. In the comparison of the base case and the case with 51% PV, a significant increase in transient stability of the network was seen for a similar fault. In the case with 51% PV, the most critical generator in the network (for a specific fault at bus 8) was replaced by a PV system and hence improving the transient stability of the network for that specific fault.

- The severity of the fault. The severity of the fault is mainly determined by two factors i.e. the type of fault and the location of the fault. In this research project only three-phase faults are considered, hence the severity of the fault is only influenced by the point at which the disturbance occurs. Logically, it has been shown that the network is most susceptible to transient instability when a fault occurs near a synchronous generator as shown in Table 5.4. Moreover, the analysis showed that with higher PV penetration levels the transient stability decreases when a disturbance is introduced near a synchronous generator. This decrease in transient stability is due to a lower amount of short-circuit current during the fault hence causing higher oscillations in reactive power of synchronous generators and thus ultimately leading to more critical operating points hence decreasing the transient stability.

- The inertia of the synchronous generator. The higher the inertia of the synchronous generator, the more transiently stable the generator is as the rotor angle changes at a slower rate i.e. the higher the critical clearing time. This relationship is defined by the swing equation provided in Equation 5.2.

The factors influencing transient stability in this study are discussed above, however, there are several other factors that play a role in the transient stability which have not been discussed in this analysis such as the internal reactance of the generator and the transmission circuit reactance [13].

5.3. Short-term Voltage Stability

To evaluate the short-term voltage stability of the various networks of the IEEE 9 bus network shown in Figure 5.1 and 5.2, a three-phase bolted fault is introduced at bus 8 at t=1s for 6 cycles amounting to a time of 120 ms and thus the clearance of the fault occurs at t=1.12s. The response of the voltage at bus 8 in the various networks is provided in Figure 5.17.
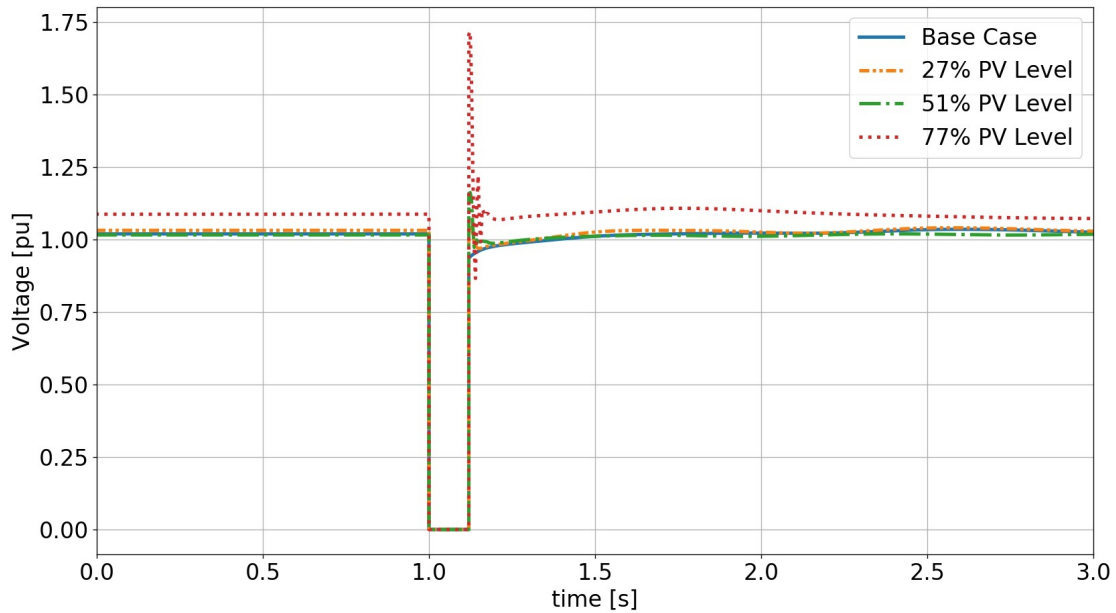
Figure 5.17: Voltage at bus 8 in IEEE 9 bus network

In Figure 5.17, it can be seen that the voltage at bus 8 goes to zero at the time of the fault since a bolted fault is introduced. The distinction in initial voltage between cases is due to the changes being made in the network e.g. addition of LV/MV transformer and collector system equivalent for cases with PV systems and the fact that the reactive power output of the PV systems has been set to zero while the replaced synchronous generator had a non-zero reactive power output leading to power flow changes in the network. The initial voltage of the 77% PV case has the biggest difference as the most changes are made for this network compared to the other cases. After clearance of the fault the voltage recovers. However, it is notable to highlight that there is quite a high voltage spike for the case with 77% PV. This voltage spike is also seen for the 27% PV and 51% PV case albeit less pronounced. This can be explained by looking into the behaviour of a PV system in the network. To explain this behaviour, the PV system at bus 11 for the 77% PV case shall be looked at. The behaviour of this PV system is shown in Figure 5.18.
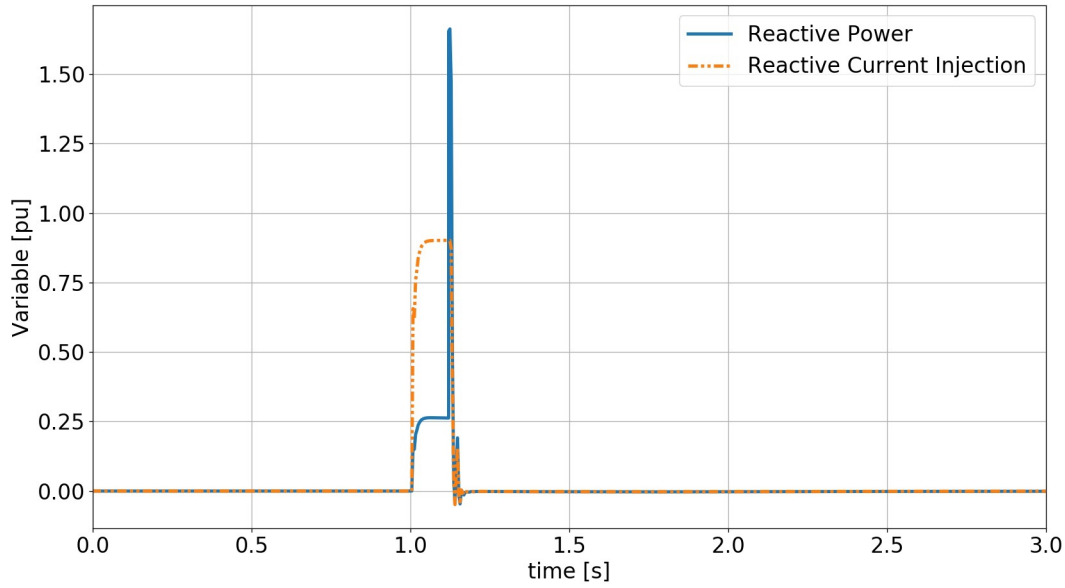
(a) Reactive power and Reactive current injection
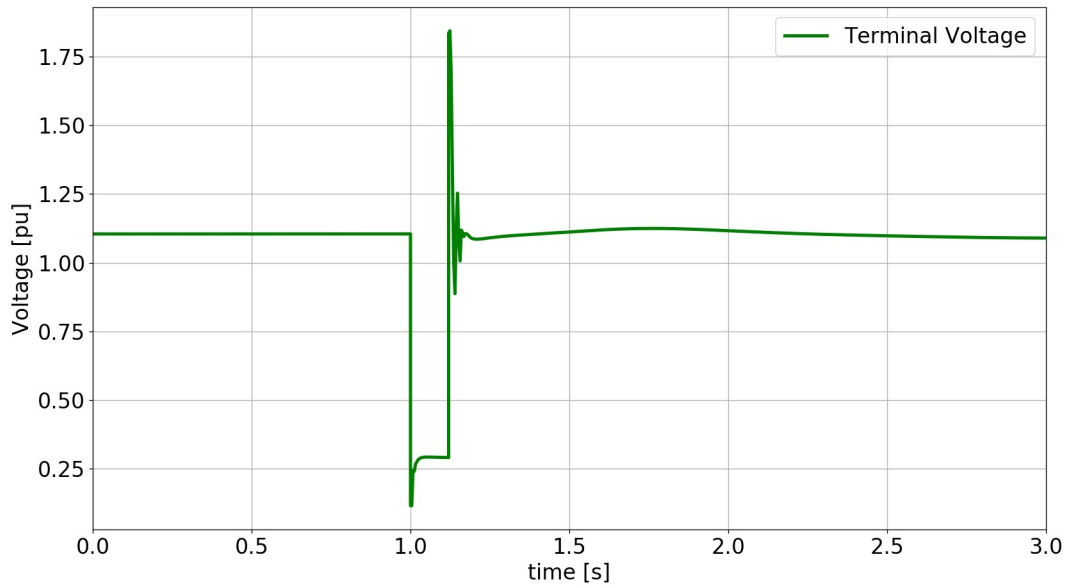
(b) Terminal Voltage

Figure 5.18: PV system at bus 11 for 77% PV level case

In Figure 5.18, the response of the PV system at bus 11 for the 77% PV case is shown when a fault is introduced at bus 8 from t=1s to t=1.12s. Firstly, it is important to highlight that the terminal voltage, reactive power output of the PV system and the reactive current injection have the relationship as shown in Equation 5.3.

$$Q(t) = V_t(t) \times I_q(t) \tag{5.3}$$

Looking at the terminal voltage of the PV system, it is shown that at t=1s the voltage decreases due to the fault. Shortly thereafter, the reactive current is injected by the PV system to contribute to the fault current injection. Consequently, the reactive power output of the PV system also increases with the relationship provided in Equation 5.3. At t=1.12s, the fault is cleared and the voltage increases with a sharp spike for a short-duration of time. This can be explained by

the fact that at the time of clearance the reactive current injection is still taking place and thus causes both the high voltage spike and reactive power output spike at the time of the clearance of the fault. This short-duration voltage spike is not representative of real PV systems and is present due to a shortcoming of the PV system model. To quote the WECC Solar Plant Dynamic Modeling Guidelines [28] regarding this shortcoming,

It should be noted that generic dynamic models for inverter-based generator tend to produce a short-duration (a cycle or shorter) voltage spike at fault inception or clearing. These spikes should be ignored in most cases, as they do not represent the performance of actual hardware. They are simply a consequence of the model's limited bandwidth, integration time step, and the way current injection models interface with the network solution.

To this end, the voltage spikes present after the clearance of the fault shall be ignored for the analysis.

To analyse the behaviour of the voltage at the different buses, the voltage drop at each bus is quantified by the following equation,

$$\% \text{ Voltage drop at bus} = \frac{\text{Initial voltage - Voltage (t=1.12s right before clearance)}}{\text{Initial voltage}} \times 100\% \tag{5.4}$$

The results at the various buses using Equation 5.4 are shown in Table 5.8.

	Bus 4	Bus 5	Bus 6	Bus 7	Bus 8	Bus 9
Base Case	30.59%	42.92%	43.49%	62.31%	100%	65.44%
27% PV Level	35.63%	46.89%	53.43%	63.64%	100%	84.00%
51% PV Level	33.77%	48.84%	45.83%	75.91%	100%	65.89%
77% PV Level	40.89%	54.89%	57.66%	78.54%	100%	85.46%

Table 5.8: Voltage drop percentages for fault at bus 8

Since a bolted three-phase fault occurs at bus 8, it is logically seen that the voltage drop in all cases at bus 8 is equivalent to 100%. In Table 5.8, it can be seen that for most of the cases the voltage drop increases when going from the base case to the 77% PV case, with some exceptions when going from 27% PV to the 51% PV case. It should also be noted that for the network with 51% PV, the total amount of short-circuit current injected is higher compared to the 27% PV case due to the fact that the PV system added is of higher capacity in the 51% PV case. The total reactive current injected by all generation units for the various cases is shown in Figure 5.19.
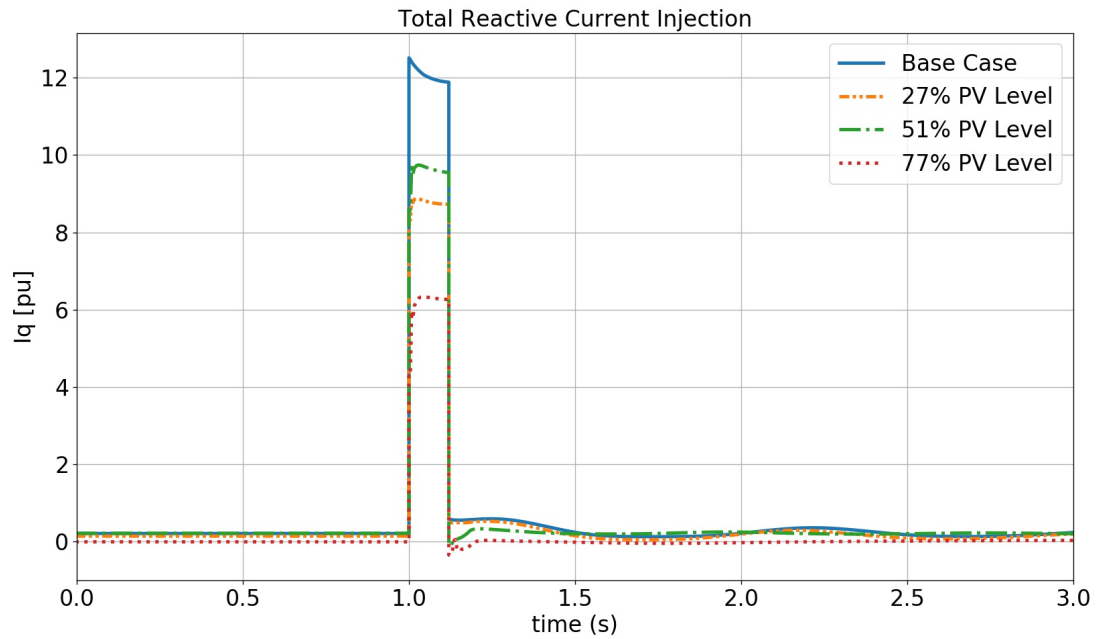
Figure 5.19: Total reactive current injection for all cases

Bus 4 and bus 6

The voltages at bus 4 and bus 6 are shown in Figure 5.20.

(a) Bus 4

(b) Bus 6
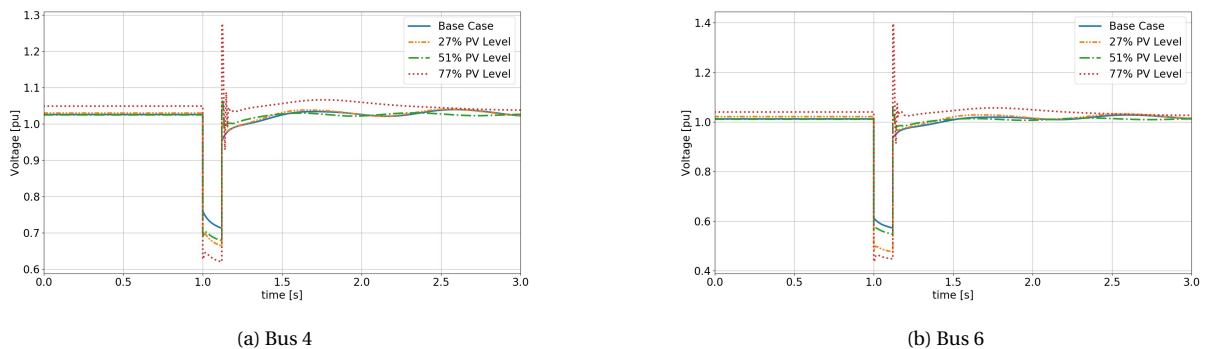
Figure 5.20: Voltage at bus 4 and bus 6

For bus 4 and bus 6, similar behaviour is seen, mainly that the voltage drops at these buses increase except when going from 27% PV to 51% PV case. This is due to the fact that the amount of short-circuit current injected for the 51% PV case is higher compared to the 27% PV case as shown in Figure 5.19 and hence influences the voltage drops witnessed at nearby buses.

Bus 5

The voltage at bus 5 is provided in Figure 5.21.
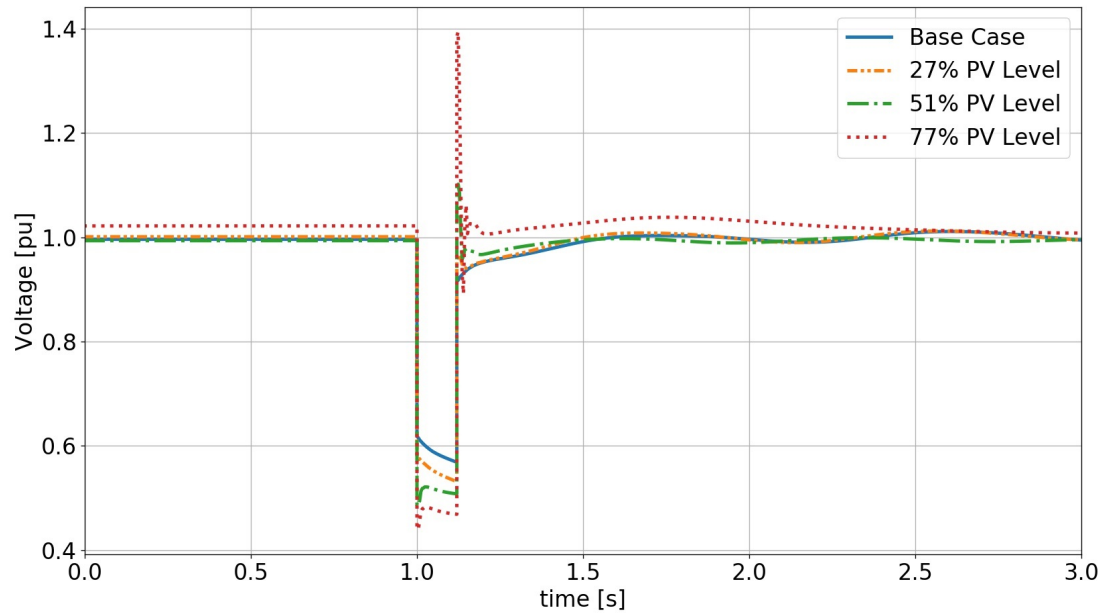
Figure 5.21: Voltage at bus 5

At bus 5, it can be seen that the voltage drop increases as the PV penetration in the network increases. Even though, a higher amount of short-circuit injection is present for the case with 51% PV compared to the case with 27% PV, an increase in voltage drop is still seen. This increase in voltage drop is due to the change in the network when going from 27% PV to the 51% PV case, as the synchronous generator 2 is being replaced by a PV system during this transition hence leading to a higher voltage drop at bus 5 for the 51% PV case.

Bus 7 and bus 9
The voltages at bus 7 and bus 9 are shown in Figure 5.22.

(a) Bus 7

(b) Bus 9
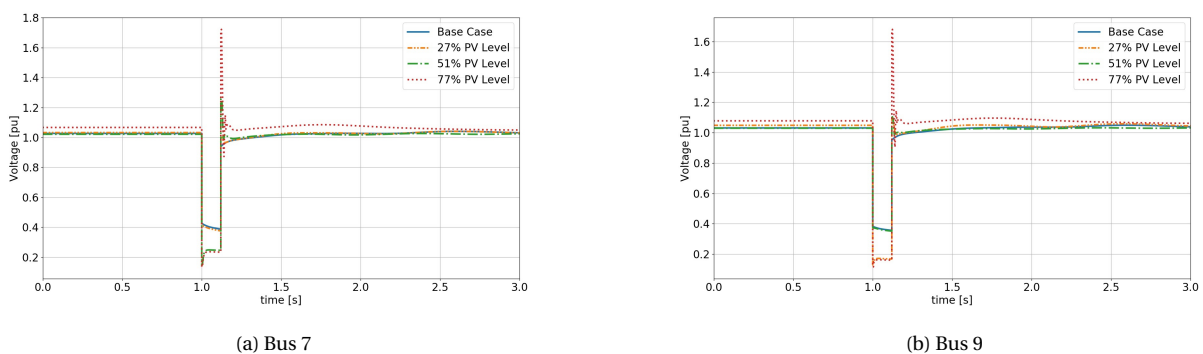
Figure 5.22: Voltage at bus 7 and bus 9

It is of interest to evaluate bus 9, here it is seen that the voltage drop initially increases from the base case to the 27% PV case. Following this increase, the voltage drop then decreases from the 27% PV case to the 51% PV case. Lastly, the voltage drop at bus 9 increases again to the highest value at this bus. When going from the base case to the 27% PV case, the generator 3 at bus 9 is replaced by a PV system. Due to the reduced reactive current injection at this bus the voltage drop significantly increases. When going from 27% PV case to the 51% PV case, the synchronous generator 3 is placed back in the network, and hence provides more reactive current injection at this particular bus thus the voltage drop decreases. And lastly, for the 77% PV case the generator 3 is once again replaced by the PV system. Similar explanation for bus 7 holds true, however, the replacement of synchronous generator 2 to a PV system occurs when going from

27% PV case to 51% PV case at that bus. At bus 7 and bus 9, it is seen that the voltage drop is highly dependent on the nearby generation unit. In the cases of a synchronous generator at bus 9 (base case and 51% PV case), the voltage drop is less compared to the cases where this generator is replaced by a PV system (27% PV and 77% PV case) as the reactive current injection from these units is significantly less. The reactive current injection from either synchronous generator 3 at bus 3 or PV system 11 at bus 11 is shown in Figure 5.23.
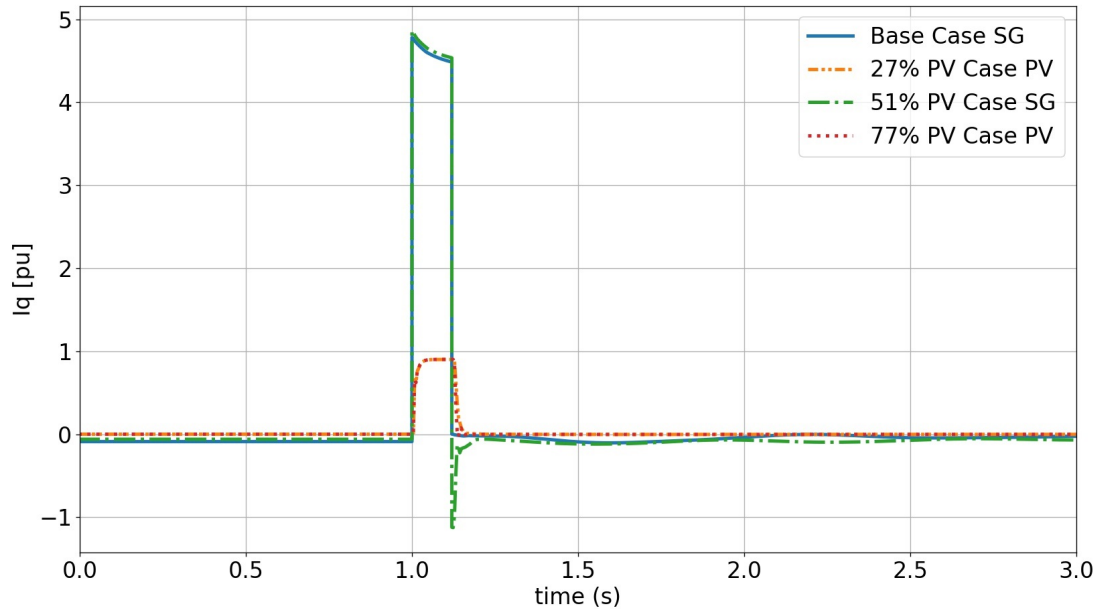
Figure 5.23: Reactive current injection SG bus 3 or PV bus 11

As explained above, when the synchronous generator is connected near bus 9, the reactive current injection is significantly larger compared to the cases when the PV system replaces the synchronous generator 3. Therefore, for the cases with the synchronous generator 3 near bus 9 the voltage drop isn't as significant compared to the cases with the PV system connected.

Comparing the buses near a generation unit i.e. bus 7 and bus 9, the voltage dip has increased most significantly at bus 9 for the cases where the generation unit nearby the bus is a PV system (for bus 7 this is represented by the transition from 27% PV case to the 51% PV case, while for bus 9 this is represented when going from the 51% PV case to the 27% PV case). This can be explained by evaluating the amount of reactive current injection of the PV system during the fault near the respective buses. The comparison between reactive current injection of the two PV systems added are shown in Figure 5.24.
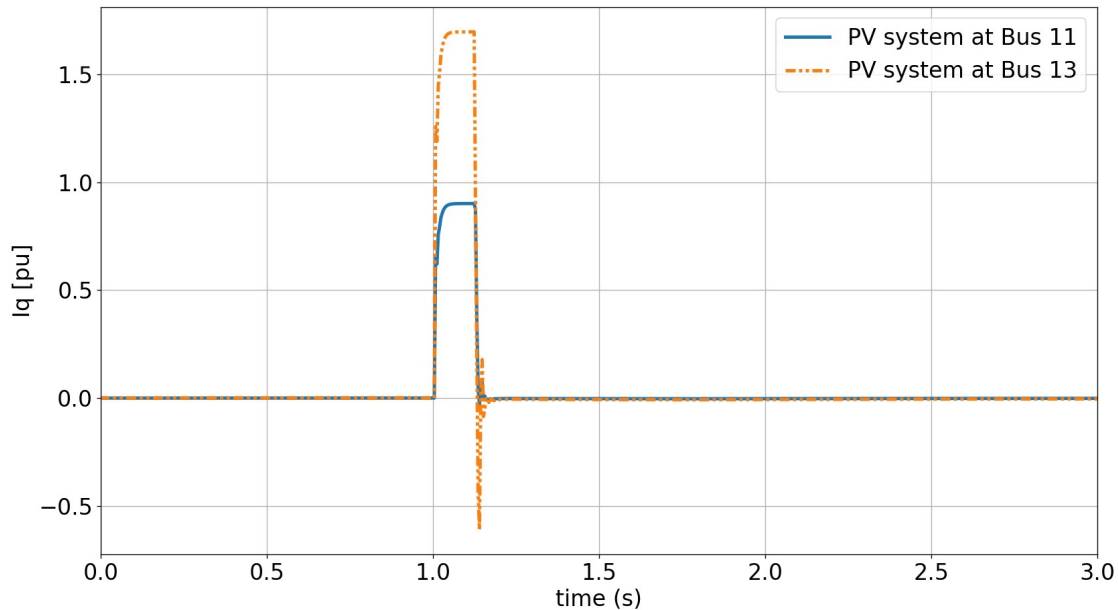
Figure 5.24: Reactive current injection PV systems

As shown in Figure 5.24, the amount of reactive current injection of the PV system at bus 11 is significantly less compared to the PV system at bus 13, since the capacity of this PV system is also less. Accordingly, the voltage drop at bus 9 is most significant for the cases where the PV system replaces a synchronous generator near the bus of interest. Additionally, the fact that bus 9 is located electrically closer to bus 8 compared to bus 7, only magnifies the voltage drop seen as the electrical distance to the fault also plays a vital role in the voltage drop witnessed.

Increase in overall voltage dips
When looking at the extent of the voltage drops at the various buses when a fault is introduced at bus 8, the voltage drops occur more severely at higher penetration levels of PV systems. Compared to the base case, the voltage drops are more severe in every other case. This stems from the fact that the total amount of short-circuit current during the fault has decreased due to the replacement of synchronous generators. As discussed for bus 9, certain instances proved that the increase of PV penetration level from 27% PV case to the 51% PV case did not always result in more severe voltage drops at certain buses. Lastly, when looking at the 77% PV level case, the worst voltage drops compared to all other cases were seen. Again, this as a result of replacing the two synchronous generators with PV systems and consequently decreasing the total amount of reactive current injection during the fault.

After the analysis provided above, there are a few key takeaways. These are given below,

- It was shown that from the base case to increased PV penetration levels, the voltage drops at all buses saw an increase. This increase is present as a result of the decreased reactive current injection during the fault as PV systems provide significantly less short-circuit current during a fault compared to synchronous generators. Additionally, it was shown that the increase of 27% PV case to the 51% PV case did not always result in an increase in voltage drop. For these cases the response of the voltage drop was dependent on the bus of interest, the impedance from the bus of interest to surrounding generation units and also changes brought upon the type of generation units.

- The voltage drop at a bus close to a generation unit is highly dependent on the type of generation unit. It was shown in the analysis that when the generation unit closely connected to the bus is a PV system, the voltage drop at the bus increases compared to when a synchronous generator is connected close to the bus of interest. This is due to the fact that synchronous generator can inject significantly more reactive current during the fault compared to PV systems. The difference in voltage drop only holds true if the bolted three-phase fault does not occur at this particular bus otherwise the voltage drop would be equal to 100%.

- When looking at the voltage drop at a bus closely near a generation unit. If this generation unit remains of the

same type, minor increase in voltage drop at this bus is seen as the PV penetration level in the network increases. This is due to the fact that the overall fault current contribution in the network is less.

6

TenneT Network Case Study

This chapter starts off with an introduction of the Investment Plan of 2020 and shortly discusses the three different scenarios devised in this plan. Ensuingly, the selection of the scenario which will be examined is argued, followed by a discussion of the selected hours which are related to the total demand and the dispatch of the generation units. Hereafter, a brief overview of the current dynamic grid model is provided and the approach taken to model the PV systems is discussed. Lastly, the analysis with respect to transient- and short-term voltage stability will be examined for the relevant areas and mitigation measures are provided accordingly.

6.1. Investment Plan of 2020

The Investment Plan of 2020 (IP2020) is developed by TenneT TSO B.V. in collaboration with Gasunie, and maps out potential realistic scenarios for the future of the TenneT grid and the state of electrical landscape in the Netherlands. The different scenarios are described in detail in various different domains such as growth of renewable energy sources, advancements in alternative energy sources such as hydrogen, growth of alternative methods for powering transportation and methods of heating and electrical storage [38]. However, since the interest of this research primary lies in the dynamic behaviour under high penetration of solar PV systems, the main focus shall be on the growth of renewable energy sources. In the Investment Plan of 2020, three scenarios are developed with the reference year 2030.

The three scenarios with reference year 2030 discussed in the IP2020 are [38],

1. Climate Agreement Scenario
2. Alternative Transition Scenario
3. Foundation for System Integration Scenario

The *Climate Agreement Scenario* (CA Scenario) is a scenario developed based on the climate agreement of the Netherlands. The climate agreement of the Netherlands comprises of the goal to reduce CO_2 emissions from 1990 by a minimum of 49% by 2030 [6]. This scenario has been created to meet that goal by taking measures such as reducing synchronous generation units and by expanding the capacity of solar PV- and wind systems [38].

The *Alternative Transition Scenario* (AT Scenario) forecasts a technological breakthrough with regards to production of green gas, which is produced by biomass. Due to the massive technological advancement in the production of green gas, solar PV- and wind systems do not possess such a strong growth as compared to the *Climate Agreement Scenario* seeing that an alternative energy source is used to predominantly reduce the CO_2 emissions [38].

The *Foundation for System Integration Scenario* (FSI Scenario) sees a larger and faster growth in solar PV- and wind systems. This leads to the need to integrate the infrastructure for gas, heating and electricity. Due to the prominent role of renewable energy sources in this scenario, the solar PV systems have the most capacity for this scenario [38].

The installed capacity of solar PV systems in the scenarios discussed above is shown in Table 6.1.

	Solar PV (GW)
Climate Agreement Scenario	25.0
Alternative Transition Scenario	14.3
Foundation for System Integration Scenario	44.3

Table 6.1: Solar PV production IP2020 Scenarios

As shown above in Table 6.1, and as previously highlighted, the *Foundation for System Integration Scenario* possesses the highest amount of installed PV capacity out of the three scenarios. Accordingly, this scenario will be exclusively examined since high penetration levels of PV are existent in this scenario. Additionally, the power dispatch of generation units can be varied to obtain varying levels of PV penetration as defined by Equation 5.1.

6.2. Selection of Hours

For all the scenarios discussed in Section 6.1, including the *Foundation for System Integration Scenario*, each scenario contains 8736 hours, the equivalent of a year, with each hour possessing a total production value, total demand value and information regarding the specific dispatch of generation units. To take into account the intermittency of solar irradiation and wind speeds, a climate year is also taken into account in the algorithm for the dispatch of generation units. The climate year yields information regarding the solar irradiation and wind speeds at each hour. The climate year of 2011 is used for dispatching of generation units in this scenario.

The load profile of the *Foundation for System Integration Scenario* for the all the 8736 hours, the whole year, is provided in Figure 6.1.
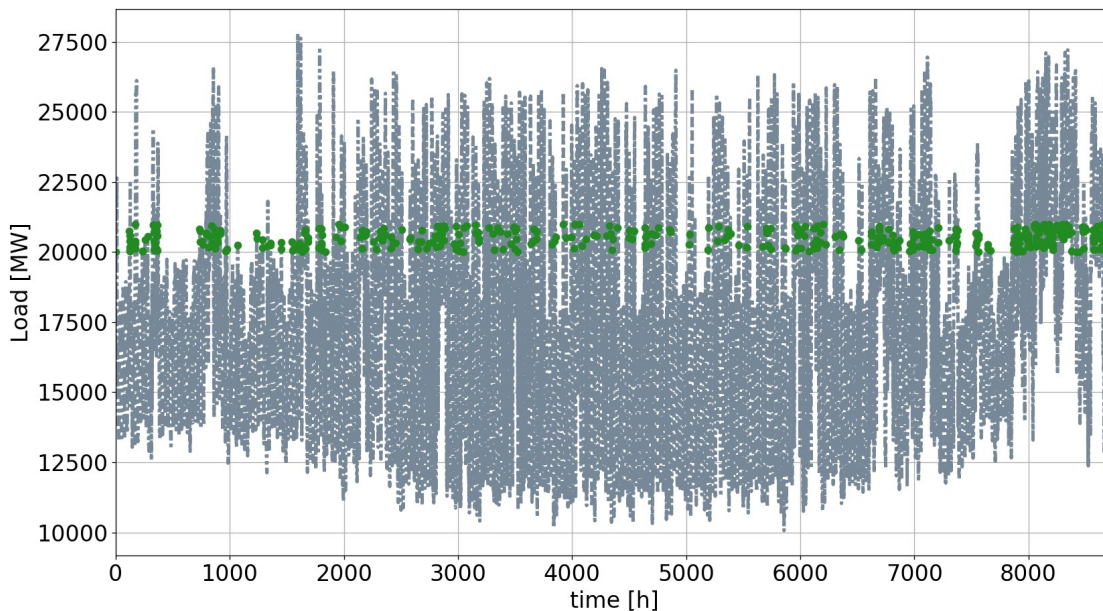
Figure 6.1: Load profile of Foundation for System Integration Scenario

As shown in Figure 6.1, the load varies over the time span of a year and is different for each hour. The green dots in the graph are the hours in which the load is in the range of 20000 to 21000 MW. This will be elaborated later on.

The profile of the generation for all the hours of the *Foundation for System Integration Scenario* is shown in Figure 6.2.

(a) Onshore Wind generation

(b) Offshore Wind generation

(c) Solar PV generation

(d) Synchronous Generators generation
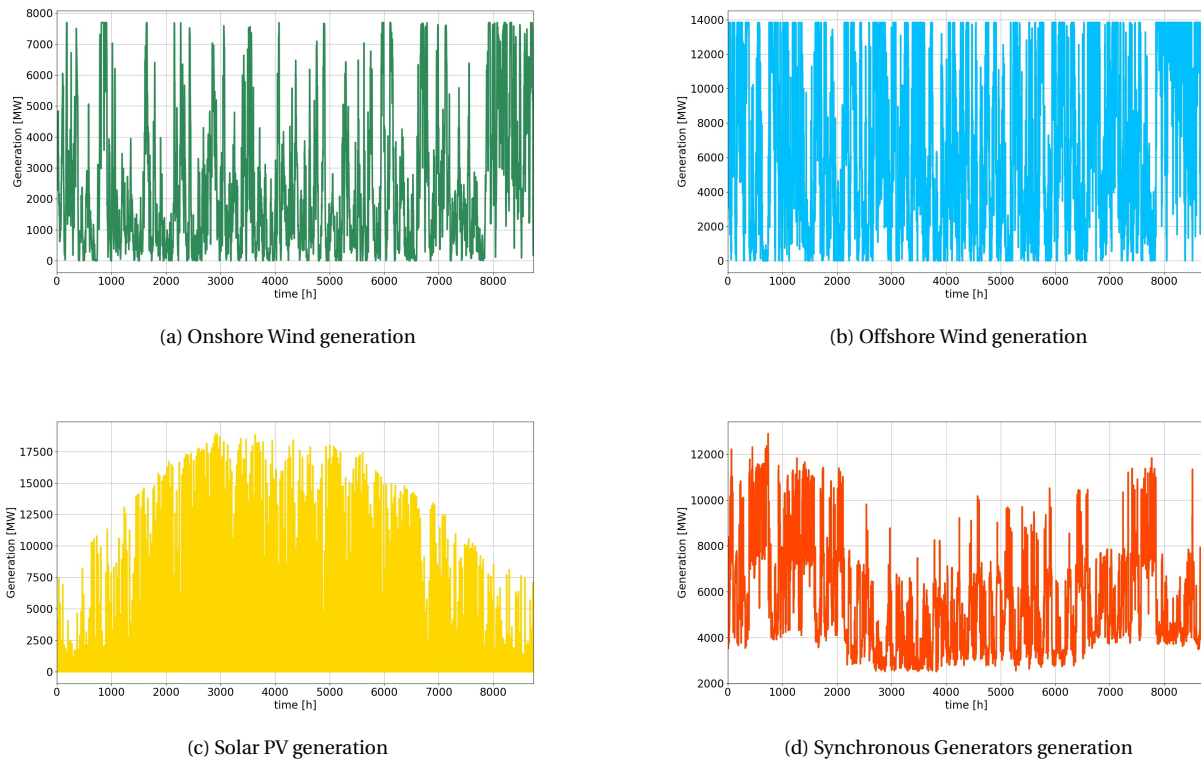
Figure 6.2: Generation profiles of Foundation for System Integration Scenario

In Figure 6.2, the behaviour of the different generation units over the time span of a year are provided for the *Foundation for System Integration Scenario*. From the provided data, the selection of hours are limited to four specific hours with the following criteria,

1. Selection of an arbitrary hour with all synchronous generator (SG) units put in-service

2. Selection of an hour with low PV dispatch and high SG dispatch

3. Selection of an hour with average PV dispatch and average SG dispatch

4. Selection of an hour with high solar PV dispatch and low SG dispatch

To evaluate the results for a comparable amount of load in the network, the latter three cases are set within a specific range of total load. Figure 6.3 provides the approach taken for the selected hours and Table 6.2 provides detailed information about the selected hours.
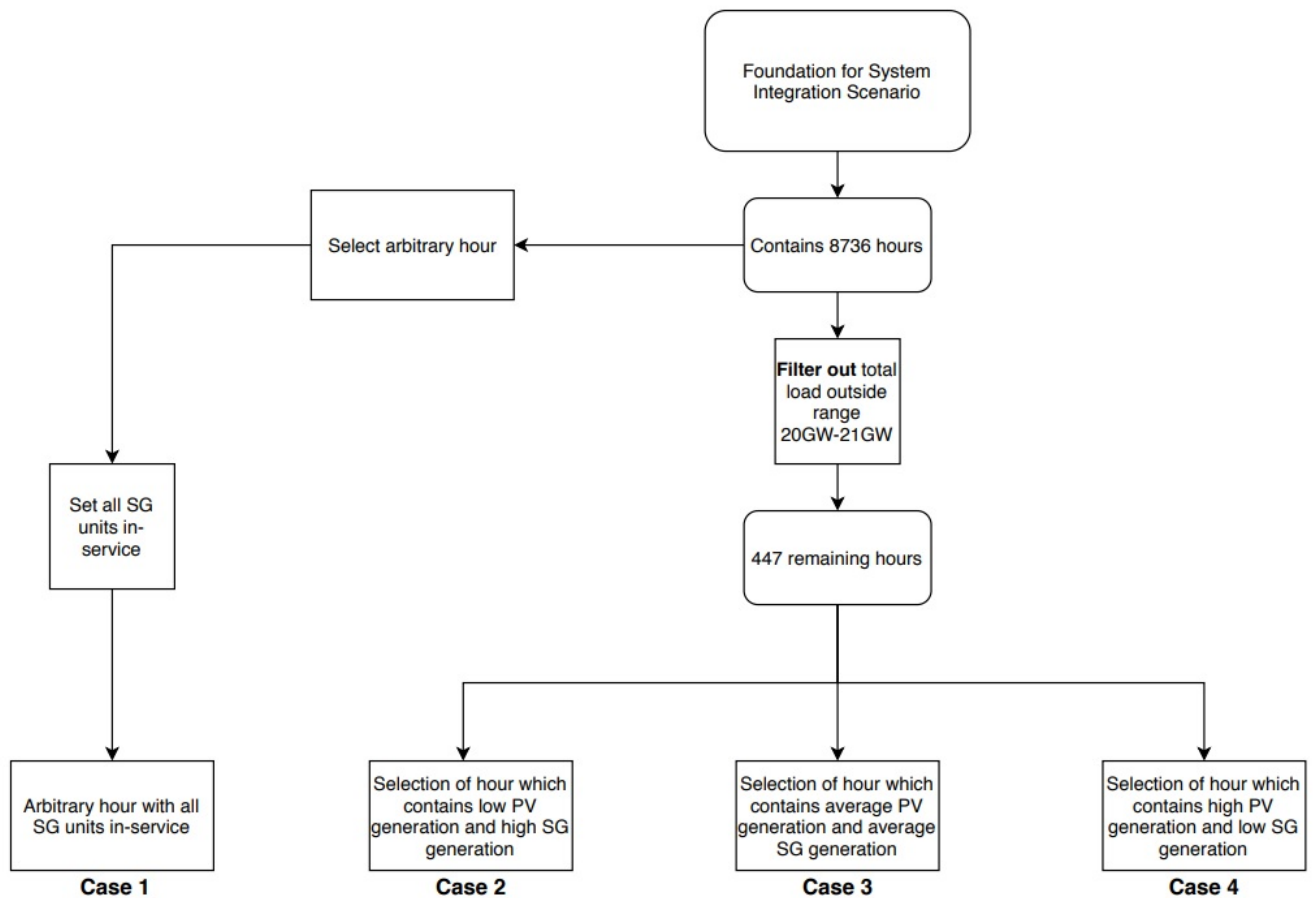
Figure 6.3: Method for the selection of hours

Case	Hour	PV production (GW)	Wind production (GW)	SG production (GW)	Total production (GW)	Total demand (GW)
1	420	2.34	2.48	8.32	15.19	18.04
2	1289	0.58	11.44	7.91	20.71	20.43
3	5389	6.98	9.31	5.62	21.76	20.64
4	2726	13.43	2.74	3.34	19.51	20.13

Table 6.2: Selected hours of Foundation for System Integration Scenario

In Figure 6.3, the method to derive the selection of the hours is provided. The Foundation for System Integration scenario contains, as previously stated, 8736 hours with varying total demand and generator dispatch values. In Table 6.2 the distribution between different generation units are provided — it must be stated that the provided generation units are not all units present in the network hence the summation of PV, wind and SG does not equal the total production. However, the remaining generation units are modelled as negative load and hence will not impact the dynamic behaviour. For the first hour an arbitrary hour is chosen in which all SG units in the Netherlands are put in-service. For the latter three cases the first step was to filter out all total load values outside of the range between 20 GW and 21 GW. This range has been selected since it is above the average total load value of 17.4 GW but on the other hand not too close to the extremum cases. After filtering out the values outside this range, 447 hours are left, which are denoted by the green dots in Figure 6.1. From the remaining hours, the selection of the cases has been done as described below.

Case 1 The selection of an hour for case 1 has been made arbitrarily. Additionally, all synchronous generation units present in the Netherlands have been put in-service for this case. This modification has been made to obtain the highest amount of total short-circuit current during contingencies.

Case 2 The requirements for case 2 is the selection of an hour which has a low solar PV production and a high synchronous generation production. To determine the selection, the average of both the solar PV production (excluding the hours with zero PV production) and the synchronous generation production for the hours in the specified range has been calculated. Thereafter, the hours are once again filtered with the following conditions,

1. Lower than solar PV generation average of remaining 447 hours (excluding hours with zero PV production)

2. Higher than synchronous generation average of remaining 447 hours

After filtering, several hours matched the set criteria. From the remaining hours, hour 1289 was selected. The details of this hour with regards to production and total load demand are shown in Table 6.2.

Case 3 The requirements for case 3 is the selection of an hour which has an average solar PV production and an average synchronous generation production. To achieve this, the average solar PV production (excluding the hours with zero PV production) and the average SG production was calculated from the remaining 447 hours. Following this, an hour was chosen which did not differ too much from these average values. The hour selected was 5389.

Case 4 The requirements for case 4 are that an hour is selected which has high solar PV production and low synchronous generation production. To determine the selection, again, the average of both the solar PV production (excluding the hours with zero PV production) and the synchronous generation production over the remaining 447 hours has been calculated. Subsequently, the hours are once more filtered with the following conditions,

1. Higher than solar PV generation average of remaining 447 hours (excluding hours with zero PV production)

2. Lower than synchronous generation average of remaining 447 hours

Again several hours were left after filtering, and the selection of hour 2726 was made. The details of this hour with regards to production and total load demand is shown in Table 6.2.

The distribution of generation between the different sources is shown in Figure 6.4 for the various cases discussed.

(a) Case 1

(b) Case 2

(c) Case 3
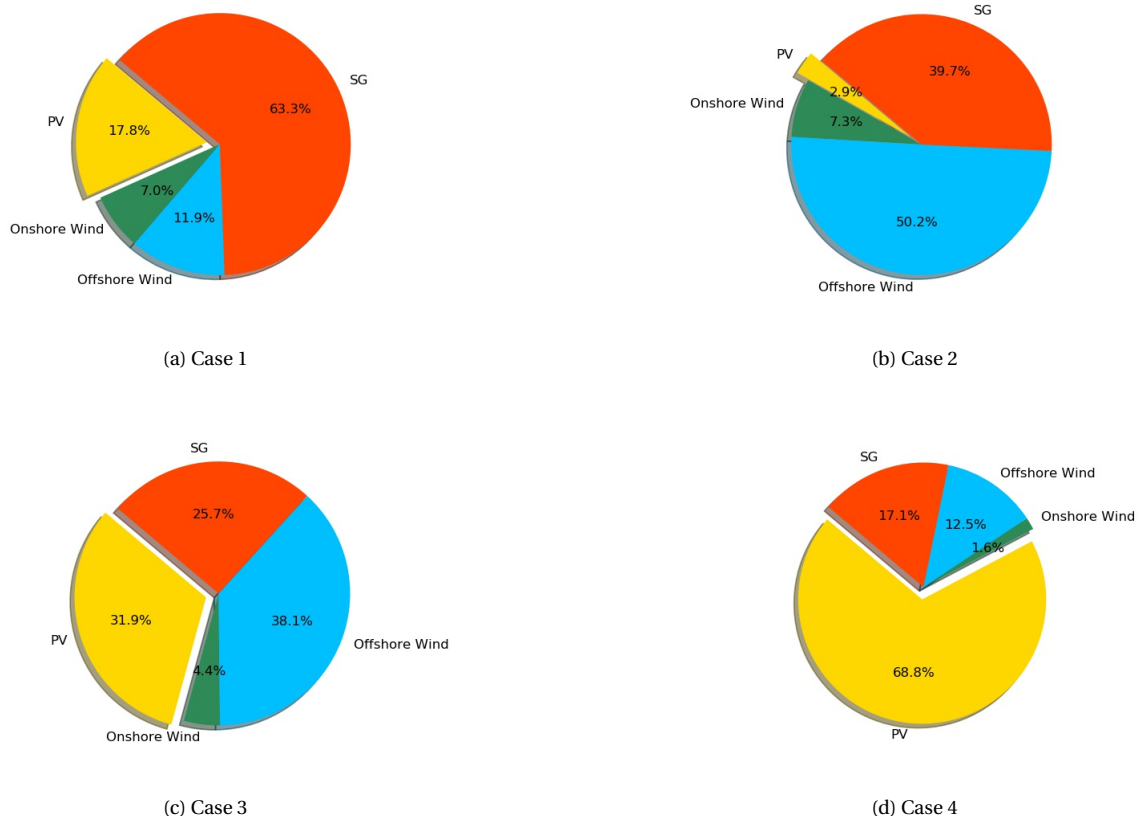
(d) Case 4

Figure 6.4: Distribution of generation for selected cases

From the selection criteria, it can be seen that ultimately several hours were still left and that the choice was made arbitrarily. However, it is of importance to keep in mind that all hours which were available adhere to the set requirements, which are for case 2 low PV generation and high SG generation, case 3 average PV generation and average SG generation and case 4 high PV generation and low SG generation.

The difference between the cases is not only the dispatch of the generation units and changes in load but also the synchronous generation units which are connected to the network. The amount of generation units connected to the network has influence on the total short-circuit current during contingencies. Henceforth, for case 1 all synchronous generation units within the Netherlands have been connected to obtain the highest total short-circuit current. In the other cases, the connection of synchronous generators varies per case hence yielding different amount of total short-circuit current injection. The amount of synchronous generators which are connected in the Netherlands per case is shown below [1],

- Case 1 – 100% of SGs connected

- Case 2 –   64% of SGs connected

- Case 3 –   59% of SGs connected

- Case 4 –   17% of SGs connected

The above introduction provides us with an overall overview of the four different cases. However, since mainly local stability phenomena is looked at such as rotor angle stability and short-term voltage stability, the areas of interest will be discussed during the analysis.

6.3. Modelling PV Systems

6.3.1. State of the TenneT dynamic grid model

Currently, the dynamic grid model of TenneT properly represents all synchronous generation units and all aggregated onshore wind PPMs. These generation units are modelled in detail in the dynamic grid model of TenneT. Solar PV systems, offshore wind PPMs and large-scale onshore wind PPMs, however, are not modelled in detail and are represented by a negative load at the concerned high voltage bus. An overview of the current modelling state of the TenneT dynamic grid model is provided in Table 6.3.

Generation type	Modelled with	Detail
Synchronous generators	Dynamic model	High detail
Large-scale onshore Wind PPMs	Negative load	Low detail
Aggregated onshore Wind PPMs	Dynamic model	High detail
Offshore Wind PPMs	Negative load	Low detail
Large-scale solar PV PPMs	Negative load	Low detail
Aggregated solar PV PPMs	Negative load	Low detail

Table 6.3: Current state of TenneT dynamic grid model

In Table 6.3, an overview is given of the current state of the dynamic grid model. Both synchronous generators and onshore wind PPMs are modelled with their respective dynamic models. Additionally, for these generation types the level of detail is high. This entails for synchronous generation units that the step-up transformer is also modelled, while for the onshore wind PPMs, the LV/MV transformer equivalent (also called pad-mounted transformer equivalent), collector system equivalent and station transformer as discussed in [39] is also added. Lastly, solar PV systems, offshore wind PPMs and large-scale onshore wind PPMs are modelled by way of a negative load hence not contributing to the dynamic response. Furthermore, they are not modelled in detail, meaning that the negative load is connected at a high voltage bus and no LV/MV transformer equivalent, collector system equivalent and station transformer are taken into account.

---

[1]The percentage of connected SGs has been determined based on the capacity of the synchronous generators.

6.3.2. Obtaining the files for a selected hour

The procedure for obtaining the final model for the selected hour (also referred to as a *snapshot*) to carry out the simulations is shown in Figure 6.5.
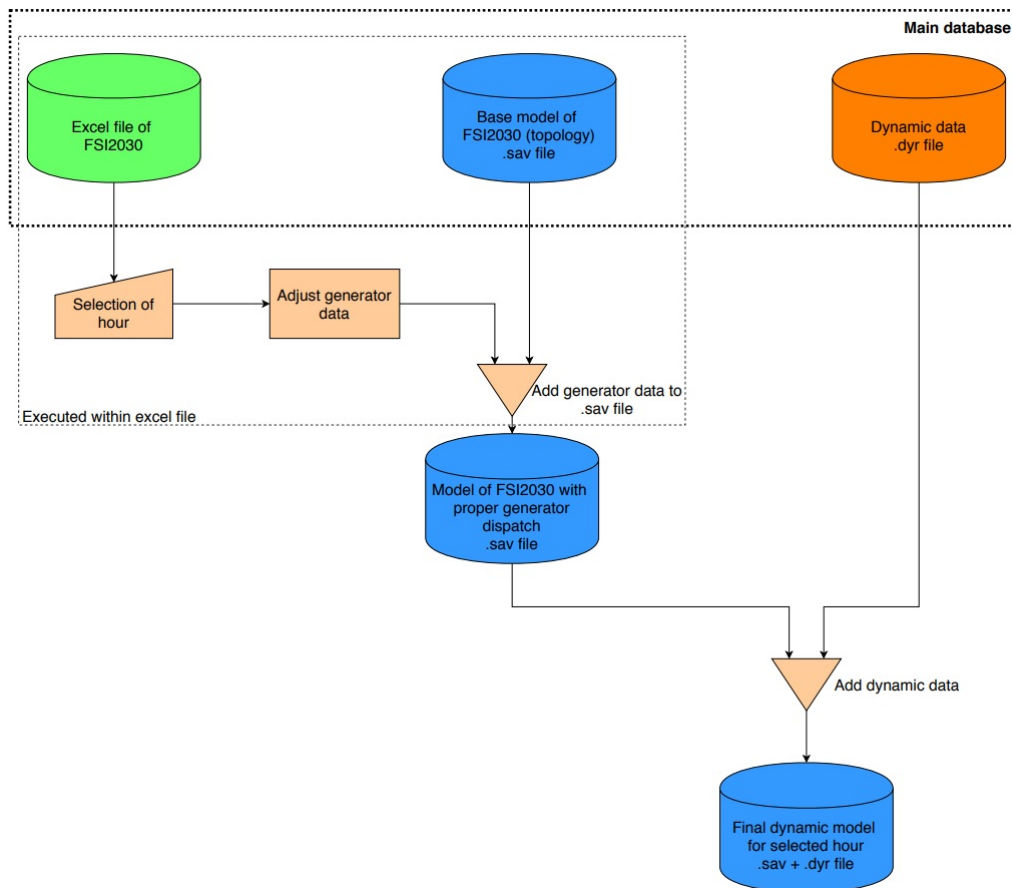
Figure 6.5: Loading in a specific hour into the dynamic grid model [40]

The main database shown in Figure 6.5, consists of:

- **Excel file of FSI2030** — The excel file of FSI2030, as also mentioned in Section 6.1, contains information of the dispatch of generation units (including PV systems) throughout the whole year. Additionally, this excel file contains a script which imports the base model, discussed subsequently, and maps the proper generation dispatch to the generators in the base model and ultimately yields the modified model (.sav file) which contains the proper generator dispatch in accordance with the selected hour.

- **Base model of FSI2030** — The base model of the Foundation for System Integration scenario for 2030 is *.sav* file, which contains the information regarding the topological structure of the network.

- **Dynamic Data** — The dynamic data database is a *.dyr* file and contains the dynamic models of the various generation units and types with their respective parameters.

To recap the working, the first step is to make a selection of the hour in the excel file. The excel file then imports the base model of the Foundation of System Integration Scenario of 2030 and changes the generator dispatch to match the selected hour and outputs a *.sav* file with the changed generator dispatch. Following this, the dynamic data is added to yield the full set of files to carry out dynamic simulations.

6.3.3. Modifications to add dynamic PV models

Section 6.3.2 provided the steps which need to be taken to obtain the final model for a selected hour in which the PV systems are modelled as negative load at high voltage buses. One of the goals of this research is to implement the proper representation of PV systems in the TenneT dynamic grid model. Since the TenneT network is an extensive network, it would be a rather lengthy process to manually add each PV system into the dynamic grid model. Hence, two automation scripts have been created to facilitate the implementation of PV systems with their proper parameters

into the dynamic grid model. Figure 6.6 provides an overview of how the current database has been modified to enable the implementation of PV systems.
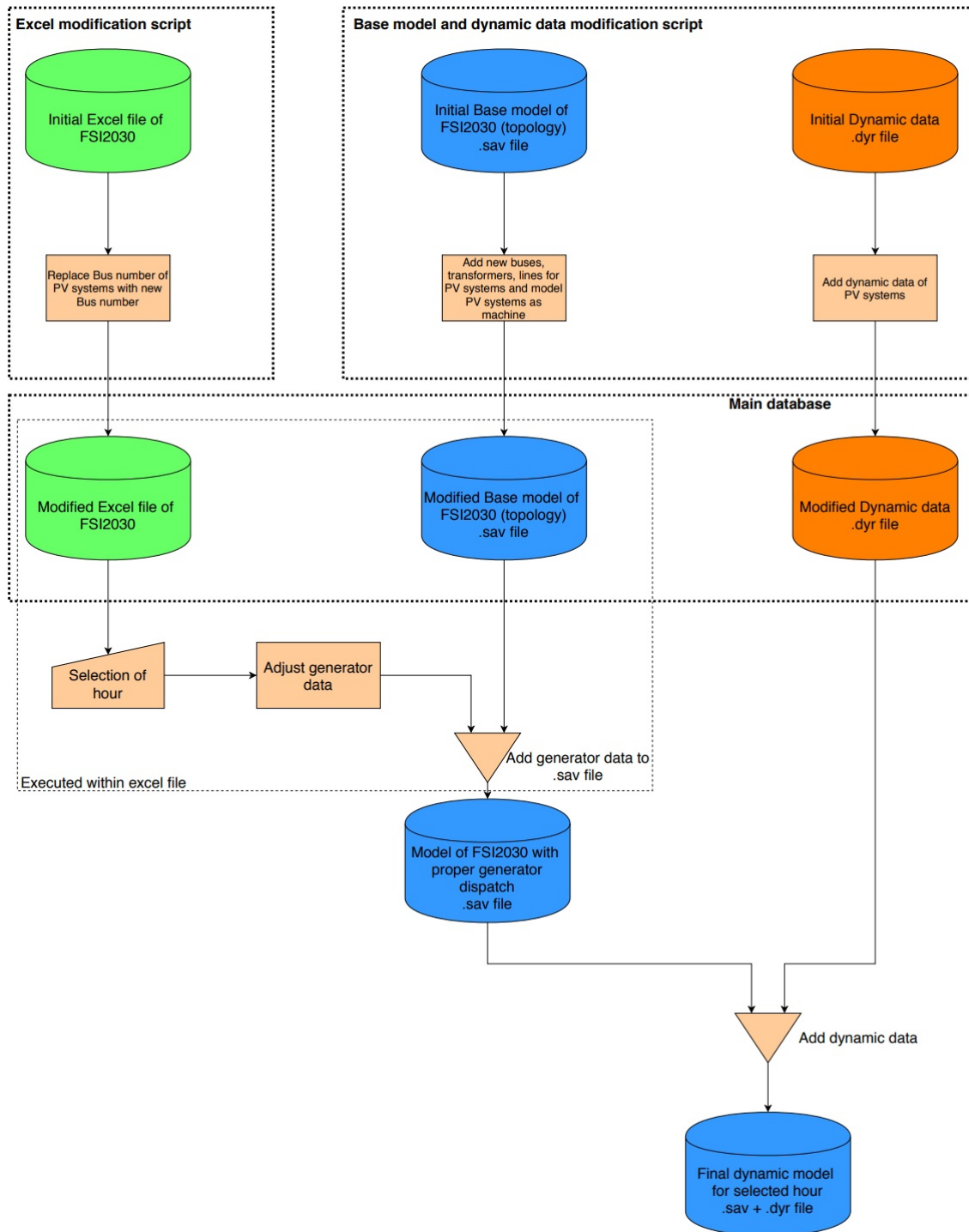
Figure 6.6: Modification made to loading in a specific hour into the dynamic grid model [40]

Two automation scripts were created in Python 2.7 to facilitate the implementation of PV systems into the TenneT dynamic grid model. The interaction of the scripts with the setup as previously explained is shown in Figure 6.6.

Excel modification script
The Excel modification script replaces the bus numbers of the PV systems (which are initially connected at high volt-

age buses) with new bus numbers which represent the low voltage bus number. Additionally, the high voltage bus number is saved in a new column with header *High voltage bus number* to serve as the bus at the point of interconnection. This step is taken to increase the level of detail of modelling the PV systems by eventually adding the necessary underlying elements (LV/MV transformer equivalent, collector system equivalent and station transformer) in between the high voltage bus and the newly created low voltage bus. This will be discussed in the subsequent script.

Base model and dynamic data modification script

The goal of this script, as the title states, is twofold. Firstly, to add the newly created LV buses alongside the transformers, line for PV systems and to add the PV system as a machine in PSS/E, by modifying the topology of the base model of the Foundation for System Integration file. The second goal of this script is to add the dynamic data of the PV systems into the dynamic data library. The changes in detail of modelling with the use of this script are shown in Figure 6.7.

(a) PV system modelling before script   (b) PV system modelling after script
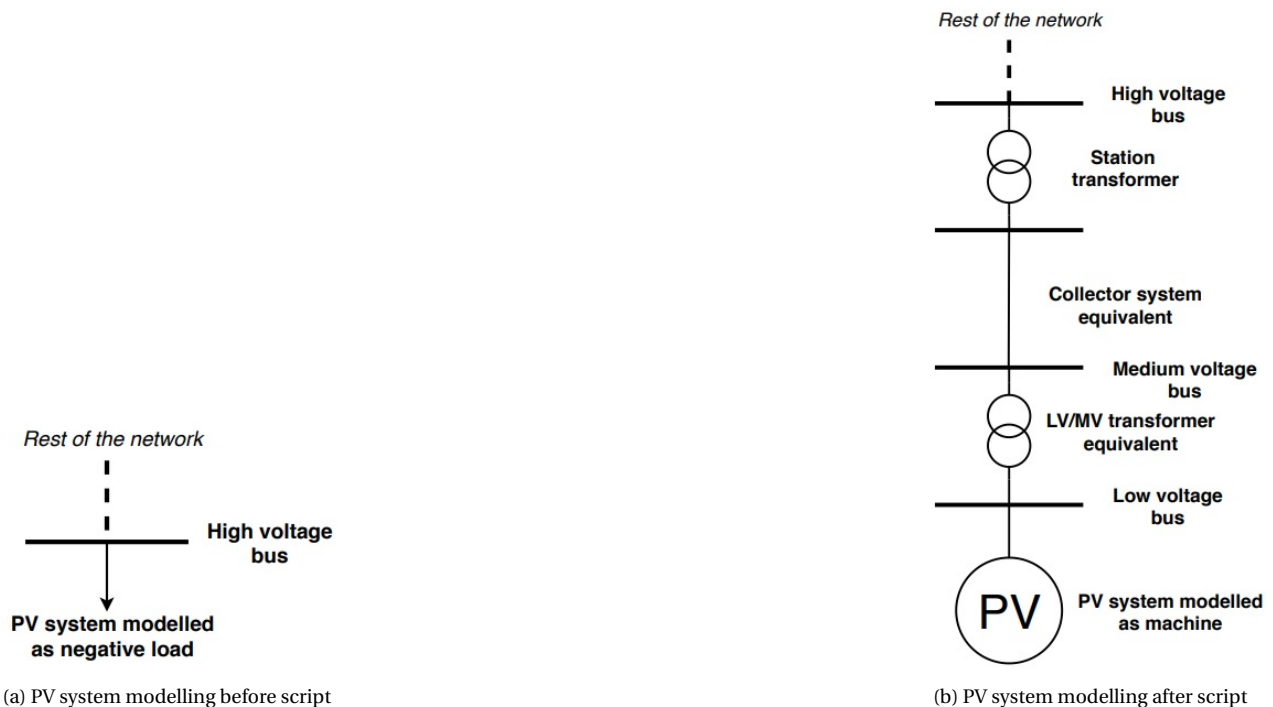
Figure 6.7: Modelling of PV systems in TenneT dynamic grid model

The level of detail for the PV systems in the *Initial Base model* of the Foundation for System Integration scenario is shown in Figure 6.7a. After running the script, the changes are made to increase the level of detail for PV system modelling as shown in Figure 6.7b to yield the *Modified Base model* of FSI2030 with detailed PV modelling. The parameters used for these underlying elements are discussed in Appendix E.

Besides modifying the level of detail of PV systems and modifying the dynamic data library with the addition of PV dynamic data, the script also makes a distinction between,

1. Large-scale PV systems (connected at or above 110kV)
2. Aggregated PV systems (connected at or below 50kV)[2]

In the excel file, PV systems are named with a certain characteristic depending on whether they are connected to the TenneT transmission network or at the voltage level of DSO's. The aggregated PV systems at DSO voltage level are of types A, B, C and D1. As discussed in Chapter 3 and 4, type A PPMs have a different parameter set compared to type B, C and D1 PPMs. The primary difference is that type A PPMs are not obliged to offer fast fault current injection during contingencies while type B, C and D1 PPMs are [18]. Hence, it is of great importance to model this distribution between type A and type B, C and D1 PPMs correctly.

---

[2]After 50kV, the next voltage level in the Netherlands is 110kV if offshore connections are excluded

The growth in 2019 of the distribution between the residential market (type A) and the business market (type B, C and D) is shown in Table 6.4.

	Growth (GW)	Growth (%)
Total	2.4	100 %
Type A	0.7	29.17 %
Type B, C and D1	1.6	66.67 %
Type D2	0.1	4.16 %

Table 6.4: Distribution of growth in PV systems in 2019 [7]

From Table 6.4, it can be seen that a very small portion of the PV systems are connected to the transmission network (≥ 110 kV). The highest growth is seen for the PPMs of type B, C and D1. The above mentioned data, serves to provide the reader with the state of the current growth of the different types of PV systems in the electrical network.

The technical potential for solar PV in 2030 is projected to be approximately equal to 14 GW [41]. As this provides an extreme case, an assumption is made that 75% of this potential is reached for 2030 and hence amounting to 10.5 GW of installed capacity of residential (type A) solar PV systems. With this in mind, the distribution of the various types solar PV systems for the *Foundation for System Integration Scenario* is shown in Table 6.5.

	Installed (GW)	Installed (%)
Total	44.3	100 %
Type A	10.5	24 %
Type B, C and D1	9.5	21 %
Type D2	24.3	55 %

Table 6.5: Distribution of PV systems in Foundation for System Integration Scenario [7],[41]

The total amount of potential residential solar PV in the year 2030 is equivalent to 10.5 GW in Table 6.5 [41]. Additionally, it is assumed that all connections equal to and above 120 MW which are categorised as aggregated PV systems are partially modelled as large-scale PV systems — this will be explained later. With the above-stated conditions, the values in Table 6.5 are found.

At distribution level, the distribution between type A PPMs and type B, C and D1 PPMs is of interest as these have different parameter sets. The distribution of type A and type B, C and D1 is shown in Table 6.6.

	Installed (GW)	Installed (%)
Total	20	100 %
Type A	10.5	53 %
Type B, C and D1	9.5	47 %

Table 6.6: Distribution of PV systems in Foundation for System Integration Scenario at distribution level [7],[41]

To this end, it is assumed that the distribution is 50% to 50% between type A PPMs and Type B, C and D1 PPMs at distribution level for this scenario. The method of PV modelling used in the TenneT dynamic grid model is shown in Figure 6.8.
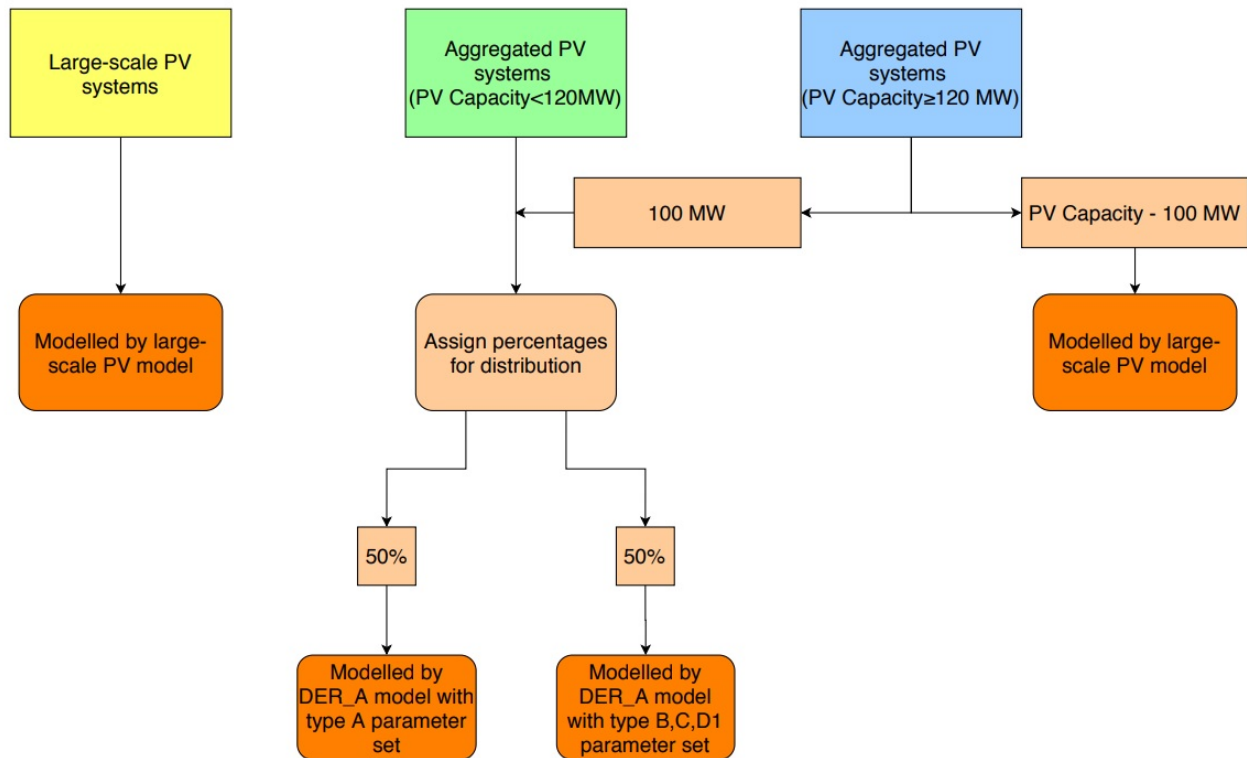
Figure 6.8: PV Modelling method in TenneT dynamic grid model

Figure 6.8 provides the approach taken to model PV systems. This approach can be divided in the following categories,

- **Large-scale PV systems** — Large-scale PV systems are considered to be PV systems connected at the transmission domain of the electrical network (≥ 110kV) and these units are modelled with the large-scale PV model.

- **Aggregated PV systems (PV capacity < 120 MW)** — Aggregated PV systems below 120 MW connected to a specific bus at the transmission domain are firstly divided based on the percentage of distribution between type A PPMs and type B, C and D1 PPMs as previously discussed and then modelled accordingly with the DER_A model with their specific parameter set. A simple example is an aggregated PV system of 100 MW connected at a bus on the transmission domain, 50 MW would then be modelled by the DER_A model with the type A parameter set, while the remaining 50 MW would be modelled by the DER_A model with the type B, C and D1 parameter set.

- **Aggregated PV systems (PV capacity ≥ 120 MW)** — Aggregated PV systems with a capacity above or equal to 120 MW are modelled in three separate ways. A portion of the capacity i.e. 100 MW is modelled in the same manner as *Aggregated PV systems (PV capacity < 120 MW)*. This threshold has been chosen considering *Article 2.25* of the Dutch netcode stating that generation up to 100 MVA shall be connected at distribution level [18]. Moreover, the remaining capacity is modelled by the large-scale PV model (hence always having a minimum of 20 MW). Essentially, an assumption is made here that if a PV system categorised as an aggregated PV system with a capacity higher than 120 MW is modelled, 100 MW is actually seen as aggregation of PV systems while the remaining capacity is seen as a large-scale PV system connected at transmission level. This assumption has been made in congruence with *Article 2.25* of the Dutch netcode. A simple example of the distribution would be an aggregated PV system with a capacity of 170 MW connected to a high voltage bus. The distribution would be as follows, 100 MW would be distributed by the percentages hence similar to the previous example 50 MW will be modelled by the DER_A Model with type A parameter set and 50 MW will be modelled by the DER_A Model with Type B, C and D1 parameter set. The remaining 70 MW will then be modelled by the large-scale PV model.

6.4. Transient stability

6.4.1. Introduction
In this section, the transient stability of the Dutch high voltage network shall be evaluated of the discussed FSI 2030 scenario and the selected snapshots. Three-phase faults shall be introduced at high voltage buses (110 kV and 150 kV) close to synchronous generation units since all PV systems are connected at these voltage levels. [42] states that

a critical clearing time in the Dutch TenneT Network has to be larger than 150 ms to avoid loss of synchronism of synchronous generation units. Additionally, for increased robustness critical clearing times of larger than 250-300 ms are required. All pu values in this Chapter are in terms of the system base of 100 MVA unless stated otherwise.

The main factors of interest that influence transient stability are [42],

- Steady state rotor angle – The steady state rotor angle of a synchronous generator is decided by the active power and reactive power output, it can also be expressed in terms of the operating point of a synchronous generator. The higher the rotor angle, the closer the synchronous generator is to it's limit and hence resulting in lower transient stability.

- Short-circuit current at point of connection – Short-circuit current at the faulted bus indicates the current contributed to the fault and the fault recovery time. The transient stability improves for higher the short-circuit current levels.

- Generator Inertia – The inertia of the generator influences the transient stability as shown in Chapter 5. The lower the inertia of the synchronous generator the lower the critical clearing time and hence reduction of the transient stability as the rotor angle accelerates at a faster rate.

- Voltage at generator bus – The voltage at a generator bus influences the amount of current injected. A lower voltage increases the rotor angle for fixed reactive power output and hence reduces the critical clearing time.

6.4.2. Assessment Method
The method to asses the transient stability in this section shall be done in a comparable manner as shown in Chapter 5. The *critical clearing time* shall be used to assess the transient stability. However, since a larger, more extensive network, is evaluated, it would be computationally very complex and time consuming to use the method as shown in Figure 5.3. To this end, an existing python script[3], used at TenneT, was used for the analysis. The flowchart explaining the method to obtain the CCT is shown in Figure 6.9.

---

[3]The script was created by Jorrit Bos
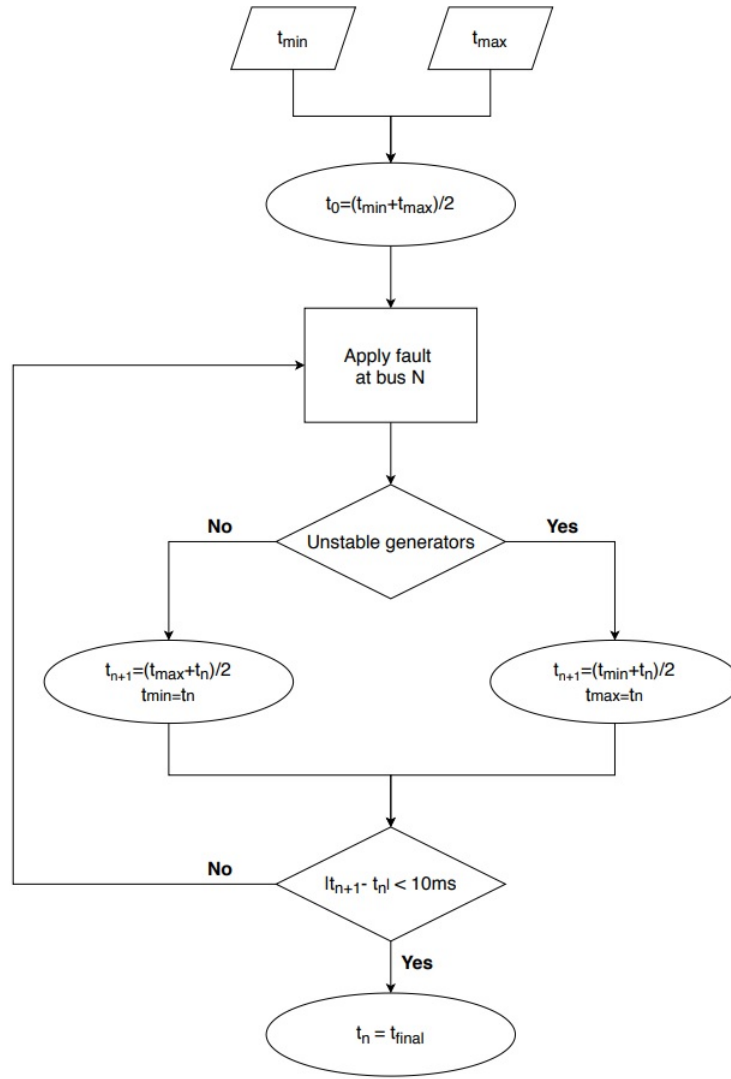
Figure 6.9: Flowchart of iterative process to obtain critical clearing time for TenneT network [42]

As shown in Figure 6.9, there are two inputs for the CCT script i.e. t_{max} and t_{min}. These two inputs indicate the time interval in which the simulation will search for the critical clearing time. The first clearing time (t_0) of the fault is calculated as shown in Equation 6.1.

$$t_0 = \frac{t_{max} + t_{min}}{2} \text{ (n=0)} \tag{6.1}$$

Following this, the fault is applied at a particular bus for t_0 seconds and then the fault is cleared and the simulation continues to run till 5 seconds. The rotor angle of all synchronous generation units are then scanned to evaluate if the rotor angle exceeds a certain threshold. If there are unstable generators present then the fault clearing time is decreased as shown in Equations 6.2 and 6.3.

$$t_{n+1} = \frac{t_{min} + t_n}{2} \tag{6.2}$$

$$t_{max} = t_n \tag{6.3}$$

If no unstable generators are present then the fault clearing time is increased as shown in Equations 6.4 and 6.5.

$$t_{n+1} = \frac{t_{max} + t_n}{2} \tag{6.4}$$

$$t_{min} = t_n \tag{6.5}$$

This iterative process is repeated until Equation 6.6 holds, yielding the critical clearing time as provided in Equation 6.7.

$$|t_{n+1} - t_n| < 10ms \tag{6.6}$$

$$\boxed{\text{Critical clearing time} = t_n} \tag{6.7}$$

6.4.3. Results & Analysis

As previously stated, the critical clearing time has been calculated for the 110 kV and 150 kV buses which are located close to synchronous generators with the method shown in Figure 6.9. The CCT of the relevant 110 kV and 150 kV buses are shown in Table 6.7.

Bus name	Substation name	CCT Case 1 (ms)	CCT Case 2 (ms)	CCT Case 3 (ms)	CCT Case 4 (ms)	Aggregated PV at bus	Large-scale PV at bus
BL110-A	Beilen 110 kV	>400	>400	>400	>400	Yes	Yes
BSL150-A	Borssele 150 kV	315	259	334	>400	Yes	Yes
DZW110-B	Delfzijl Weiwerd 110 kV	240	231	240	240	No	No
EBK150-A	Eerbeek 150 kV	277	268	>400	277	Yes	No
GT150-B	Geertruidenberg 150 kV	287	268	>400	>400	Yes	Yes
GVN150-A	Geervliet Noorddijk 150 kV	>400	>400	>400	>400	No	No
HGLB110-B	Hengelo Boldershoek 110 kV	315	306	>400	325	Yes	No
HGV110-A	Hoogeveen 110 kV	>400	>400	>400	>400	Yes	Yes
HW150-A	Amsterdam Hemweg 150 kV	>400	>400	>400	>400	Yes	Yes
LLS150-A	Lelystad 150 kV	>400	>400	>400	>400	Yes	No
MBT-150A1	Maasbracht 150 kV	>400	>400	>400	>400	Yes	Yes
MDK150-A	Moerdijk 150 kV	381	>400	>400	>400	Yes	Yes
RSB150-A	Roosendaal Borchwerf 150 kV	371	362	371	334	No	No
RTW150-A2	Rotterdam Waalhaven 150 kV	>400	>400	>400	>400	No	No
TNZ150-A	Terneuzen 150 kV	381	362	>400	371	Yes	No
ULW150-B1	Utrecht Lage Weide 150 kV	>400	>400	>400	>400	No	No
VO110-A	Veenoord 110 kV	352	>400	362	>400	No	No

Table 6.7: Critical clearing time at 110 kV and 150 kV buses

Overall it can be seen that the critical clearing times provided in Table 6.7 will not lead to loss of synchronism if the fault is cleared appropriately. It is, however, shown that the bus *DZW110-B* leads to the lowest critical clearing time of the results shown in Table 6.7. This is due to the fact that the generator which loses synchronism is in close proximity to the faulted bus and possesses high operating points for all four cases. The discrepancies at the other buses between cases is due to different operating conditions such as different operating points of synchronous generators, varying voltages at generator buses and out of service generators.

In the following sub-sections, the transient stability at individual buses of interest shall be looked at. For the analysis of the individual buses, the critical clearing time script discussed in Figure 6.9 has been modified to acquire an increased accuracy. The modification is shown in Equation 6.8.

$$|t_{n+1} - t_n| < 3ms \tag{6.8}$$

Additionally, for the remainder of the analysis it is important to define the various methods of PV representation which will be used subsequently. This distinction is made to clearly identify the factors in play which influence the impact of PV penetration on transient stability. The four different modelling representations which shall be studied are,

- Representation of all PV systems with their respective dynamic models. This representation shall be referred to as *All dynamic models*.

- Representation of all PV systems with negative load. This representation shall be referred to as *All negative load*.

- Representation of the PV systems connected at the faulted bus with dynamic models while all others are represented by negative load. This representation shall be referred to as *Dynamic local 1*. A further elaboration of this representation is shown in Figure 6.10a (The underlying elements of the PV system have been omitted in the figure for simplicity purposes).

- Representation of PV systems connected to at the faulted bus and PV systems connected at a bus directly connected to the faulted bus are represented with dynamic models. All other PV systems are represented with negative load. This representation shall be referred to as *Dynamic local 2*. A further elaboration of this representation is provided in Figure 6.10b.
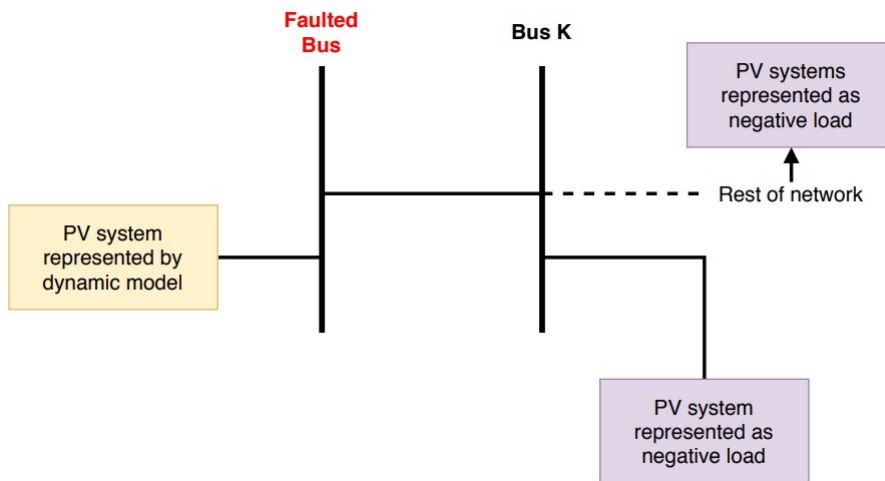
(a) Dynamic local 1 representation
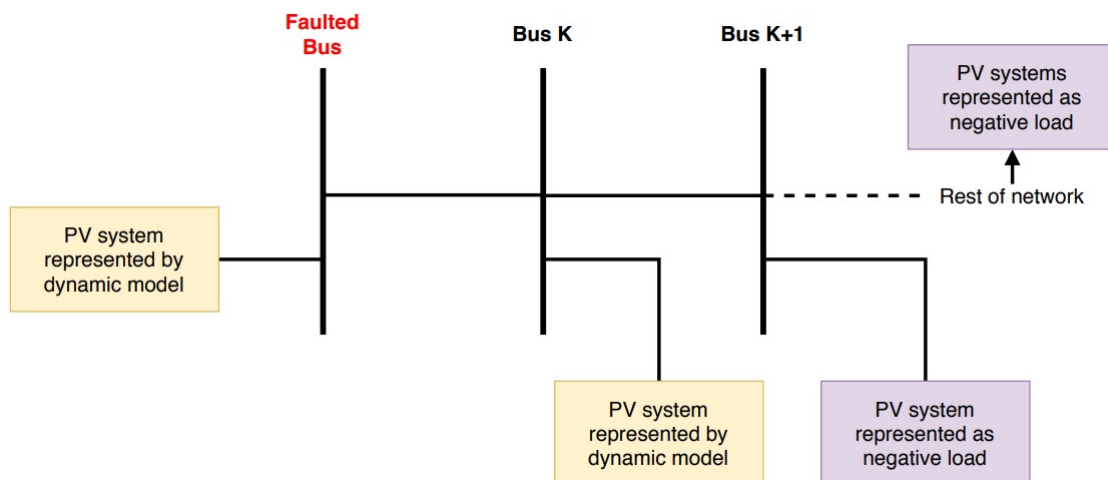
(b) Dynamic local 2 representation

Figure 6.10: Scenarios of PV representation

Geertruidenberg 150 kV
The first bus which will be examined is the bus at Geertruidenberg with a voltage level of 150 kV also referred to as

GT150-B. This bus was chosen since a synchronous generator and PV systems are in close proximity. Additionally, distinction between the short-circuit current at this bus can be clearly seen between the various cases. An overview of the relevant connections at this bus is shown in Figure 6.11. An aggregated wind PV system was also connected to this bus, but has been put out of service to solely evaluate the impact of solar PV systems.
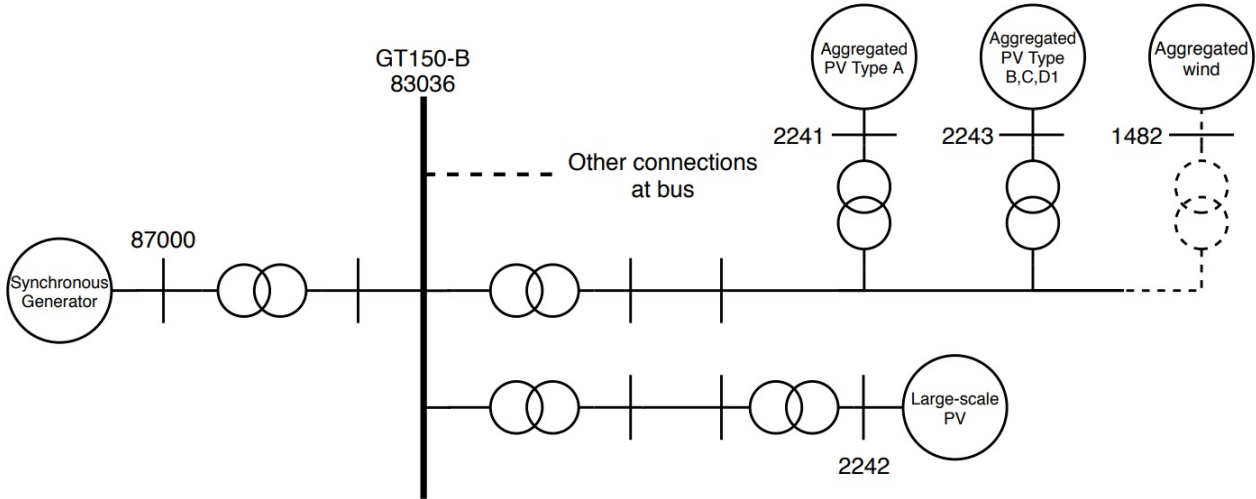
Figure 6.11: Connections at GT150-B bus

First it will be briefly demonstrated why the critical clearing time is low for case 1 and 2 compared to the other two cases. The initial operating points of the synchronous generator at bus 87000 are shown in Table 6.8.

Case number	P (MW)	Q (Mvar)
Case 1	620	93.38
Case 2	620	90.64
Case 3	248	32.93
Case 4	248	21.64

Table 6.8: Initial operating points of synchronous generator at bus 87000

As presented in Chapter 5, the steady-state operating point of the synchronous generator plays an important role in the transient stability. The operating point and the generator bus voltage are the main cause for the differences in critical clearing time.

The impact of the PV systems on the transient stability is of interest. To isolate the impact of PV systems on the transient stability, the synchronous generator at bus 87000 has been provided one operating point for all four cases while all other generation dispatch remains unchanged. Additionally, the voltage at the generator bus has been brought within a range of 0.01 pu of each other to obtain comparable cases. The voltages at the generator bus are displayed in Table 6.9. By doing this, the impact of varying PV generation and the short-circuit current on the transient stability can be clearly seen. Moreover, the impact of the total system inertia on the transient stability for the different cases is neglected as the network is widely interconnected to European countries and thus the disconnection of certain SGs within the Netherlands has an insignificant influence on the total system inertia. The modification of the synchronous generator and the generation of the PV systems at bus 87000 for the various cases is presented in Table 6.10.

Bus SG	Voltage Case 1 (pu)	Voltage Case 2 (pu)	Voltage Case 3 (pu)	Voltage Case 4 (pu)
87000	0.9758	0.9752	0.9779	0.9738

Table 6.9: Voltage at generator bus 87000

	SG 87000			PV 2241			PV 2242			PV 2243		
	P (MW)	Q (Mvar)	S (MVA)	P (MW)	Q (Mvar)	S (MVA)	P (MW)	Q (Mvar)	S (MVA)	P (MW)	Q (Mvar)	S (MVA)
Case 1	620	90.64	812.50	1.88	0	55.56	7.06	0	208.79	1.88	0	55.56
Case 2	620	90.64	812.50	0.58	0	55.56	2.18	0	208.79	0.58	0	55.56
Case 3	620	90.64	812.50	6.56	0	55.56	24.64	0	208.79	6.56	0	55.56
Case 4	620	90.64	812.50	11.63	0	55.56	43.69	0	208.79	11.63	0	55.56

Table 6.10: Generation of SG and PV systems near bus *GT150-B*

As shown in Table 6.10 the synchronous generation unit has been set to 620 MW and 90.64 Mvar for all four cases to obtain an identical steady-state operating point. The production of the PV systems differ for the four cases with case 2 having the lowest amount of PV production while case 4 has the highest amount of PV production. Furthermore, it's important to realise that the PV systems (i.e. the large-scale PV system and the PV system representing type B,C,D1) inject reactive current equivalent to their respective rating. In other words, the amount of reactive current injected by the PV systems is similar for all four cases. It is also worth to mention that the PV system at bus 2241, representing type A aggregated PV units, does not contribute to the fault current as per the grid connection requirements.

The critical clearing times for the four cases are provided in Table 6.11.

Representation	CCT Case 1 (ms)	CCT Case 2 (ms)	CCT Case 3 (ms)	CCT Case 4 (ms)
All dynamic models	279	274	274	272
All negative load	268	256	256	237
Dynamic local 1	270	256	261	242
Dynamic local 2	274	261	265	247

Table 6.11: CCT with constant operating point of SG at bus 87000

When firstly comparing the representation *All dynamic models* for the different cases provided in Table 6.11, it can be seen that the critical clearing time is nearly identical for all cases. The minor difference witnessed in case 1 is due to the increased short-circuit current at the faulted bus. Additionally, the difference witnessed in case 4 is due to the reduction of short-circuit current at the faulted bus as several synchronous generators are put out of service for this case (i.e. low SG case). The short-circuit current[4] of the different cases is shown in Table 6.12. The equation used to calculate *SCC PV Ratio* in Table 6.12 is provided in Equation 6.9 and shows the percentage of short-circuit contribution of all the PV systems in the network relative to the total short-circuit contribution.

Case	SCC Case 1 (kA)	SCC Case 2 (kA)	SCC Case 3 (kA)	SCC Case 4 (kA)
Total SCC	59.64	57.26	57.32	54.25
Total SCC PV	9.09	9.38	9.46	9.97
SCC PV Ratio	15.25%	16.37%	16.50%	18.37%

Table 6.12: Short-circuit current at bus *GT150-B*

$$\text{SCC PV Ratio} = \frac{\text{Short-circuit current provided by all PV systems at faulted bus}}{\text{Total short-circuit current at faulted bus}} \times 100\% \qquad (6.9)$$

As shown in Table 6.12, the short-circuit current for case 1 is the highest. For this case it is also seen that the SCC PV ratio is the lowest. Hence for the four cases presented, the PV systems contribute the least for case 1 relative to the total short-circuit current. This is also reflected when looking at the critical clearing time of case 1 when comparing the

---

[4]Calculated with the IEC 60909 method in PSS/E

representations *All dynamic models* and *All negative load*, as the lowest decrease is seen for this case. In other words, in case 1 the PV systems have the smallest effect on the transient stability due to the lowest SCC PV ratio. Additionally, for case 2 and 3, similar results are witnessed for the different representations as for these cases the SCC PV ratio is approximately identical. For case 4 a drastic decrease in transient stability is seen when comparing the representations *All dynamic models* and *All negative load*. This increased difference stems from the fact that the short-circuit current in this case has decreased (due to out of service of certain SGs) and thus the contribution of the PV systems to the total short-circuit current is more prevalent, as indicated by the SCC PV ratio for this case.

From the results provided in Table 6.11, it is shown that the PV systems do have an effect on the transient stability for this particular bus as the transient stability reduces when removing the dynamic behaviour of the PV systems. Additionally, it is shown that the impact of the PV systems increase when their short-circuit current contribution increases with respect to the total short-circuit current at the faulted bus — this is expressed by an increasing SCC PV ratio. Furthermore, when comparing the critical clearing time of the various representations, it is shown that the PV systems located at the faulted bus and to another bus nearby, do provide a significant contribution to the transient stability, but not a predominant one. As the remaining PV systems also aid the transient stability. This distinction between the contribution of *local* PV systems and PV systems located electrically further away from the fault is highly dependent on the capacity and the distribution of the PV systems in the two different areas.

Eerbeek 150 kV
The second bus of interest is *Eerbeek* abbreviated by *EBK150-A*. This bus has an aggregated PV system connected and a synchronous generator connected to it but no large-scale PV system. The relevant connections of bus *EBK150-A* are provided in Figure 6.12.
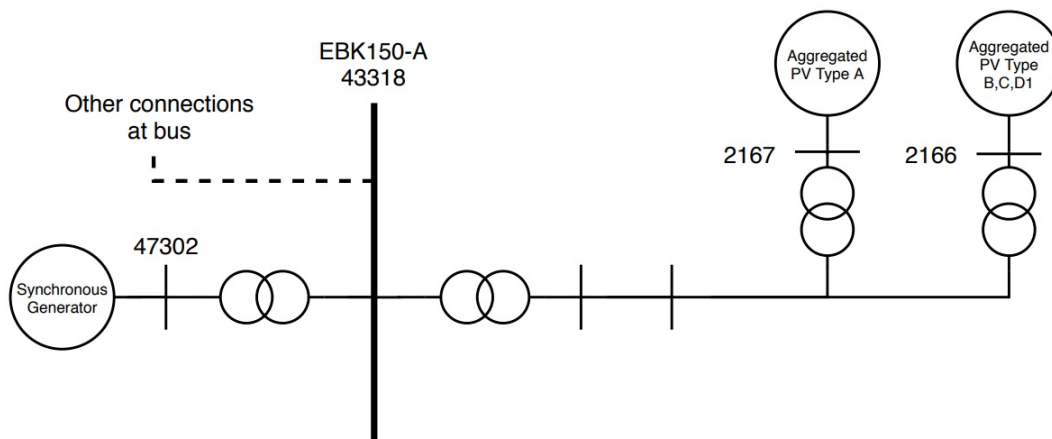
Figure 6.12: Connections at EBK150-A bus

Again, the results provided in Table 6.7 shall be firstly looked at. The steady-state operating points of the synchronous generator at bus 47302 are shown in Table 6.13. The operating points once again are predominantly responsible for the difference in critical clearing time shown in Table 6.7.

Synchronous Generator (47302)	**P (MW)**	**Q (Mvar)**
Case 1	35.58	3.70
Case 2	35.58	4.89
Case 3	24.17	3.61
Case 4	35.00	3.57

Table 6.13: Initial operating points of synchronous generator at bus 47302

The modification of the synchronous generator and the generation of the PV systems at bus 43318 for the various cases is shown in Table 6.14. The voltage at the generator bus for the four different cases is shown in Table 6.15.

	SG 47302			PV 2166			PV 2167		
	P (MW)	Q (Mvar)	S (MVA)	P (MW)	Q (Mvar)	S (MVA)	P (MW)	Q (Mvar)	S (MVA)
Case 1	35.58	4.89	66.00	1.76	0	32.39	1.76	0	32.39
Case 2	35.58	4.89	66.00	0.60	0	32.39	0.60	0	32.39
Case 3	35.58	4.89	66.00	6.28	0	32.39	6.28	0	32.39
Case 4	35.58	4.89	66.00	12.76	0	32.39	12.76	0	32.39

Table 6.14: Generation of SG and PV systems near bus *EBK150-A*

Bus SG	Voltage Case 1 (pu)	Voltage Case 2 (pu)	Voltage Case 3 (pu)	Voltage Case 4 (pu)
47302	1.0516	1.0513	1.0516	1.0514

Table 6.15: Voltage at generator bus 47302

The critical clearing times for the four cases is provided in Table 6.16.

Representation	CCT Case 1 (ms)	CCT Case 2 (ms)	CCT Case 3 (ms)	CCT Case 4 (ms)
All dynamic models	272	268	270	270
All Negative load	272	268	268	268
Dynamic local 1	272	268	268	268
Dynamic local 2	272	268	268	268

Table 6.16: CCT with constant operating point of SG at bus 47302

The results provided in Table 6.16 are contrastingly different compared to the results presented for *Geertruidenberg*. In Table 6.16, the critical clearing time changes slightly or not at all for the different representations and different cases presented. To obtain better insight as to why this is the case, the short-circuit current at the faulted bus is presented in Table 6.17.

Case	SCC Case 1 (kA)	SCC Case 2 (kA)	SCC Case 3 (kA)	SCC Case 4 (kA)
Total SCC	25.35	25.34	25.28	25.06
Total SCC PV	2.46	2.48	2.51	2.61
SCC PV Ratio	9.70%	9.80%	9.94%	10.41%

Table 6.17: Short-circuit current at bus *EBK150-A*

Firstly, it is seen that the short-circuit current presented in Table 6.17 for the different cases does not vary significantly. From this it can concluded that the synchronous generators which are out of service for the varying cases do not provide any significant contribution to the faulted bus. Moreover, in Table 6.16, it is shown that the critical clearing times vary slightly or not at all for the presented representations and cases. This is due to the fact that the short-circuit contribution of the PV systems at this bus is low — this is expressed in the low percentages of the SCC PV ratio. In other words, this area is not populated densely by PV systems in close vicinity hence leading to a small contribution to the short-circuit current by the PV systems which in consequence leads to the PV systems having a limited role in the transient stability for this faulted bus.

Hengelo Boldershoek 110 kV
The third case which shall analysed is the bus at Hengelo Boldershoek at a voltage level of 110 kV, this bus is also referred to as *HGLB110-B*. An overview of the important connections at this bus is provided in Figure 6.13.
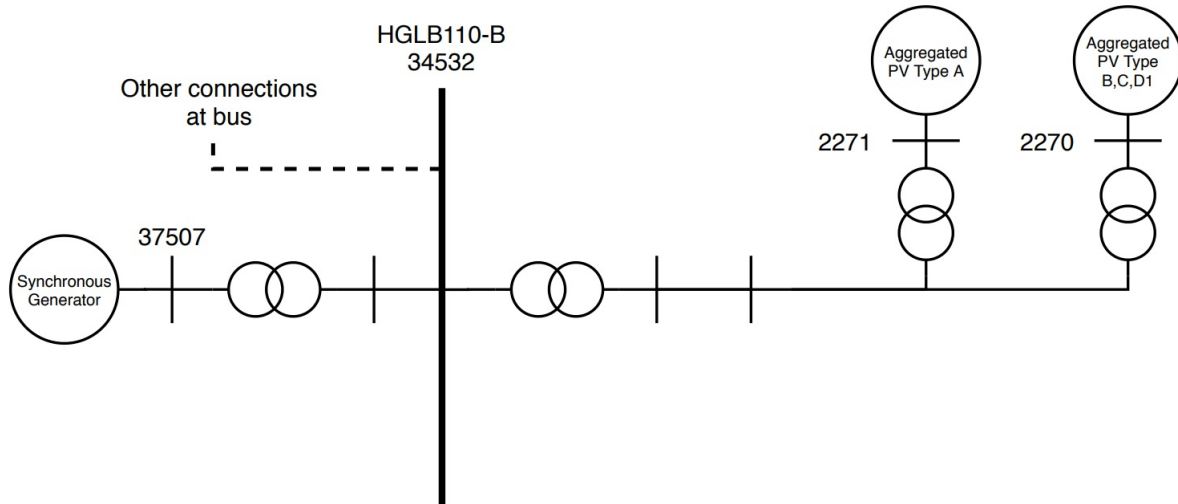
Figure 6.13: Connections at HGLB110-B bus

Again, the results provided in Table 6.7 shall be looked at first. The initial operating points of the synchronous generator at bus 37507 is shown in Table 6.18 and are mainly responsible for the distinction in critical clearing time shown in Table 6.7.

Synchronous Generator (37507)	P (MW)	Q (Mvar)
Case 1	32.73	4.56
Case 2	32.73	4.29
Case 3	22.23	3.03
Case 4	32.20	3.29

Table 6.18: Initial operating points of synchronous generator at bus 37507

The modification of the synchronous generator and the generation the PV systems at bus 37507 for the various cases is shown in Table 6.19. The voltage at the generator bus for the four different cases is shown in Table 6.20.

	SG 37507			PV 2270			PV 2271		
	P (MW)	Q (Mvar)	S (MVA)	P (MW)	Q (Mvar)	S (MVA)	P (MW)	Q (Mvar)	S (MVA)
Case 1	35.58	4.89	56.25	0.95	0	24.21	0.95	0	24.21
Case 2	35.58	4.89	56.25	0.25	0	24.21	0.25	0	24.21
Case 3	35.58	4.89	56.25	3.00	0	24.21	3.00	0	24.21
Case 4	35.58	4.89	56.25	5.46	0	24.21	5.46	0	24.21

Table 6.19: Generation of SG and PV systems near bus *HGLB110-B*

Bus SG	Voltage Case 1 (pu)	Voltage Case 2 (pu)	Voltage Case 3 (pu)	Voltage Case 4 (pu)
37507	1.0277	1.0280	1.0270	1.0278

Table 6.20: Voltage at generator bus 37507 for cases

The critical clearing times for the four cases are provided in Table 6.21. At this bus the representation *Dynamic local 1* is equivalent to *Dynamic local 2* as no PV systems are connected to neighbouring buses of bus *HNGL110-B*.

Representation	CCT Case 1 (ms)	CCT Case 2 (ms)	CCT Case 3 (ms)	CCT Case 4 (ms)
All dynamic models	322	320	320	322
All negative load	320	315	317	317
Dynamic local 1	320	315	317	317
Dynamic local 2	320	315	317	317

Table 6.21: CCT with constant operating point of SG at bus 37507

The results provided in Table 6.21 are in line with the results provided for *Eerbeek* as the critical clearing time contains very minor changes for the various representations. This can explained, again, by looking at the amount of short-circuit current provided in different cases and the amount provided by the PV systems as shown in Table 6.22.

Case	SCC Case 1 (kA)	SCC Case 2 (kA)	SCC Case 3 (kA)	SCC Case 4 (kA)
Total SCC	32.23	32.14	32.04	32.14
Total SCC PV	2.53	2.59	2.63	2.70
SCC PV Ratio	7.86%	8.05%	8.20%	8.41%

Table 6.22: Short-circuit current at bus *HGLB110-B*

Similarly as the results provided for *Eerbeek*, it is shown that for a fault at bus *Hengelo Boldershoek*, the critical clearing time is impacted barely by the presence of PV systems. For this bus, however, the short-circuit current contribution is higher compared to that seen in *Eerbeek*. Relative to the total short-circuit current, the average contribution of PV systems is less — as expressed by the SCC PV ratios. In similar fashion, the PV systems have a limited say in the transient stability at this bus due to the small short-circuit contribution by the PV systems.

Summary & Overview
In the analysis, certain variables which influence the transient stability (e.g. voltage at generator bus, operating point of synchronous generator) were set to fixed values or within a certain range to try and isolate the behaviour of PV systems on the transient stability. From the analysis it was demonstrated that PV systems play an important role in one of the variables affecting transient stability i.e. the short circuit current at the faulted bus. Two main distinctions in terms of the relation between the total short-circuit current and short-circuit current contribution by the PV systems can be made, these are,

- *High SCC PV ratio* — The first distinction which can be made is for a faulted bus which possesses a high SCC PV ratio, this entails that the amount of short-circuit contribution of PV systems is high relative to the total short-circuit current at the faulted bus. Such an example was presented when evaluating the bus at *Geertruidenberg*. In this studied case, the PV systems affected the transient stability notably. Additionally, for higher SCC PV ratios as case 4, it was shown that the transient stability was affected the most for this case when removing the dynamic behaviour of the PV systems as the SCC PV ratio was the highest.

- *Low SCC PV ratio* — The second distinction which can be made is for an area or faulted bus which possesses a low SCC PV ratio, meaning that the amount of short-circuit contribution of PV systems is low compared to the total short-circuit current at the faulted bus. Examples of cases with low SCC PV ratios are *Eerbeek* and *Hengelo Boldershoek*. For these cases it was shown that the low contribution to the total short-circuit current by the PV systems led to them having little to no influence on the transient stability.

Looking into the future, power system networks shall continue to phase out synchronous generators and add renewable energy sources such as solar PV systems. Consequently, the short-circuit current in the various regions shall decline as synchronous generators provide significantly more short-circuit current compared to renewable energy sources. This overall decline in short-circuit current and increase of short-circuit current contribution by PV systems shall progress a lot of areas towards higher *SCC PV ratios* and thus PV systems (and other RES) shall have a continuingly increasing influence on the transient stability.

The remarks above state the impact which PV systems have on the transient stability. It is also important to highlight when significant decrease in transient stability is witnessed. If the total short-circuit current at a faulted bus is highly contributed by synchronous generation units, then for certain situations in which SG units are put out of service, the short-circuit current at such a bus might decrease significantly henceforth potentially leading to harmful effects for the transient stability. Also, if a fault occurs at a bus near a synchronous generation unit which contains a low short-circuit current, transient stability problems might arise when such a synchronous generation unit is operating at a high operating point (close to it's active power limit and under-excited).

6.4.4. Mitigation measure(s)

In this sub-section mitigation measures shall be proposed to increase the critical clearing time at a faulted bus and hence the transient stability. The measures which will be discussed are,

1. Operating point of synchronous generator

2. Addition of reactive compensation devices

3. Decreasing reactance between synchronous generator and faulted bus

Operating point of synchronous generator

As also demonstrated in Chapter 5, the operating point of the synchronous generator plays an important role in the transient stability. To illustrate this point once more and to delve a bit deeper, the bus at *Geertruidenberg* (connections at this bus are shown in Figure 6.11) shall be evaluated and the operating point of the synchronous generator nearby (SG 87000) shall be given varying operating points. To examine the impact of operating point of the synchronous generator on the transient stability, case 2 has been used. The maximum active power output (*Pmax*) and the MVA base of the generator at bus 87000 near *GT150-B* is provided in Table 6.23.

SG at bus	**Pmax (MW)**	**S (MVA)**
87000	650	812.50

Table 6.23: Parameters of synchronous generator at bus 87000

The different operating points are provided in Table 6.24.

Synchronous Generator (87000)	**P (MW)**	**Q (Mvar)**
Operating Point 1	620	90.00
Operating Point 2	620	0.00
Operating Point 3	620	-45.00
Operating Point 4	450	30.00
Operating Point 5	450	-30.00
Operating Point 6	250	0

Table 6.24: Operating points of synchronous generator at bus 87000

The critical clearing times for the above mentioned cases are shown in Table 6.25.

Case	CCT (ms)
Operating Point 1	274
Operating Point 2	256
Operating Point 3	242
Operating Point 4	387
Operating Point 5	359
Operating Point 6	>400

Table 6.25: CCT for different operating points of synchronous generator at bus 87000

In Table 6.25, it is seen that the critical clearing time for operating point 1 till 3 yields the lowest critical clearing times compared to the other cases. For these operating points only the reactive power output of the synchronous generator has been varied, while the active power output is close to it's limit. These operating points yield the lowest critical clearing times due to the fact that the rotor angle is at a higher operating point yielding less margin for transient stability. In these cases, it is due to the high amount of active power being generated relative to the Pmax of the generator. Additionally, it is also seen that the critical clearing time for operating point 3 is the worst. Thus, the synchronous generator is at it's most critical when a combination of high amount of active power generation and an under-excited generator is present. Similar conclusions can be drawn when looking at operating point 4 and 5, where it is seen that the under-excited generator decreases the critical clearing time significantly. On the other hand, it is seen that the active power generation is not as high compared to operating points 1 till 3 and hence the critical clearing time is not as low. Concludingly, it is illustrated that the transient stability is highly dependent on the operating point of the synchronous generator. Furthermore, the operating point of the generator has the most significant effect on the transient stability when the active power generation is close to it's limits and the generator is under-excited. Ensuingly, for critical areas where synchronous generators are in danger of losing synchronism, limitations can be set on the synchronous generators near such relevant areas w.r.t. the active power production and reactive power output to improve the transient stability.

Addition of reactive compensation device
As presented in the analysis of Section 6.4.3, the short-circuit current at the faulted bus also has a significant say in the transient stability. To illustrate this phenomena, case 2 at the bus of *Eerbeek* is looked at without and with the addition of a reactive compensation device. The reactive compensation device has been added to the high voltage bus, in this case bus *EBK150-A*. The added reactive compensation device details are provided in Table 6.26.

	S (MVA)
Synchronous condenser (SC)	500

Table 6.26: Addition of reactive compensation device

The critical clearing time of these two cases is shown in Table 6.27.

Case	CCT (ms)
Without SC	268
With SC	293

Table 6.27: CCT with and without synchronous condenser

As shown in Table 6.27, the critical clearing time for the case with reactive compensation device has increased compared to the case without. This is due to the short-circuit current contribution of the added device. An example of such devices are synchronous condensers or static compensators (STATCOM). Conclusively, it was shown that by adding a reactive compensation device such as a synchronous condenser or STATCOM, the total short-circuit current at the faulted bus increases hence improving the transient stability. Additionally, such devices also contribute to the voltage

support which will be discussed in the following section.

Decrease reactance

Another mitigation measure which can be taken, albeit a very cost intensive one, is decreasing the reactance of the lines/cables in between the synchronous generator and the faulted bus. To demonstrate this point, case 2 has been looked at and modified by decreasing the reactance of the line between the synchronous generator at bus 87000 and the faulted bus *GT150-B*. The initial and modified reactance is provided in Table 6.28.

Case	X (pu)
Initial reactance	0.001430
Modified reactance	0.0004

Table 6.28: Modified reactance of line between SG at bus 87000 and GT150-B

The critical clearing time for the two cases is shown in Table 6.29.

Case	CCT (ms)
Initial reactance	274
Decreased reactance	279

Table 6.29: CCT initial and modified reactance line of synchronous generator at bus 87000

As shown in Table 6.29, by decreasing the reactance between the synchronous generator and the faulted bus, the critical clearing time increases. This can be explained by looking at the power flow transfer equation shown in Equation 6.10 and 6.11.

$$P = \frac{V_r \times V_s}{X} \cdot sin\delta \tag{6.10}$$

$$Q = \frac{V_r}{X}(V_s \cdot cos\delta - V_r) \tag{6.11}$$

As shown in Equation 6.10 and 6.11, the reactance is inversely proportional to the amount of active and reactive power transferred. Hence, when decreasing the reactance of the line from the synchronous generator to the faulted bus, less losses occur in terms of reactive power when the reactance is decreased, hence leading to a wider transient stability margin. Realistically, this can be achieved by two methods,

- By replacing the line/cable from the synchronous generator to the faulted bus with a line/cable with lower reactance. This alternative is very costly and does not provide any direct benefits other than an improved robustness and transfer capacity of added line. However, since the line will be completely replaced, the replacing line/cable can yield a low reactance.

- By adding a parallel line from synchronous generator to the faulted such that the equivalent reactance is hence decreased. This alternative offers redundancy and the ability to spread the transfer over two lines. However, as the equivalent reactance is also a function of the existing line/cable, this poses a limitation for the decrease in equivalent reactance.

6.5. Short-term voltage stability

6.5.1. Introduction

In this section, the short-term voltage stability for the four cases discussed in Section 6.2 shall be evaluated. The analysis shall look at the selected snapshots and evaluate the differences among them. Three-phase faults shall be introduced in areas with high short-circuit contribution by synchronous generation units so that the differences between cases can be distinctly seen. The main important factor influencing short-term voltage stability is the short-circuit current. The two factors which shall be studied are,

- The magnitude of the voltage dips and the spread in the network
- The voltage recovery

6.5.2. Results & Analysis

In this section, the voltage stability shall be evaluated, in particular the amplitude of the voltage dips, the depth of the voltage spread throughout the network and the voltage recovery witnessed for the different cases. The analysis shall be conducted by looking at the short circuit current at a particular bus.

Voltage drop and spread

For the analysis concerning voltage drop and spread, a fault is simulated at a bus of interest for a duration of 100 ms. In a similar manner as presented in Chapter 5, the voltage dips at nearby buses shall be evaluated with Equation 6.12.

$$\% \text{ Voltage drop at bus} = \frac{\text{Initial voltage - Voltage (t=1.1s right before clearance)}}{\text{Initial voltage}} \times 100\% \qquad (6.12)$$

The bus named *Geertruidenberg* also abbreviated by *GT150-B* with a voltage level of 150 kV shall be evaluated. This bus is located in North Brabant, this area contains a lot of PV systems in the FSI 2030 scenario. Additionally, the synchronous generation units contribute significantly to the short-circuit current, hence for case 4 (reduced SG case) the impact of the out of service SGs on voltage stability can be clearly witnessed. A three-phase bolted fault has been introduced at this bus at t=1s, lasting for a total of 100 ms. The propagation of the voltage dips to the nearby buses shall be evaluated. A bus (ZBH150 Z) directly connected to the faulted bus is evaluated. Then from this bus (ZBH150 Z) another bus connected to this bus (MDK150-A) has been evaluated, and so forth. This has been done to evaluate the voltage propagation as the electrical distance from the fault increases. The buses of interest are shown in Figure 6.14.
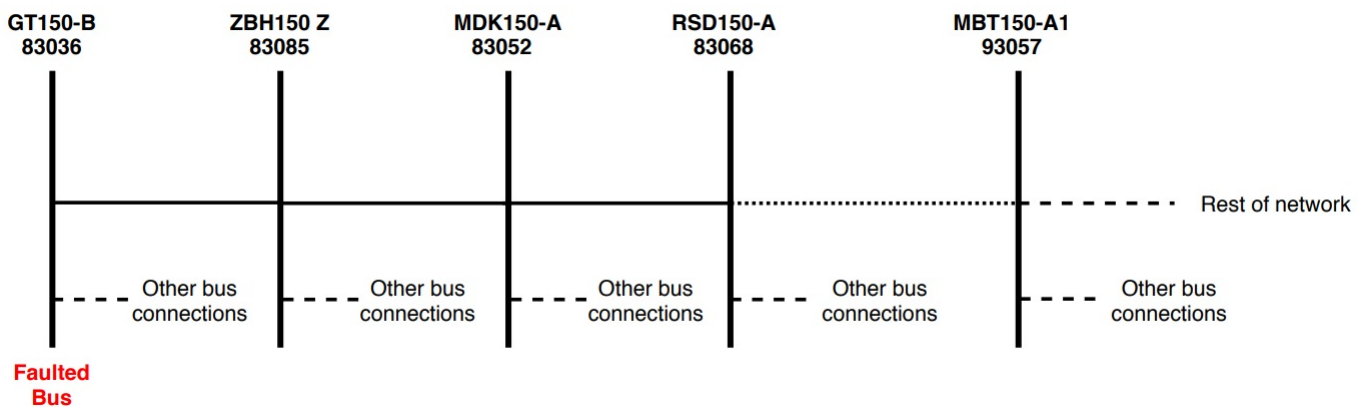
Figure 6.14: Buses near *GT150-B*

Besides looking at the behaviour of the voltage drops for the four cases, four other scenarios are also viewed in which the contribution of the PV systems is nullified. The voltage drops at the buses provided in Figure 6.14 are shown in Table 6.30. The abbreviation *DM* refers to the case with dynamic models for the PV systems while *NL* refers to the representation of PV systems with negative load.

	GT150-B	ZBH 150 Z	MDK150-A	RSD150-A
Case 1 DM	100%	81.60%	71.84%	64.16%
Case 1 NL	100%	86.18%	78.85%	75.70%
Case 2 DM	100%	84.75%	76.62%	67.24%
Case 2 NL	100%	89.56%	84.00%	79.15%
Case 3 DM	100%	84.07%	75.52%	65.89%
Case 3 NL	100%	89.21%	83.42%	78.36%
Case 4 DM	100%	88.24%	81.93%	69.77%
Case 4 NL	100%	94.21%	91.11%	83.96%

Table 6.30: Voltage drops for fault at bus *GT150-B*

Table 6.30 yields information regarding the voltage dips at the buses of interest. First of all, it can be seen that the voltage dips decrease, as the electrical distance from the faulted bus increases. This behaviour is expected and was also demonstrated in Chapter 5. The further a bus is located from the faulted bus in terms of electrical distance, the lower voltage dip witnessed at that bus. Additionally, when comparing the individual cases with dynamic models and with negative load, it is shown that the voltage dips are more pronounced at the buses for the negative load cases. This is also to be expected, as the contribution of short-circuit current of the PV systems has been excluded.

Now the focus shall be turned to the cases with dynamic models. For a better overview of the various cases with dynamic models, the values are once again provided in Table 6.31.

	GT150-B	ZBH 150 Z	MDK150-A	RSD150-A
Case 1 DM	100%	81.60%	71.84%	64.16%
Case 2 DM	100%	84.75%	76.62%	67.24%
Case 3 DM	100%	84.07%	75.52%	65.89%
Case 4 DM	100%	88.24%	81.93%	69.77%

Table 6.31: Voltage drops for fault at bus *GT150-B* of cases with dynamic models

When comparing the cases with dynamic models, it is seen that case 1 has the least severe voltage dips. Additionally, case 2 and 3 have approximately similar voltage dips at the evaluated buses. Moreover, case 4 witnesses a significantly higher voltage dip at the different buses compared to the other cases. This is demonstrated in Figure 6.15 [5].

---

[5]The figures provided show that the voltage level following the fault remain a bit higher than the initial voltage, this is due to an assertive reactive current injection by the SG 87000. Eventually, the voltage values stabilise to their initial value.

(a) Voltage at bus *GT150-B*

(b) Voltage at bus *ZBH 150 Z*

(c) Voltage at bus *MDK150-A*

(d) Voltage at bus *RSD150-A*
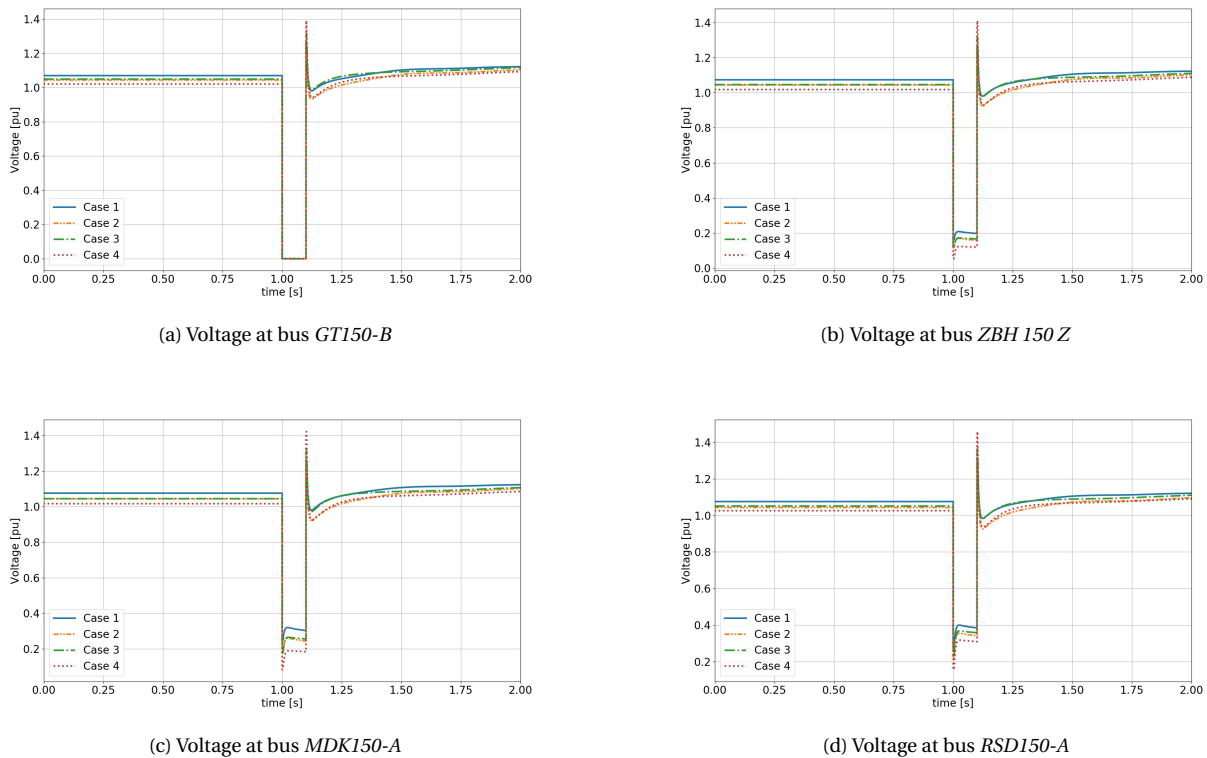
Figure 6.15: Voltages at buses near and at *GT150-B*

The results provided in Table 6.30 are confirmed by the Figures 6.15, where it is shown that the voltage dip for case 1 is the least severe, the voltage dip for case 2 and 3 are approximately similar while the voltage dip for case 4 relative to it's initial voltage is the highest. This variation can be explained by looking at the short-circuit current at the faulted *GT150-B* bus. The short-circuit current at this bus is provided in Table 6.32.

Case	**Short-circuit current (kA)**
Case 1	59.64
Case 2	57.26
Case 3	57.32
Case 4	54.25

Table 6.32: Short-circuit current at bus *GT150-B*

In Table 6.32, it is shown that case 1 possesses a high short-circuit current at the faulted bus. In consequence, the voltage dips for this case are the lowest. Moreover, case 2 and 3 yield a similar short-circuit current at the faulted bus, and hence the voltage dips for these cases are congruous. When looking at case 4, the short-circuit current has diminished as certain synchronous generators which contributed in case 1, 2 and 3, have been put out of service. This decreased short-circuit current at the faulted bus is the primary cause for the increase of magnitude in voltage dips.

It is also of interest to evaluate the voltage dips at a location further away from the buses discussed above. Consequently, the behaviour of a bus located in Limburg, bus *MBT150-A1*, shall be evaluated. This bus is connected via the 380 kV network to the faulted bus, hence is located electrically very far from the faulted bus. The voltage dips of the various cases at this bus are provided in Table 6.33. The voltage behaviour of the various cases is shown in Figure 6.16.

	MBT150-A1
Case 1 DM	8.16%
Case 2 DM	9.96%
Case 3 DM	9.28%
Case 4 DM	11.56%

Table 6.33: Voltage drops at *MBT150-A1* for fault at bus *GT150-B*
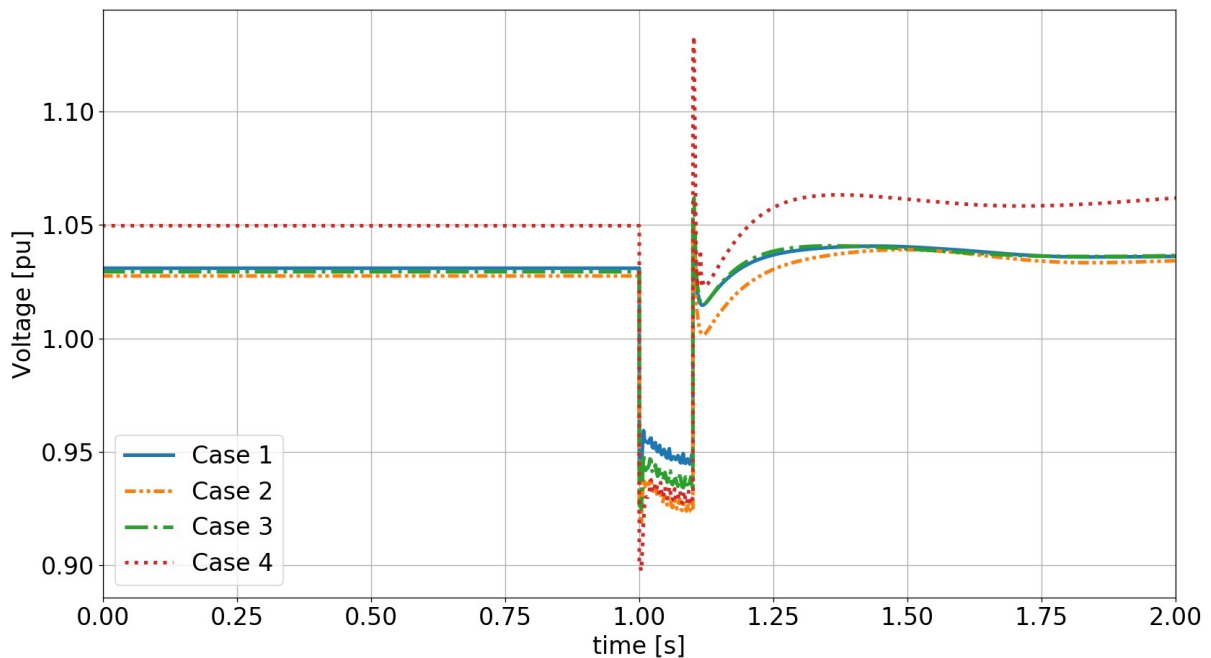
Figure 6.16: Voltage at bus *MBT150-A1*

As illustrated in Figure 6.16 and Table 6.33, similarly as the voltage dips shown for the buses nearby the faulted bus, it is seen that for bus *MBT150-A1* the magnitude of the voltage dip seen for case 1 is the lowest while for cases 2 and 3 the dips are of higher magnitude and approximately equal for these two cases. Furthermore, the highest voltage drop is witnessed for case 4 when evaluating the bus located electrically far from the fault. Hence, it can be concluded that a lower total short-circuit current in the network causes the voltage dips to be more severe and to penetrate further into the network. In similar fashion as discussed for transient stability, by phasing out synchronous generators and adding new PV systems, the short-circuit current in the various regions is decreasing. To this end, the voltage dips shall increase in magnitude while the fault shall influence a larger part of the system with regards to voltage. Additionally, as shown in Table 6.30, for areas with a high SCC PV ratio, the PV systems play a vital role in limiting the voltage drop due to their short-circuit contribution. This is most clearly seen when comparing the dynamic model and negative load scenario of case 4 of Table 6.30.

Voltage recovery
Another important aspect of voltage stability is the manner in which the voltage recovers following the clearance of a fault. For this analysis, a three-phase bus fault introduced at *Veenoord*, abbreviated by *VO110-B*, shall be evaluated. At this particular bus, PV systems are connected and a SG generator is connected nearby as shown in Figure 6.17.
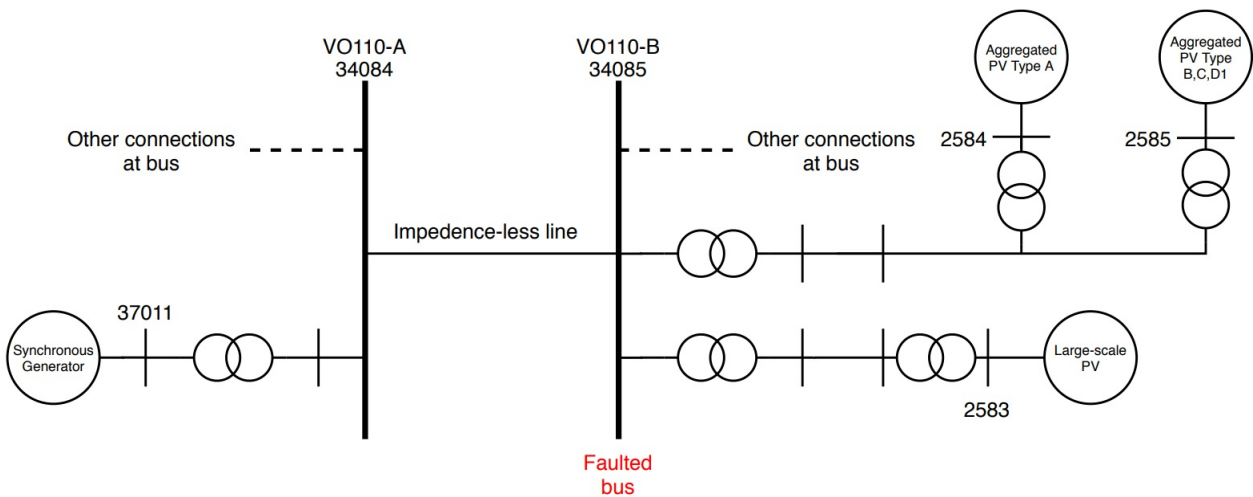
Figure 6.17: Connections at VO110-B bus

The first comparison compares the cases in which PV systems are represented with dynamic models to the cases in which the PV systems are represented as negative load. This comparison is provided in Figure 6.18.

(a) Case 1

(b) Case 2

(c) Case 3

(d) Case 4
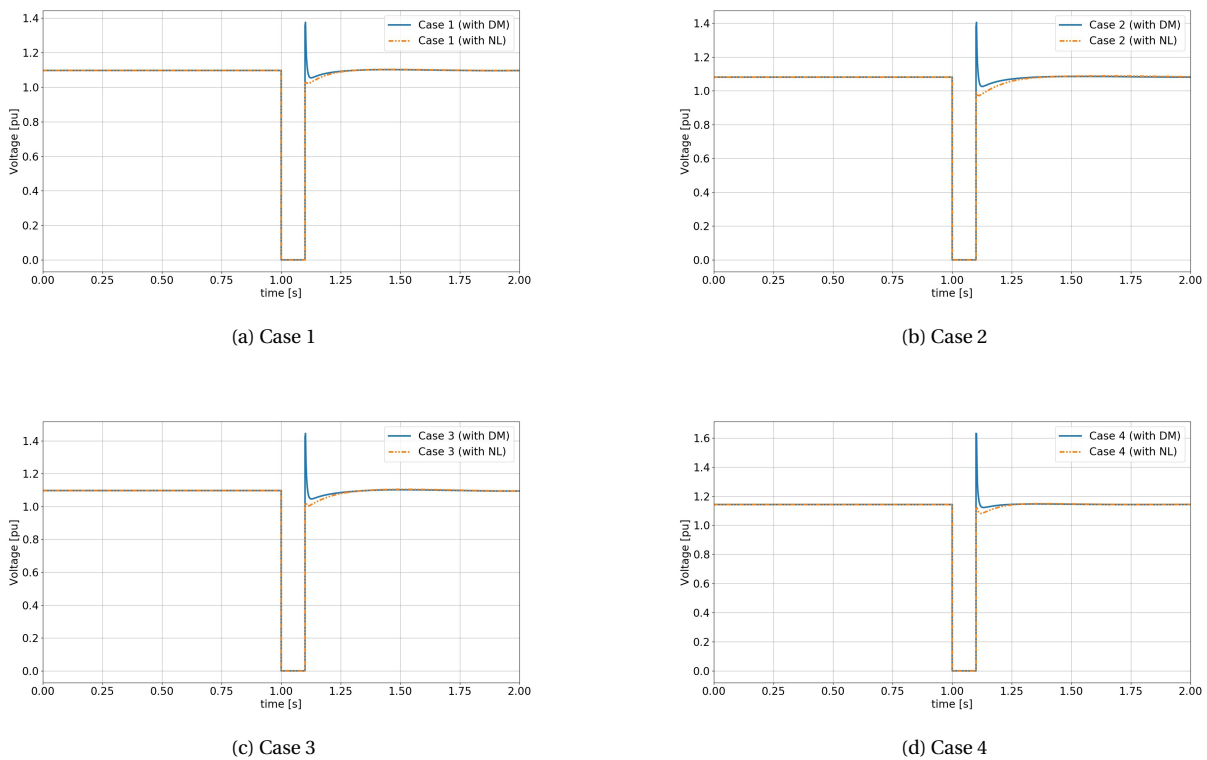
Figure 6.18: Comparison of voltage recovery between DM and NL at VO110-B

As shown in Figures 6.18, the voltage recovery for the PV systems represented as dynamic model is slightly better compared to the representation with negative load. Again, this is to be expected as the short-circuit contribution of the PV systems aids the voltage recovery. The voltage peak at the time instance of fault clearing can be neglected as discussed in Chapter 5.

Furthermore, it is also interesting to evaluate the voltage at the terminals of the large-scale PV system at bus 2583. In this evaluation a comparison is made for different reactive current gains (Kqv) of the large-scale PV system. Additionally, the FRT profile according to the grid connection requirements is also displayed to determine if the voltage of the PV system drops below this profile. Figure 6.19 provides the comparison.
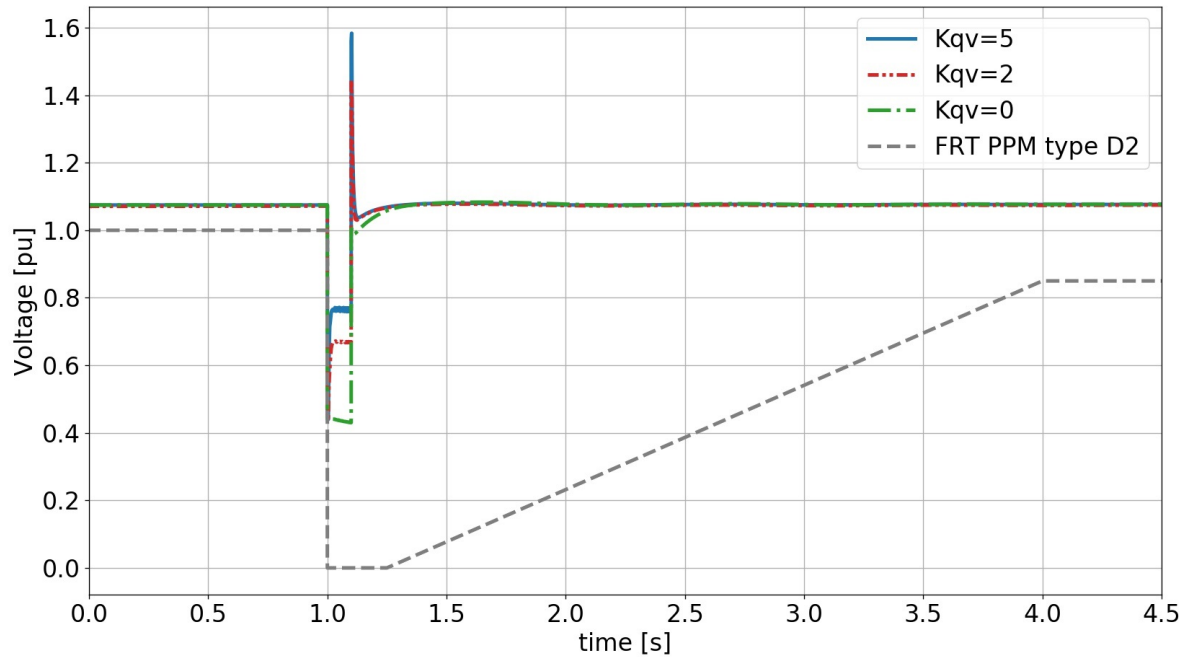
Figure 6.19: Voltage at large-scale PV system at bus 2583 for case 2

Figure 6.19 displays the voltage of the large-scale PV systems at bus 2583 connected at the faulted bus *VO110-B*. The first thing that stands out in Figure 6.19, is that the voltage at the terminals of the PV system does not drop below the FRT profile thus the PV system should remain connected to the grid. Additionally, the figure shows that the voltage drop for the various cases differ. The distinction in voltage drop stems from the changes made to the reactive current gain (Kqv). For the reactive current gain value 5, the voltage drop is the least severe as the most reactive current is injected by the PV system for this value. In stark contrast stands the case with a reactive current gain of 0, here the voltage drop is the most severe as no reactive current is injected from the PV system. To gain a bit more insight into the voltage drops for the various cases, the reactive current injection of this PV system is provided in Figure 6.20.
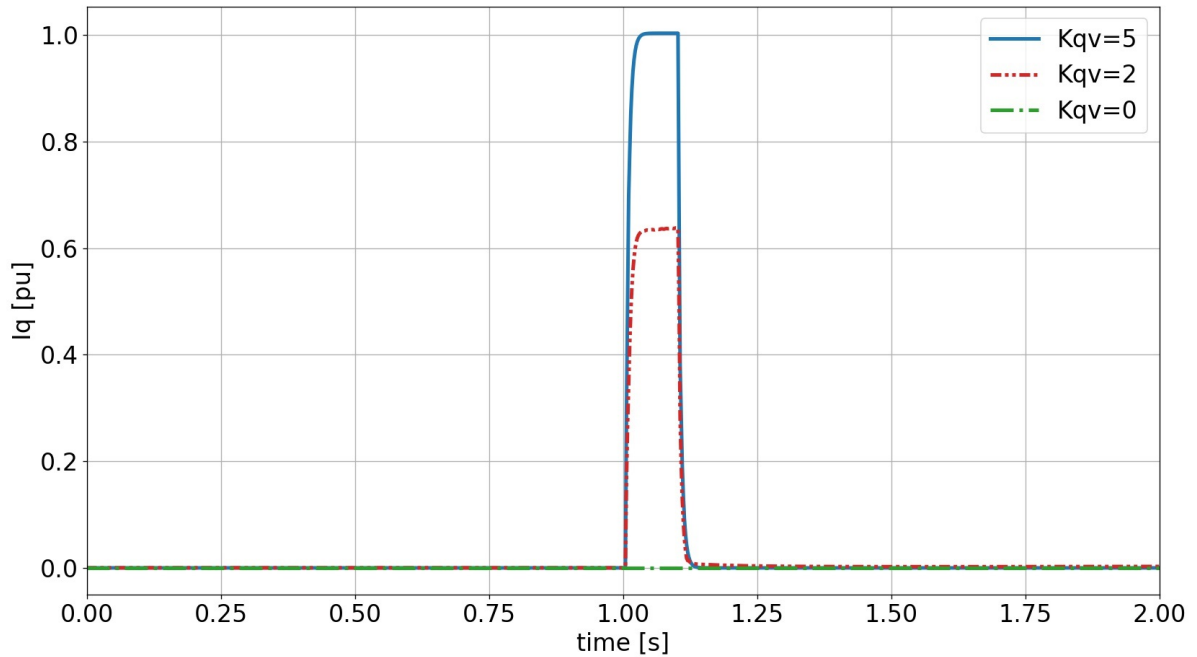
Figure 6.20: Reactive current injection from large-scale PV system at bus 2583 for case 2

The values provided in Figure 6.20 are based on the base of the PV system. As shown in Figure 6.20, the reactive current injection for the various cases is consistent with the results shown in Figure 6.19 — the higher the reactive current injection of the PV system, the lower the voltage dip witnessed at the terminals of the PV system.

Lastly, it is also of importance to evaluate the voltage at the terminals of the synchronous generator nearby i.e. the SG at bus 37011. Similarly, the voltage at the terminals of the synchronous generator is compared to the FRT profile established in the grid connection requirements for synchronous generators. The voltage at the terminals of the synchronous generator at bus 37011 is provided in Figure 6.21[6]. The FRT profile before the occurrence of the fault should not be taken into account. Figure 6.21 shows that the synchronous generator for this particular fault does not drop below the FRT profile.

---

[6]For case 4 the generator at bus 37011 was out of service hence the response is not shown
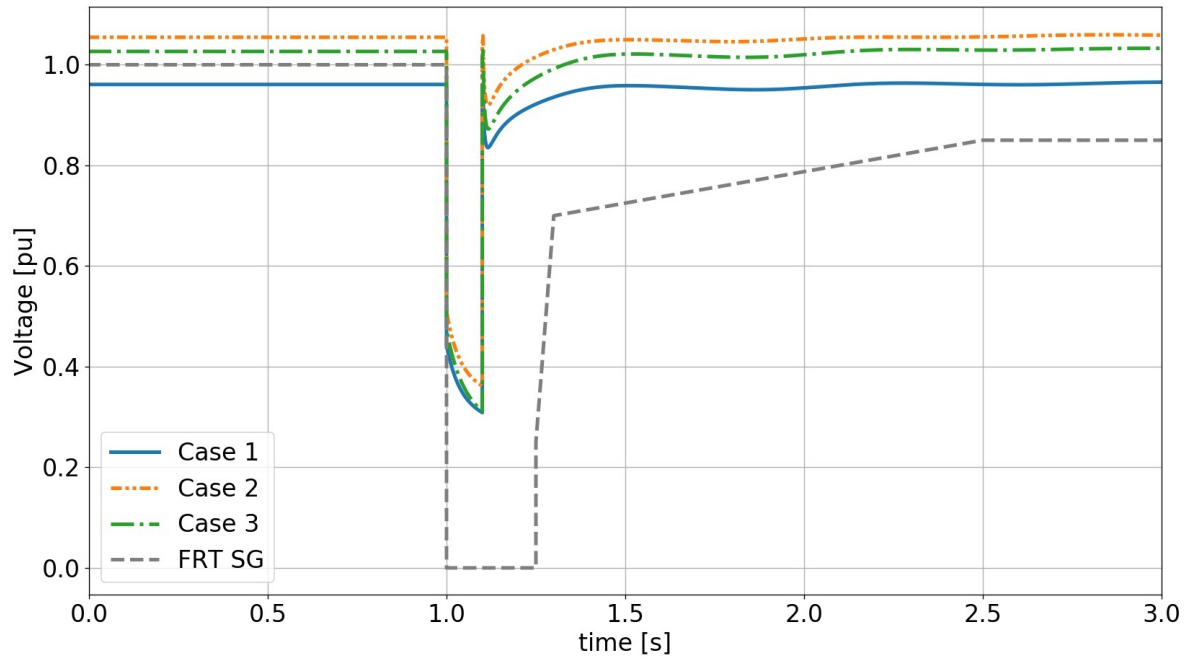
Figure 6.21: Voltage at synchronous generator at bus 37011

Summary & Overview
In the analysis above, the magnitude of the voltage dips and the spread of the voltage dips were evaluated by examining a bus fault at *Geertruidenberg*. In this analysis, the voltage dips of surrounding buses were evaluated and a bus located electrically distanced from the faulted bus. The analysis pointed out that as the total short-circuit current reduced at the faulted bus, the voltage dips seen at nearby and the bus located further away, increased. Additionally, from the bus located far away from the fault, it was concluded that the voltage spread is more extensive for cases with a lower total short-circuit current. Evidently, it was also shown that the PV systems also contribute to decreasing the voltage dips witnessed as the comparison of PV representation with dynamic models and negative load yielded deeper voltage drops for the negative load cases.

For voltage recovery, a comparison was made between the representation of PV systems with dynamic models and as negative load. From this analysis, the voltage recovery for the PV systems represented with dynamic models was slightly better compared to the negative load case. The improvement in voltage recovery is once more due to the provided short-circuit current contribution of the PV systems.

Furthermore, it was shown that the voltage at the PV system terminals and also the rest of the network is also dependent on the reactive current gain of the PV systems with the highest value of 5 yielding the lowest voltage drops. Moreover, it was shown that the PV systems and the synchronous generators did not drop below their respective FRT profiles for the evaluated case.

Similarly as concluded for transient stability but even more so for voltage stability (since transient stability is also generally dependent on other factors while short-term voltage stability is predominately dependent on the short-circuit current), the short-circuit current plays a vital role in the magnitude of the voltage drops, voltage spread and voltage recovery. As more synchronous generators are phased out, and RES such as PV systems are added to the network, areas/regions shall shift towards lower short-circuit ratios hence the power system networks shall be at greater risk of being confronted with voltage instability phenomena should mitigation measures not be taken.

6.5.3. Mitigation measure(s)
In the analysis it was demonstrated that the voltage stability (i.e. magnitude of voltage dips and voltage recovery) is highly dependent on the amount of short-circuit current available. Henceforth, a mitigation measure which could increase the voltage stability is to increase the amount of short-circuit current available. As also discussed in transient

stability, this can be achieved with the use of reactive compensation devices such as synchronous condenser or static compensator/condenser. To show the effectiveness of the addition of a reactive compensation device on the voltage stability, the case of *Geertruidenberg* is once again looked at with the addition of a synchronous condenser with the capacity as shown in Table 6.34.

	S (MVA)
Synchronous condenser (SC)	500

Table 6.34: Addition of synchronous condenser to improve voltage stability at bus *RSD150-A*

The synchronous condenser has been added to the HV bus *RSD150-A*. The voltage drop with the added synchronous condenser for the various cases is provided in Table 6.35.

	GT150-B	ZBM 150 Z	MDK150-A	RSD150-A
Case 1 DM	100%	81.60%	71.84%	64.16%
Case 1 with SC	100%	79.68%	68.90%	58.09%
Case 2 DM	100%	84.75%	76.62%	67.24%
Case 2 with SC	100%	82.65%	73.39%	60.79%
Case 3 DM	100%	84.07%	75.52%	65.89%
Case 3 with SC	100%	82.03%	72.39%	59.72%
Case 4 DM	100%	88.24%	81.93%	69.77%
Case 4 with SC	100%	85.82%	78.23%	62.83%

Table 6.35: Voltage drops for fault at bus *GT150-B* with added synchronous condenser

As shown in Table 6.35, the voltage dips witnessed at the buses nearby bus *GT150-B* have decreased. This decrease is achieved due to the added synchronous condenser at bus *RSD150-A* as the total short-circuit current is increased.

It should also be noted that when looking at bus *MBT150-A1*, located electrically further, the voltage dips presented in Table 6.36 are seen.

	MBT150-A1
Case 1 DM	8.16%
Case 1 with SC	8.15%
Case 2 DM	9.96%
Case 2 with SC	9.77%
Case 3 DM	9.28%
Case 3 with SC	9.23%
Case 4 DM	11.56%
Case 4 with SC	11.60%

Table 6.36: Voltage drops for fault at bus *GT150-B* with added synchronous condenser at bus *RSD150-A*

As presented in Table 6.36, the added synchronous condenser at bus *RSD150-A* has limited to no effect on the voltage dips witnessed further in the network. This is due to the fact that the added synchronous condenser is not located near the bus *MBT150-A1*, and the transfer of reactive power through this bus remains more or less equivalent to the initial

case. Henceforth, the placement of such a reactive compensation device is of high importance towards the increase in short-term voltage stability. A method for optimal allocation of dynamic var sources is described in detail in [43].

7

Conclusions & Future Work

7.1. Conclusions

The research questions defined in Chapter 1 shall be repeated and answered subsequently.

RQ1 *How can a model structure and default parameter set be developed for individual (future) solar PV PPMs?*

The selection of a dynamic model for representing the generic behaviour of (future) large-scale PV systems has been appointed to the large-scale PV Model. This model is the standard for modelling large-scale PV systems for stability studies. Additionally, the IEC 614700-12-2 would also be a possibility to represent the behaviour of large-scale PV, however, since this model has not been made publicly available it has been excluded from the selection procedure. The large-scale PV model consists of 3 separate modules with their own parameter sets. The parameters of the modules which aligned with the grid connection requirements were determined by the grid connection requirements — such important parameters are the reactive current gain and the reactive current injection deadband. Parameters which are manufacturer dependent were assigned values of existing PV systems in the Dutch grid. Furthermore, certain parameters did not have influence on the dynamic behaviour of the PV system, these were assigned by typical values. Finally, for the remaining parameters, a sensitivity study and literature research were combined to assign these values. With the above-mentioned steps a full parameter set was attained for the large-scale PV model.

RQ2 *How does the transient stability in the Dutch high voltage grid change with increased penetration levels of solar PV?*

The analysis of the transient stability was conducted in such a manner as to isolate the behaviour of the short-circuit current on the transient stability. This was achieved by evaluating a certain bus and setting the synchronous generator near that bus to a fixed operating point across all cases. Additionally, the voltage of this generator bus was brought within a range of 0.01 pu across the cases. These changes have been made to solely evaluate the impact of short-circuit current on the transient stability. The analysis concluded that the impact of PV systems (at a bus near a synchronous generator) on the transient stability is predominantly determined by the SCC PV ratio equation defined. This relationship defined the amount of short-circuit contribution by the PV systems relative to the total short-circuit current at the faulted bus. As this ratio became higher, the PV systems started to have a bigger impact on the transient stability. On the other hand, when the SCC PV ratio was low, it was shown that PV systems had minimal impact on the transient stability. As PV systems are being added to power systems and synchronous generation units are being decommissioned, more areas will tend towards high SCC PV ratios hence the impact of the PV systems on the transient stability will only increase. Concerning the overall transient stability, it was shown that the total short-circuit current will diminish in power systems as synchronous generation units are being replaced by PV systems therefore leading to an overall decrease in transient stability.

RQ3 *What impact does increased penetration of solar PV have on the voltage stability of the Dutch high voltage grid?*

For the voltage stability analysis three different aspects were evaluated namely the voltage drop, voltage spread and voltage recovery. For the first two aspects, a fault was introduced at a bus and it was shown that the voltage drop decreased for distances further away from the faulted bus. The first comparison which was made was between a case with dynamic models and negative load representing PV systems. In this comparison, the cases with negative load yielded deeper voltage dips as the reactive current contribution of the PV systems was omitted. Additionally, when comparing the cases with all dynamic models, the conclusion was made that the

case with the highest total short-circuit current at the faulted bus yielded the least severe voltage drops. On the contrary, the case with the lowest total short-circuit current provided the highest voltage drops. From this was concluded that the voltage drops witnessed at nearby buses are highly dependent on the total short-circuit current at the faulted bus. Moreover, a bus located electrically very far from the faulted bus was evaluated. The analysis yielded similar results, as the voltage drop at this far located bus was most severe for lowest total short-circuit current case. Hence, it was demonstrated that the lower the total short-circuit current, the wider the spread of voltage witnessed in the network. In similar fashion, it was shown that the voltage recovery was also dependent on the total short-circuit current with high levels yielding faster recovery times. In addition, it was demonstrated that no breach of the FRT profile was found in the studied cases. Ultimately, as synchronous generation units are eliminated and PV systems are added, the short-circuit ratios in various regions shall decrease and thus lead to deeper voltage dips, larger areas of the network being affected by a contingency and slower voltage recovery times.

RQ4 *How can a rule of thumb be developed to determine at which penetration level mitigation measures are needed in the relevant areas?*

From the studied cases of both transient- and voltage stability, none of the cases yielded very critical scenarios. However, a certain number of aspects can lead a certain area to be more vulnerable to power system instability. Concerning transient stability, it was shown that a fault occurring at a bus in close proximity to a synchronous generator, which is operating close to it's limits, significantly deteriorates the transient stability. Another influencing factor was the total short-circuit current present at the faulted bus. Henceforth, areas are most vulnerable for transient instability when synchronous generators are operating close to their limits and the area possesses a low short-circuit ratio. For voltage stability, as also discussed in the analysis, the main influencing factor happens to be the short-circuit current at the faulted bus. Henceforth, voltage is most vulnerable to instability in areas with low short-circuit ratios.

RQ5 *What type of mitigation measures can be introduced to reduce the potential consequences of high penetration solar PV?*

In the analysis mitigation measures were proposed to enhance the transient- or short-term voltage stability. As regards transient stability, it was firstly discussed that the operating points of synchronous generators influence the transient stability drastically. More specifically, when a critical synchronous generator operates close to it's active power limits and is under-excited, the transient stability declines. Henceforth, by limiting the operating region of critical synchronous generators, this influencing factor on the transient stability can be minimised. Additionally, it was shown that the short-circuit current plays an important role in the transient stability. By adding a reactive compensation device which aids the short-circuit current, the transient stability can also be improved. Furthermore, by decreasing the reactance between the synchronous generator and the faulted HV bus, the amount of reactive power losses are reduced hence the transient stability increases. Concerning voltage stability, the main important factor is the short-circuit current. Hence, similar as proposed for transient stability, by adding a reactive compensation device which can contribute to the short-circuit current, the voltage stability can be improved.

7.2. Future Work

- Currently, the large-scale PV model does not posses an inherent module to provide the fault-ride-through profile. An expansion of this model would be to implement a fault-ride-through logic so that the unit represented can be disconnected accordingly.

- In this research project, the underlying elements (LV/MV transformer equivalent, collector system equivalent and the station transformer) were represented by standard parameters discussed in Appendix E. A more detailed set of standard parameters is discussed in [44]. The implementation of these parameters, however, leaded to convergence problems. To this end, a future work proposal is to resolve these convergence problems and to implement a more detailed set of parameters for the underlying elements.

- This research focused on the development of a standard parameter set for PV systems. Additionally, the transient- and short-term voltage stability were examined under high levels of solar PV systems. A similar study can be conducted for wind farms.

A
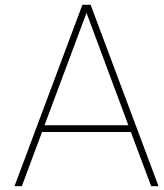
Parameter Sensitivity Study and Plant Controller Impact

A.1. Network
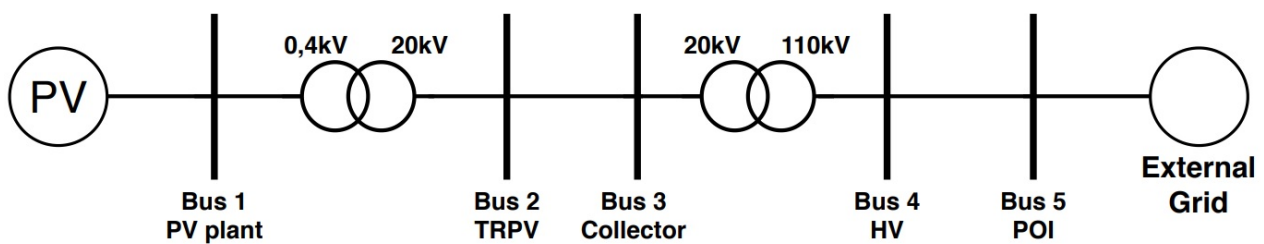
Figure A.1: Network for parameter sensitivity study

A.2. Parameters

PV plant:

Pmax with unity power factor (MW)
100

Table A.1: Parameters PV system

Transformers:

Transformer	From Bus (Voltage level)	To Bus (Voltage level)	R (pu)	X (pu)
1	1 (0,4 kV)	2 (20kV)	0.009	0,085
2	3 (20kV)	4 (110kV)	0.004	0.120

Table A.2: Transformer parameters

Transmission Lines:

Transmission Line	From Bus (Voltage)	To Bus (Voltage)	R (pu)	X (pu)	B (pu)	Length
1	2 (20kV)	3 (20kV)	0,000045	0,00012	0,00013	0.05
2	4 (110kV)	5 (110kV)	0,0037	0,0052	0,038	5.00

Table A.3: Transmission line parameters

External Grid:

Mbase (MVA)	Inertia	Damping Constant
2000	5	0

Table A.4: External grid parameters

A.3. Parameters of PV Models

A.3.1. REGC_A Module

Parameter	Description	Unit	Values
Lvplsw	Low Voltage Power Logic switch (0: LVPL not present, 1: LVPL present)	–	0
Tg	Converter time constant	s	0.005
Rrpwr	Low Voltage Power Logic (LVPL) ramp rate limit	pu	2.0
Brkpt	LVPL characteristic voltage 2	pu	0.70
Zerox	LVPL characteristic voltage 1	pu	0.10
Lvpl1	LVPL gain	pu	0
Volim	Voltage limit for high voltage reactive current management	pu	2
Lvpnt1	High voltage point for low voltage active current management	pu	0.8
Lvpnt0	Low voltage point for low voltage active current management	pu	0
Iolim	Current limit for high voltage reactive current management (specified as a negative value)	pu	-1.12
Tfltr	Voltage filter time constant for low voltage active current management	s	0.01
Khv	Overvoltage compensation gain used in the high voltage reactive current	–	0
Iqrmax	Upper limit on rate of change for reactive current	pu	99.0
Iqrmin	Lower limit on rate of change for reactive current	pu	-99.0
Accel	acceleration factor (0 < Accel ≤ 1)	–	1

Table A.5: Parameters of REGC_A used for sensitivity study

A.3.2. REEC_B Module

Parameter	Description	Unit	Values
Vdip	low voltage threshold to activate reactive current injection logic	pu	0.9
Vup	Voltage above which reactive current injection logic is activated	pu	1.1
Trv	Voltage filter time constant	s	0.01
dbd1	Voltage error dead band lower threshold (≤0)	pu	-0.1
dbd2	Voltage error dead band upper threshold (≥0)	pu	0.1
Kqv	Reactive current injection gain during over and undervoltage conditions	pu	2
Iqh1	Upper limit on reactive current injection Iqinj	pu	1
Iql1	Lower limit on reactive current injection Iqinj	pu	-1
Vref0	User defined reference (if 0, model initialises it to initial terminal voltage)	pu	0
Tp	Filter time constant for electrical power	s	0.02
QMax	limit for reactive power regulator	pu	0.6
QMin	limit for reactive power regulator	pu	-0.6
VMAX	Max. limit for voltage control	pu	1.5
VMIN	Min. limit for voltage control	pu	0.5
Kqp	Reactive power regulator proportional gain	pu	10
Kqi	Reactive power regulator integral gain	pu	0.1
Kvp	Voltage regulator proportional gain	pu	0.1
Kvi	Voltage regulator integral gain	pu	0
Tiq	Reactive current regulator time constant	s	1
dPmax	(>0) Power reference max. ramp rate	pu/s	10
dPmin	(<0) Power reference min. ramp rate	pu/s	-10
PMAX	Max. power limit	pu	1
PMIN	Min. power limit	pu	0
Imax	Maximum limit on total converter current	pu	1.12
Tpord	Power filter time constant	s	0.2

Table A.6: Parameters of REEC_B used for sensitivity study

A.3.3. REPC_A Module

Parameter	Description	Unit	Value
Tfltr	Voltage or reactive power measurement filter time constant	s	0.05
Kp	Reactive power PI control proportional gain	pu	0.2
Ki	Reactive power PI control integral gain	pu	0.058
Tft	Lead time constant	s	0.05
Tfv	Lag time constant	s	0
Vfrz	Voltage below which State s2 is frozen	pu	0
Rc	Line drop compenstation resistance	pu	0
Xc	Line drop compenstation reactance	pu	0
Kc	Reactive current compensation gain	pu	0
emax	upper limit on deadband output	pu	1
emin	lower limit on deadband output	pu	-1
dbd1	lower threshold for reactive power control deadband (≤ 0)	pu	-0.01
dbd2	upper threshold for reactive power control deadband (≥ 0)	pu	0.01
Qmax	Upper limit on output of V/Q control	pu	0.4
Qmin	Lower limit on output of V/Q control	pu	-0.4
Kpg	Proportional gain for power control	pu	0.04
Kig	Proportional gain for power control	pu	0.08
Tp	Real power measurement filter time constant	s	0.05
fdbd1	Deadband for frequency control, lower threshold (≤ 0)	Hz	0.2
fdbd2	Deadband for frequency control, upper threshold (≥ 0)	Hz	10
femax	frequency error upper limit	pu	1
femin	frequency error lower limit	pu	-1
Pmax	upper limit on power reference	pu	1.05
Pmin	lower limit on power reference	pu	0
Tg	Power Controller lag time constant	s	0.1
Ddn	droop for over-frequency conditions	pu	0
Dup	droop for under-frequency conditions	pu	0

Table A.7: Parameters of REPC_A Module used for sensitivity study

A.4. Plant Controller (REPC_A) Impact
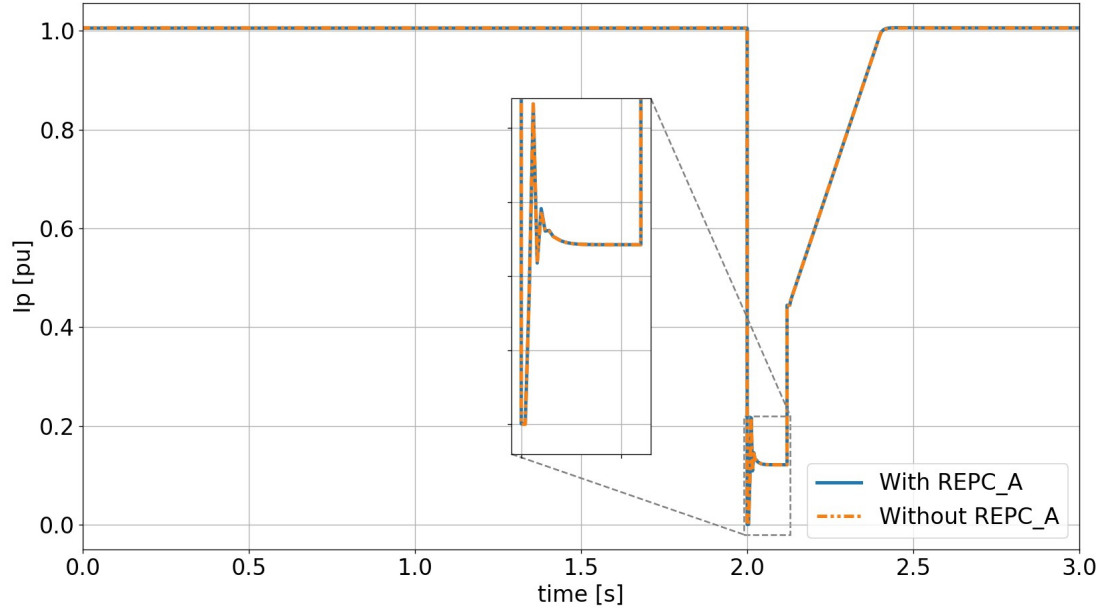
Figure A.2: Active current injection of PV system with and without REPC_A module
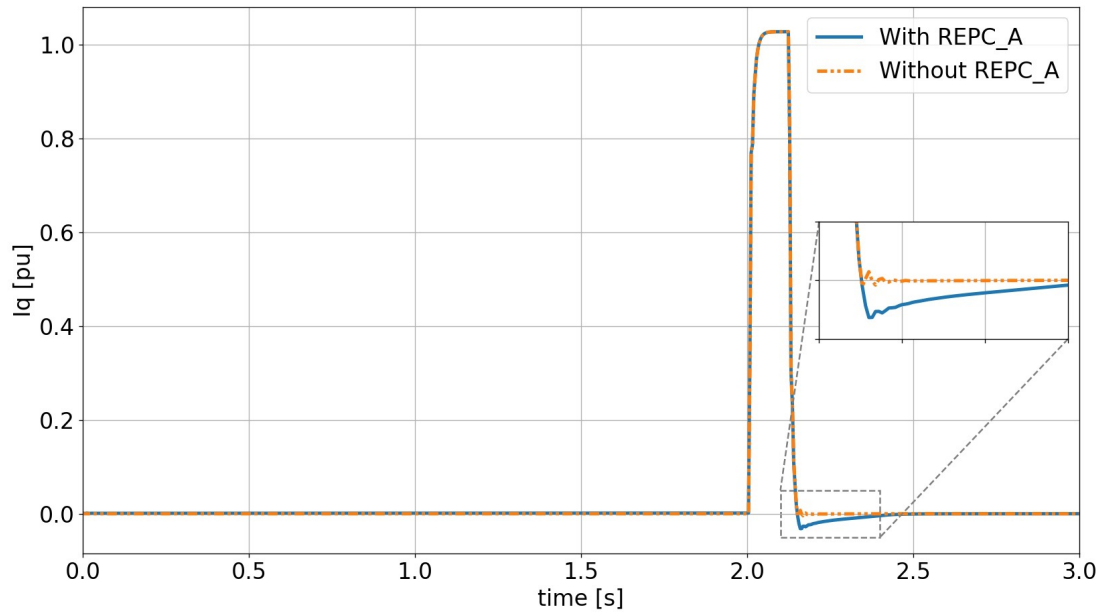
Figure A.3: Reactive current injection of PV system with and without REPC_A module
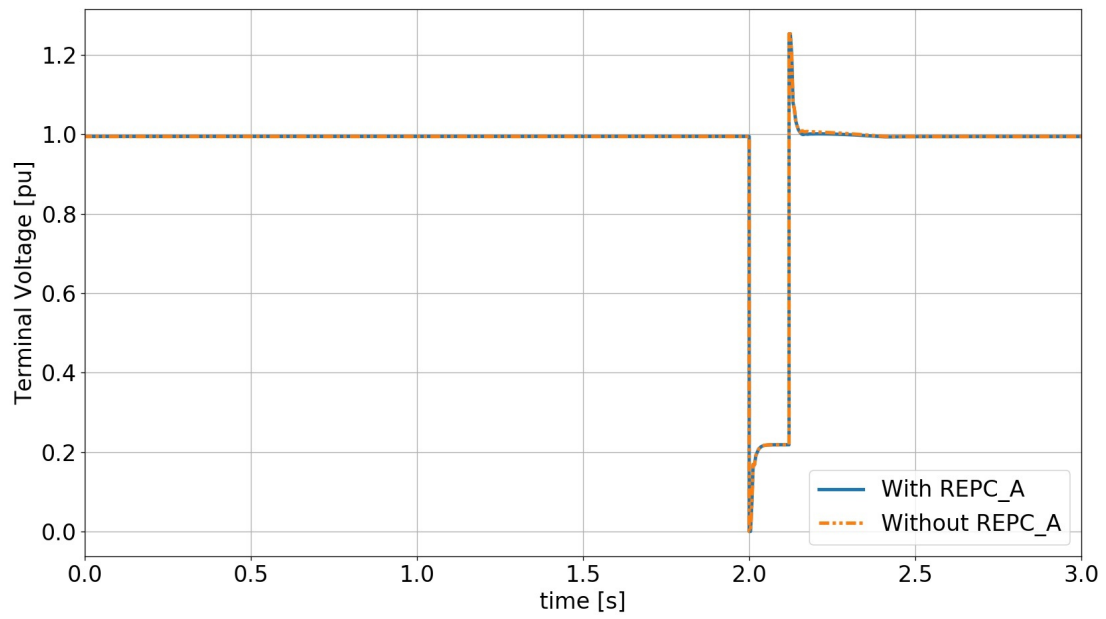
Figure A.4: Terminal voltage of PV system with and without REPC_A module

B
Proposed Parameter Set

B.1. REGC_A Module

Parameter	Description	Unit	Values
Tg	Converter time constant	s	0.005
Rrpwr	Low Voltage Power Logic (LVPL) ramp rate limit	pu	10.0
Brkpt	LVPL characteristic voltage 2	pu	0.70
Zerox	LVPL characteristic voltage 1	pu	0.10
Lvpl1	LVPL gain	pu	0
Volim	Voltage limit for high voltage reactive current management	pu	2
Lvpnt1	High voltage point for low voltage active current management	pu	0.8
Lvpnt0	Low voltage point for low voltage active current management	pu	0
Iolim	Current limit for high voltage reactive current management (specified as a negative value)	pu	-1.1
Tfltr	Voltage filter time constant for low voltage active current management	s	0.01
Khv	Overvoltage compensation gain used in the high voltage reactive current	–	0
Iqrmax	Upper limit on rate of change for reactive current	pu	99.0
Iqrmin	Lower limit on rate of change for reactive current	pu	99.0
Accel	acceleration factor (0 < Accel ≤ 1)	–	1

Table B.1: Parameters of REGC_A

B.2. REEC_B Module

Parameter	Description	Unit	Values
Vdip	low voltage threshold to activate reactive current injection logic	pu	0.90
Vup	Voltage above which reactive current injection logic is activated	pu	1.10
Trv	Voltage filter time constant	s	0.01
dbd1	Voltage error dead band lower threshold (≤ 0)	pu	-0.1
dbd2	Voltage error dead band upper threshold (≥ 0)	pu	0.1
Kqv	Reactive current injection gain during over and undervoltage conditions	pu	5
Iqh1	Upper limit on reactive current injection Iqinj	pu	1
Iql1	Lower limit on reactive current injection Iqinj	pu	-1
Vref0	User defined reference (if 0, model initialises it to initial terminal voltage)	pu	0
Tp	Filter time constant for electrical power	s	0.01
QMax	limit for reactive power regulator	pu	0.6
QMin	limit for reactive power regulator	pu	-0.6
VMAX	Max. limit for voltage control	pu	1.1
VMIN	Min. limit for voltage control	pu	0.9
Kqp	Reactive power regulator proportional gain	pu	10
Kqi	Reactive power regulator integral gain	pu	0.1
Kvp	Voltage regulator proportional gain	pu	0.1
Kvi	Voltage regulator integral gain	pu	0
Tiq	Reactive current regulator time constant	s	0.01
dPmax	(>0) Power reference max. ramp rate	pu/s	10
dPmin	(<0) Power reference min. ramp rate	pu/s	-10
PMAX	Max. power limit	pu	1
PMIN	Min. power limit	pu	0
Imax	Maximum limit on total converter current	pu	1.1
Tpord	Power filter time constant	s	0.01

Table B.2: Parameters of REEC_B

B.3. REPC_A Module

Parameter	Description	Unit	Value
Tfltr	Voltage or reactive power measurement filter time constant	s	0.01
Kp	Reactive power PI control proportional gain	pu	0.1
Ki	Reactive power PI control integral gain	pu	0.15
Tft	Lead time constant	s	0.05
Tfv	Lag time constant	s	0
Vfrz	Voltage below which State s2 is frozen	pu	0
Rc	Line drop compenstation resistance	pu	0
Xc	Line drop compenstation reactance	pu	0
Kc	Reactive current compensation gain	pu	0.33
emax	upper limit on deadband output	pu	1
emin	lower limit on deadband output	pu	-1
dbd1	lower threshold for reactive power control deadband (≤ 0)	pu	-0.005
dbd2	upper threshold for reactive power control deadband (≥ 0)	pu	0.005
Qmax	Upper limit on output of V/Q control	pu	0.4
Qmin	Lower limit on output of V/Q control	pu	-0.4
Kpg	Proportional gain for power control	pu	0.04
Kig	Proportional gain for power control	pu	0.08
Tp	Real power measurement filter time constant	s	0.05
fdbd1	Deadband for frequency control, lower threshold (≤ 0)	Hz	0
fdbd2	Deadband for frequency control, upper threshold (≥ 0)	Hz	0
femax	frequency error upper limit	pu	1
femin	frequency error lower limit	pu	-1
Pmax	upper limit on power reference	pu	1
Pmin	lower limit on power reference	pu	0
Tg	Power Controller lag time constant	s	0.1
Ddn	droop for over-frequency conditions	pu	20
Dup	droop for under-frequency conditions	pu	0

Table B.3: Parameters of REPC_A Module

B.4. DER_A Model

Parameter	Description	Unit	Values
VtripFlag	Flag to enable/disable voltage trip logic. 1: enable, 0: disable	–	[0 1]
FtripFlag	Flag to enable/disable frequency trip logic. 1: enable, 0: disable	–	[0 1]
Trv	voltage measurement transducer time constant	s	0.01
Trf	frequency measurement transducer time constant	s	0.01
dbd1	lower voltage deadband (≤ 0)	pu	-0.1
dbd2	upper voltage deadband ($\geq$)	pu	0.1
Kqv	proportional voltage control gain	pu	[0 2 5]
Vref0	user specified voltage set-point	pu	0
Tp	power measurement transducer time constant	s	0.01
Tiq	Q-control time constant	s	0.01
Ddn	reciprocal of droop for over-frequency conditions (<0)	pu	20
Dup	reciprocal of droop for under-frequency conditions (>0)	pu	0
fdbd1	deadband for frequency control, lower threshold	Hz	0
fdbd2	deadband for frequency control, upper threshold	Hz	0
femax	frequency error upper limit	Hz	1
femin	frequency error lower limit	Hz	-1
PMAX	Maximum power limit	pu	1
PMIN	Minimum power limit	pu	0
dPmax	Power reference maximum ramp rate (>0)	pu/s	99
dPmin	Power reference minimum ramp rate (<0)	pu/s	-99
Tpord	Power filter time constant	s	0.01
Kpg	PI controller proportional gain	pu	0.1
Kig	PI controller integral gain	pu	10
Imax	Maximum converter current	pu	1.1
vl0	inverter voltage break-point for low voltage cut-out	pu	0.7
vl1	inverter voltage break-point for low voltage cut-out (vl1$\geq$vl0)	pu	0.7
vh0	inverter voltage break-point for high voltage cut-out	pu	1.1
vh1	inverter voltage break-point for high voltage cut-out (vh1$\leq$vh0)	pu	1.1
tvl0	low voltage cut-out timer corresponding to voltage vl0	s	0.2
tvl1	low voltage cut-out timer corresponding to voltage vl1	s	0.2
tvh0	high voltage cut-out timer corresponding to voltage vh0	s	2
tvh1	high voltage cut-out timer corresponding to voltage vh1	s	2
Vrfrac	fraction of device that recovers after voltage comes back to within vl1$<$V$<$vh1 (0$\leq$Vrfrac$\leq$1)	–	1
fl	inverter frequency break-point for low frequency cut-out	Hz	47.5
fh	inverter frequency break-point for high frequency cut-out	Hz	51.5
tfl	low frequency cut-out timer corresponding to frequency fl	s	2
tfh	high frequency cut-out timer corresponding to frequency fh	s	2
Tg	current control time constant (to represent behaviour of inner control loops) (>0)	s	0.005
rrpwr	ramp rate for real power increase following a fault	pu/s	10
Tv	time constant on the output of the multiplier	s	0.01
Vpr	voltage below which frequency tripping is disabled	pu	0.3
Iqhl	upper limit on reactive current injection	pu	1
Iqll	lower limit on reactive current injection	pu	-1

Table B.4: Parameters of DER_A Model

C

Freeze Function

The freeze function is active when the PV system enters a state of fault condition which is determined by Equation 4.1. The freeze function, just like the name implies, freezes the state variables of the control blocks active during normal operation [14]. The function is illustrated by a simple integral block as shown in Figure C.1. The impact of the freeze function is shown in Figure C.2, where $y(t) = sin(t)$[1] and *Voltage_dip* is equal to 1 during the time period 2s to 4.2s.
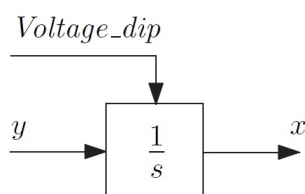
Figure C.1: Integral Block used to demonstrate freeze function
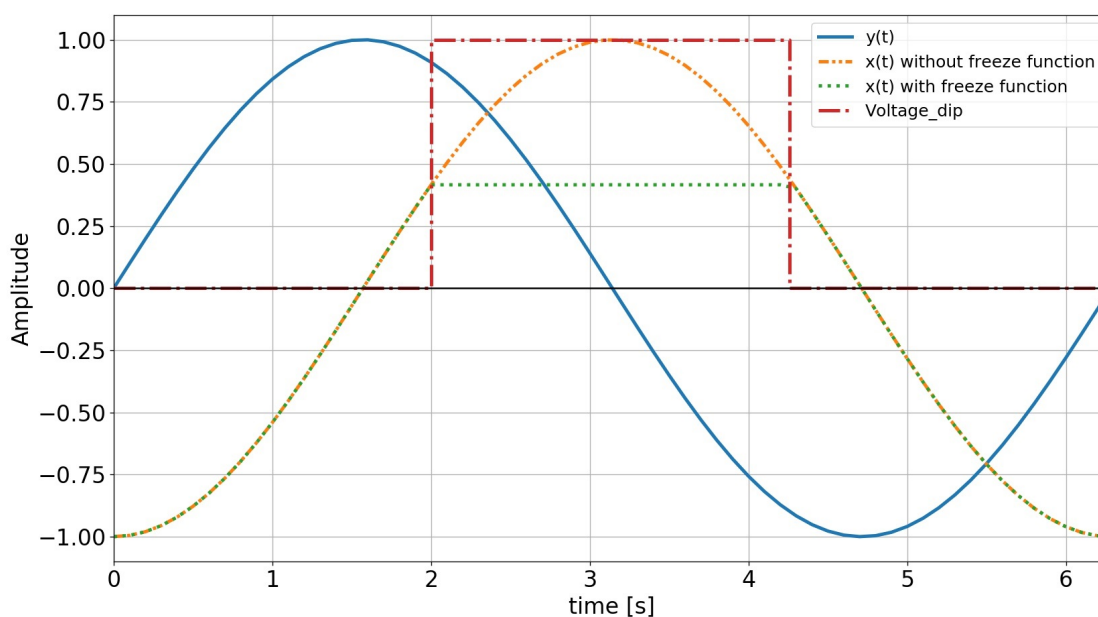
Figure C.2: Freeze function

[1]The constant of the integration is considered to be zero for this illustration

D

Parameters IEEE 9 Bus system

D.1. Load flow parameters

Transformers:

From Bus (Voltage)	To Bus (Voltage)	R (pu)	X (pu)
1 (16.5kV)	4 (230kV)	0	0.0576
2 (18kV)	7 (230kV)	0	0.0625
3 (13.8kV)	9 (230kV)	0	0.0586
11 (0.4kV)	10 (13.8 kV)	0.009	0.0850
13 (0.4 kV)	12 (18 kV)	0.009	0.0850

Table D.1: Transformer parameters of various IEEE 9 bus networks

Transmission Lines:

From Bus (Voltage)	To Bus (Voltage)	R (pu)	X (pu)	B (pu)
2 (18kV)	12 (18kV)	0.000045	0.00012	0.00013
3 (13.8kV)	10 (13.8kV)	0.000045	0.000045	0.000045
4 (230kV)	5 (230kV)	0.01	0.085	0.176
4 (230kV)	6 (230kV)	0.017	0.092	0.158
5 (230kV)	7 (230kV)	0.032	0.161	0.306
6 (230kV)	9 (230kV)	0.039	0.17	0.358
7 (230kV)	8 (230kV)	0.0085	0.072	0.149
8 (230kV)	9 (230kV)	0.0119	0.0602	0.209

Table D.2: Transmission line parameters of various IEEE 9 bus networks

Fixed shunts:

Case	Fixed Shunt at Bus 2 (Mvar)	Fixed Shunt at Bus 3 (Mvar)
27% PV Level	-	8.45
51% PV Level	20.95	-
77% PV level	26.75	7.00

Table D.3: Fixed shunts added to IEEE 9 bus networks

D.2. Dynamic parameters

Dynamic data *Base Case*:

```
// IEEE_9.dyr
1 'GENSAL' 1 8.96 0.05 0.05  9.55 1.60 0.3615  0.24 0.1508  0.10     0.06 1.01 1.02    /
2 'GENROU' 1 6.00 0.05 0.535 0.05 3.33 0.67    1.72 1.66    0.23     0.37 0.21 0.10  1.01 1.02 /
3 'GENROU' 1 5.89 0.05 0.60  0.05 2.35 0.47    1.68 1.61    0.23206  0.32 0.21 0.1536 1.01 1.02 /
// exciter
1 'IEEET1' 1 0.0 20.0 0.2 3.0 −3.0 1.0 0.314 0.063 0.35  0.0 2.8 0.3034 3.73 1.2884 /
2 'IEEET1' 1 0.0 20.0 0.2 3.0 −3.0 1.0 0.314 0.063 0.35  0.0 2.8 0.3034 3.73 1.2884 /
3 'IEEET1' 1 0.0 20.0 0.2 3.0 −3.0 1.0 0.314 0.063 0.35  0.0 2.8 0.3034 3.73 1.2884 /
// governor
1,  'IEESGO', 1, 25.0, 0,1.0,1.0,12.5,  0, 5.0,3.0,0.5,  1.0,    0,/
2,  'IEESGO', 1, 25.0, 0,1.0,1.0,12.5,  0, 5.0,3.0,0.5,  1.0,    0,/
3,  'IEESGO', 1, 25.0, 0,1.0,1.0,12.5,  0, 5.0,3.0,0.5,  1.0,    0,/
// stabilizer
1,'PSS2A',1,1,0,3,0,5,1,2,2,0.1,2,4,2,0.250,1,0.5,0.1,30,0.15,0.03,0.15,0.03,0.1,−0.1,/
2,'PSS2A',1,1,0,3,0,5,1,2,2,0.1,2,4,2,0.250,1,0.5,0.1,30,0.15,0.03,0.15,0.03,0.1,−0.1,/
3,'PSS2A',1,1,0,3,0,5,1,2,2,0.1,2,4,2,0.250,1,0.5,0.1,30,0.15,0.03,0.15,0.03,0.1,−0.1,/
```

Dynamic data *27% PV level case:*

```
// IEEE_9.dyr
1 'GENSAL' 1 8.96 0.05 0.05  9.55 1.60 0.3615  0.24 0.1508  0.10     0.06 1.01 1.02    /
2 'GENROU' 1 6.00 0.05 0.535 0.05 3.33 0.67    1.72 1.66    0.23     0.37 0.21 0.10  1.01 1.02 /

// exciter
1 'IEEET1' 1 0.0 20.0 0.2 3.0 −3.0 1.0 0.314 0.063 0.35  0.0 2.8 0.3034 3.73 1.2884 /
2 'IEEET1' 1 0.0 20.0 0.2 3.0 −3.0 1.0 0.314 0.063 0.35  0.0 2.8 0.3034 3.73 1.2884 /
// governor
1,  'IEESGO', 1, 25.0, 0,1.0,1.0,12.5,  0, 5.0,3.0,0.5,  1.0,    0,/
2,  'IEESGO', 1, 25.0, 0,1.0,1.0,12.5,  0, 5.0,3.0,0.5,  1.0,    0,/

// stabilizer
1,'PSS2A',1,1,0,3,0,5,1,2,2,0.1,2,4,2,0.250,1,0.5,0.1,30,0.15,0.03,0.15,0.03,0.1,−0.1,/
2,'PSS2A',1,1,0,3,0,5,1,2,2,0.1,2,4,2,0.250,1,0.5,0.1,30,0.15,0.03,0.15,0.03,0.1,−0.1,/

// PV dynamic data
11 'REGCA1' 1 0 0.50000E−02 10.0000 0.70000 0.10000 0.0000 2.0000 0.80000 0.0000
−1.10000  0.10000E−01 0.0000 99.000 −99.000 1.000 /
11 'REECB1' 1 0 0 1 1 0 0.95 1.05 0.01 −0.05 0.05 5.0000 1.0000 −1 0 0.01 0.6 −0.6
1.1 0.9 10 0.1 0.1 0 0.01 10.00 −10 1.0000 0.0000 1.1000 0.01 /
11  'REPCA1' 1 9 3 9 '1 ' 0 0 0 0.01 0.1 0.15 0.05 0.0000 0.0 0.0000 0.00000 0.3300
1.0000 −1.0000 −0.0050 −0.00500 0.4 −0.4 0.04 0.08 0.05 0 0 1.0 −1 1.0000 0.0000 0.10000
20.0000 0.0000 /
```

Dynamic data *51% PV level case*:

```
// IEEE_9.dyr
1 'GENSAL' 1 8.96 0.05 0.05  9.55 1.60 0.3615  0.24 0.1508  0.10     0.06 1.01 1.02    /
3 'GENROU' 1 5.89 0.05 0.60  0.05 2.35 0.47    1.68 1.61    0.23206  0.32 0.21 0.1536 1.01 1.02 /
```

```
// exciter
1 'IEEET1' 1 0.0 20.0 0.2 3.0 −3.0 1.0 0.314 0.063 0.35   0.0 2.8 0.3034 3.73 1.2884 /
3 'IEEET1' 1 0.0 20.0 0.2 3.0 −3.0 1.0 0.314 0.063 0.35   0.0 2.8 0.3034 3.73 1.2884 /
// governor
1,   'IEESGO', 1, 25.0, 0,1.0,1.0,12.5,   0, 5.0,3.0,0.5,   1.0,     0,/
3,   'IEESGO', 1, 25.0, 0,1.0,1.0,12.5,   0, 5.0,3.0,0.5,   1.0,     0,/
// stabilizer
1,'PSS2A',1,1,0,3,0,5,1,2,2,0.1,2,4,2,0.250,1,0.5,0.1,30,0.15,0.03,0.15,0.03,0.1,−0.1,/
3,'PSS2A',1,1,0,3,0,5,1,2,2,0.1,2,4,2,0.250,1,0.5,0.1,30,0.15,0.03,0.15,0.03,0.1,−0.1,/
// PV dynamic data
13 'REGCA1' 1 0 0.50000E−02 10.0000 0.70000 0.10000 0.0000 2.0000 0.80000 0.0000
−1.10000  0.10000E−01 0.0000 99.000 −99.000 1.000 /
13 'REECB1' 1 0 0 1 1 0 0.95 1.05 0.01 −0.05 0.05 5.0000 1.0000 −1 0 0.01 0.6 −0.6
1.1 0.9 10 0.1 0.1 0 0.01 10.00 −10 1.0000 0.0000 1.1000 0.01 /
13  'REPCA1' 1 7 2 7 '1 ' 0 0 0 0.01 0.1 0.15 0.05 0.0000 0.0 0.0000 0.00000 0.3300
1.0000 −1.0000 −0.0050 −0.00500 0.4 −0.4 0.04 0.08 0.05 0 0 1.0 −1 1.0000 0.0000 0.10000
20.0000 0.0000 /
```

Dynamic data *77% PV level case*:

```
// IEEE_9.dyr
1 'GENSAL' 1 8.96 0.05 0.05  9.55 1.60 0.3615  0.24 0.1508  0.10     0.06 1.01 1.02    /
// exciter
1 'IEEET1' 1 0.0 20.0 0.2 3.0 −3.0 1.0 0.314 0.063 0.35   0.0 2.8 0.3034 3.73 1.2884 /
// governor
1,   'IEESGO', 1, 25.0, 0,1.0,1.0,12.5,   0, 5.0,3.0,0.5,   1.0,     0,/
// stabilizer
1,'PSS2A',1,1,0,3,0,5,1,2,2,0.1,2,4,2,0.250,1,0.5,0.1,30,0.15,0.03,0.15,0.03,0.1,−0.1,/
// PV dynamic data
11 'REGCA1' 1 0 0.50000E−02 10.0000 0.70000 0.10000 0.0000 2.0000 0.80000 0.0000
−1.10000  0.10000E−01 0.0000 99.000 −99.000 1.000 /
11 'REECB1' 1 0 0 1 1 0 0.95 1.05 0.01 −0.05 0.05 5.0000 1.0000 −1 0 0.01 0.6 −0.6
1.1 0.9 10 0.1 0.1 0 0.01 10.00 −10 1.0000 0.0000 1.1000 0.01 /
11  'REPCA1' 1 9 3 9 '1 ' 0 0 0 0.01 0.1 0.15 0.05 0.0000 0.0 0.0000 0.00000 0.3300
1.0000 −1.0000 −0.0050 −0.00500 0.4 −0.4 0.04 0.08 0.05 0 0 1.0 −1 1.0000 0.0000 0.10000
20.0000 0.0000 /
13 'REGCA1' 1 0 0.50000E−02 10.0000 0.70000 0.10000 0.0000 2.0000 0.80000 0.0000
−1.10000  0.10000E−01 0.0000 99.000 −99.000 1.000 /
13 'REECB1' 1 0 0 1 1 0 0.95 1.05 0.01 −0.05 0.05 5.0000 1.0000 −1 0 0.01 0.6 −0.6
1.1 0.9 10 0.1 0.1 0 0.01 10.00 −10 1.0000 0.0000 1.1000 0.01 /
13  'REPCA1' 1 7 2 7 '1 ' 0 0 0 0.01 0.1 0.15 0.05 0.0000 0.0 0.0000 0.00000 0.3300
1.0000 −1.0000 −0.0050 −0.00500 0.4 −0.4 0.04 0.08 0.05 0 0 1.0 −1 1.0000 0.0000 0.10000
20.0000 0.0000 /
```

D.3. Other Calculations
Calculation steady-state stability limit generators:

Generator	Vt (pu)	Xd (pu)	$\frac{Vt^2}{Xd}$ (pu)
2	1.025	1.72	0.6108
3	1.025	1.68	0.6254

Table D.4: Steady-state stability limit of generators IEEE 9 bus networks

E

Parameters of added elements in dynamic grid model

This Appendix discusses the method used for assigning parameters to the underlying elements (LV/MV transformer equivalent, collector system equivalent and station transformer) added to the dynamic grid model as shown in Figure E.1.
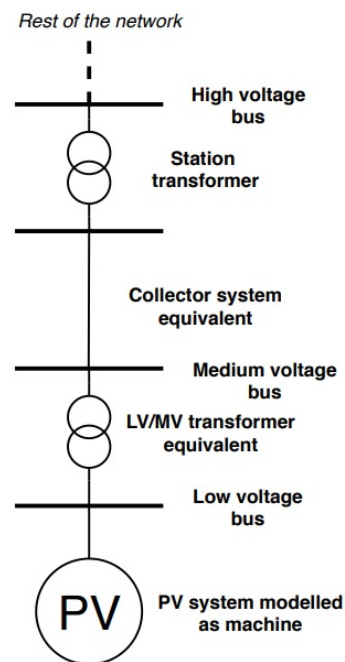
Figure E.1: Detail of PV modelling after using script

The assignment of values is shown below.

Station transformer
The station transformer is assigned the parameters shown below.

$$S_{equivalent} = \frac{\text{Total Capacity of PV systems at this bus}}{0.9} \tag{E.1}$$

$$\text{rating\_transformer} = \frac{S_{equivalent}}{60} \tag{E.2}$$

$$R = \frac{0.00317}{\text{rating\_transformer}} \tag{E.3}$$

$$X = \frac{0.19}{rating\_transformer} \tag{E.4}$$

Collector System equivalent

The collector system equivalent is assigned the parameters shown below.

$$S_{equivalent} = \frac{\text{Total Capacity of PV systems at this bus}}{0.9} \tag{E.5}$$

$$\text{Length of equivalent cable} = 3\text{km} \tag{E.6}$$

$$\text{rating\_cables} = \frac{S_{equivalent}}{10} \tag{E.7}$$

$$R = \frac{0.03 \times \text{length of cable}}{rating\_cables} \tag{E.8}$$

$$X = \frac{0.05 \times \text{length of cable}}{rating\_cables} \tag{E.9}$$

$$B = \frac{0.0035 \times \text{length of cable}}{rating\_cables} \tag{E.10}$$

LV/MV transformer equivalent

The LV/MV transformer equivalent is assigned the parameters shown below.

$$S_{equivalent} = \frac{\text{Total Capacity of PV systems at this bus}}{0.9} \tag{E.11}$$

$$R = 0.009 \tag{E.12}$$

$$X = 0.07 \tag{E.13}$$

Bibliography

[1] D. Qin, M. Manning, Z. Chen, M. Marquis, K. Averyt, M. Tignor, and H. Miller, "Contribution of Working Group I to the Fourth Assessment Report of the Intergovernmental Panel on Climate Change," *Climate Change 2007: The Physical Science Basis*, January 2007.

[2] NASA Team, "Global Surface Temperature," Apr 2019. [Online]. Available: https://climate.nasa.gov/vital-signs/global-temperature/ [Accessed: 13 December 2019]

[3] C. Butler, "Climate Change, Health and Existential Risks to Civilization: A Comprehensive Review (1989-2013)," *International journal of environmental research and public health*, vol. 15, October 2018. [Online]. Available: https://www.ncbi.nlm.nih.gov/pmc/articles/PMC6210172/ [Accessed: 19 December 2019]

[4] P. Ruyssenaars, P. Coenen, P. Zijlema, E. Arets, K. Baas, R. Dröge, G. Geilenkirchen, M. T Hoen, E. Honig, B. Huet, E. Huis, W. Koch, L. Lagerwerf, R. Molder, J. Montfoort, C. Peek, J. Vonk, and M. van Zanten, "Greenhouse Gas Emissions in the Netherlands 1990-2017: National Inventory Report 2019," May 2019. [Online]. Available: https://www.rivm.nl/bibliotheek/rapporten/2019-0020.pdf [Accessed: 19 December 2019]

[5] United Nations, "Paris Agreement," 2015. [Online]. Available: https://unfccc.int/sites/default/files/english_paris_agreement.pdf [Accessed: 12 December 2019]

[6] "Klimaatakkoord," June 2019. [Online]. Available: https://www.klimaatakkoord.nl/documenten/publicaties/2019/06/28/klimaatakkoord [Accessed: 13 December 2019]

[7] Dutch New Energy Research (DNE Research), "Nationaal Solar Trendrapport 2020 samenvatting," 2019. [Online]. Available: https://www.solarsolutions.nl/trendrapport/ [Accessed: 14 February 2020]

[8] J. Boemer, "On Stability of Sustainable Power Systems: Network Fault Response of Transmission Systems with Very High Penetration of Distributed Generation," Ph.D. dissertation, June 2016. [Online]. Available: https://pure.tudelft.nl/portal/files/4368591/JCBoemer_On_Stability_of_Sustainable_Power_Systems_June2016.pdf [Accessed: 19 December 2019]

[9] V. N. Sewdien, M. van der Meijden, T. Breithaupt, L. Hofmann, D. Herwig, A. Mertens, B. W. Tuinema, and J. L. Rueda Torres, "Effects of Increasing Power Electronics on System Stability: Results from MIGRATE Questionnaire," pp. 1–9, Oct 2018. [Online]. Available: https://ieeexplore.ieee.org/document/8635602 [Accessed: 14 February 2020]

[10] K. Yamashita, H. Renner, S. Martinez Villanueva, K. Vennemann, J. Martins, P. Aristidou, T. Van Cutsem, Z. Song, G. Lammert, L. Pabon, L. Zhu, I. Green, G. Irwin, D. Geibel, S. Jankovic, C. Zhan, F. Ciausiu, K. Karoui, K. Chan, and M. Steurer, "Modelling of Inverter-Based Generation for Power System Dynamic Studies," pp. 81 – 87, June 2018. [Online]. Available: http://cired.net/uploads/default/files/727-web.pdf [Accessed: 19 December 2019]

[11] Leonard L. Grigsby, *Electric Power Engineering Handbook Second Edition*, 2019.

[12] P. Kundur, J. Paserba, V. Ajjarapu, G. Andersson, A. Bose, C. Canizares, N. Hatziargyriou, D. Hill, A. Stankovic, C. Taylor, T. Van Cutsem, and V. Vittal, "Definition and Classification of Power System Stability IEEE/CIGRE Joint Task Force on Stability Terms and Definitions," *IEEE Transactions on Power Systems*, vol. 19, no. 3, pp. 1387–1401, August 2004. [Online]. Available: https://ieeexplore.ieee.org/document/1318675 [Accessed: 19 December 2019]

[13] P. Kundur, N. Balu, and M. Lauby, *Power System Stability and Control*, ser. EPRI power system engineering series. McGraw-Hill Education, 1994. [Online]. Available: https://books.google.nl/books?id=2cbvyf8Ly4AC

[14] G. Lammert, "Modelling, Control and Stability Analysis of Photovoltaic Systems in Power System Dynamic Studies," Ph.D. dissertation, 2019. [Online]. Available: https://www.uni-kassel.de/upress/online/OpenAccess/978-3-7376-0716-2.OpenAccess.pdf [Accessed: 23 January 2020]

[15] T. Breithaupt, D. Herwig, L. Hofmann, A. Mertens, R. Meyer, N. Farrokhseresht, B. Tuinema, D. Wang, J. Rueda Torres, S. Ruberg, and V. Sewdien, "Deliverable D1.1 Report on systemic issues," December 2016. [Online]. Available: https://www.h2020-migrate.eu/downloads.html [Accessed: 19 December 2019]

[16] Eirgrid, "All Island TSO Facilitation of Renewables Studies," 2010. [Online]. Available: http://www.eirgridgroup.com/site-files/library/EirGrid/Facilitation-of-Renewables-Report.pdf [Accessed: 3 August 2020]

[17] Commission Regulation (EU) , "Establishing a network code on requirements for grid connection of generators," *Official Journal of the European Union,* April 2016. [Online]. Available: https://eur-lex.europa.eu/legal-content/EN/TXT/?uri=OJ:JOL_2016_112_R_0001#d1 [Accessed: 6 January 2020]

[18] De Autoriteit Consument en Markt, "Netcode Elektriciteit," April 2016. [Online]. Available: https://wetten.overheid.nl/BWBR0037940/2019-10-22 [Accessed: 6 January 2020]

[19] European Network of Transmission System Operators for Electricity (ENTSO-E), "Implementation Guideline for Network Code "Requirements for Grid Connected Applicable to All Generators"," October 2013. [Online]. Available: https://www.entsoe.eu/fileadmin/user_upload/_library/resources/RfG/131016_-_NC_RfG_implementation_guideline.pdf [Accessed: 9 January 2020]

[20] Netbeheer Nederland, "Netcode elektriciteit met onderhanden zijnde codewijzigingenvoorstellen," July 2019. [Online]. Available: https://www.netbeheernederland.nl/_upload/Files/E02_-_Netcode_elektriciteit_112.pdf [Accessed: 17 January 2020]

[21] S. Ruberg, V. Sewdien, J. Rueda Torres, E. Rakshani, D. Wang, B. Tuinema, N. Farrokhseresht, D. Gusain, A. Perilla, J. Mola Jumenez, C. LongáRes Viejo, T. Breithaupt, F. Goudarzi, R. Meyer, F. Stallmann, M. Herrmann, L. Hofmann, A. Mertens, T. Hennig, M. Val Escudero, J. Kilter, T. Prevost, and G. Denis, "Demonstration of Mitigation Measures and Clarification of Unclear Grid Code Requirements," December 2019. [Online]. Available: https://www.h2020-migrate.eu/downloads.html [Accessed: 11 March 2020]

[22] TenneT (AMN-GDS), "Fast Fault Current Injection Requirements," January 2020.

[23] Göksu, P. Sorensen, J. Fortmann, A. Morales, S. Weigel, and P. Pourbeik, "Compatility of IEC 61400-27-1 Ed 1 and WECC 2nd Generation Wind Turbine Models," November 2016. [Online]. Available: https://www.researchgate.net/publication/310442555_Compatibility_of_IEC_61400-27-1_Ed_1_and_WECC_2nd_Generation_Wind_Turbine_Models [Accessed: 5 February 2020]

[24] WECC Renewable Energy Modeling Task Force, "Generic Solar Photovoltaic System Dynamic Simulation Model Specification," September 2012. [Online]. Available: https://www.wecc.biz/Reliability/WECC-Solar-PV-Dynamic-Model-Specification-September-2012.pdf [Accessed: 30 January 2020]

[25] Electric Power Research Institure (EPRI), "The New Aggregated Distributed Energy Resources (der_a) Model for Transmission Planning Studies: 2019 Update," March 2019. [Online]. Available: https://www.epri.com/#/pages/product/000000003002015320/?lang=en-US [Accessed: 5 February 2020]

[26] North American Electric Reliability Corporation (NERC), "Reliability Guideline Parameterization of the DER_A Model," September 2019. [Online]. Available: https://www.nerc.com/comm/PC_Reliability_Guidelines_DL/Reliability_Guideline_DER_A_Parameterization.pdf [Accessed: 19 December 2019]

[27] R. T. Elliott, A. Ellis, P. Pourbeik, J. J. Sanchez-Gasca, J. Senthil, and J. Weber, "Generic photovoltaic system models for WECC - A status report," pp. 1–5, July 2015. [Online]. Available: https://ieeexplore.ieee.org/document/7285992 [Accessed: 23 January 2020]

[28] WECC Renewable Energy Modeling Task Force, "WECC Solar Plant Dynamic Modeling Guidelines," April 2014.

[29] PSS/E 34 Documentation, "Model Library," 2018.

[30] P. Zhou, X. Yuan, J. Hu, and Y. Huang, "Stability of DC-link voltage as affected by phase locked loop in VSC when attached to weak grid," in *2014 IEEE PES General Meeting | Conference Exposition,* July 2014, pp. 1–5. [Online]. Available: https://ieeexplore.ieee.org/document/6939460 [Accessed: 31 January 2020]

[31] Electric Power Research Institure (EPRI), "Model User Guide for Generic Renewable Energy System Models," June 2015. [Online]. Available: https://www.epri.com/#/pages/product/3002006525/?lang=en-US [Accessed: 3 February 2020]

[32] P. Pourbeik, J. Weber, D. Ramasubramanian, J. Sanchez-Gasca, J. Senthil, P. Zadkhast, J. Boemer, A. Gaikwad, I. Green, S. Tacke, R. Favela, S. Wang, S. Zhu, and M. Torgesen, "An aggregate dynamic model for distributed energy resources for power system stability studies," vol. 14, pp. 38–48, June 2019. [Online]. Available: https://www.researchgate.net/publication/334081370_An_Aggregate_Dynamic_Model_for_Distributed_Energy_Resources_for_Power_System_Stability_Studies [Accessed: 5 February 2020]

[33] K. Yamashita, H. Renner, S. Martinez Villanueva, K. Vennemann, J. Martins, P. Aristidou, T. Van Cutsem, Z. Song, G. Lammert, L. Pabon, L. Zhu, I. Green, G. Irwin, D. Geibel, S. Jankovic, C. Zhan, F. Ciausiu, K. Karoui, K. Chan, and M. Steurer, "Modelling of inverter-based generation for power system dynamic studies," vol. No. 298, pp. 81 – 87, June 2018. [Online]. Available: http://cired.net/uploads/default/files/727-web.pdf [Accessed: 5 February 2020]

[34] P. Pourbeik, J. Weber, D. Ramasubramanian, J. Sanchez-Gasca, J. Senthil, P. Zadkhast, J. Boemer, A. Gaikwad, I. Green, S. Tacke, R. Favela, S. Wang, S. Zhu, and M. Torgesen, "An aggregate dynamic model for distributed energy resources for power system stability studies," vol. 14, pp. 38–48, June 2019. [Online]. Available: https://www.researchgate.net/publication/334081370_An_Aggregate_Dynamic_Model_for_Distributed_Energy_Resources_for_Power_System_Stability_Studies [Accessed: 19 December 2019]

[35] P. Pourbeik, J. J. Sanchez-Gasca, J. Senthil, J. D. Weber, P. S. Zadehkhost, Y. Kazachkov, S. Tacke, J. Wen, and A. Ellis, "Generic dynamic models for modeling wind power plants and other renewable technologies in large-scale power system studies," *IEEE Transactions on Energy Conversion*, vol. 32, no. 3, pp. 1108–1116, September 2017. [Online]. Available: https://ieeexplore.ieee.org/document/7782402 [Accessed: 17 March 2020]

[36] North American Electric Reliability Corporation (EPRI), "Reliability Guideline Distributed Energy Resource Modeling," September 2017. [Online]. Available: https://www.nerc.com/comm/PC_Reliability_Guidelines_DL/Reliability_Guideline_-_DER_Modeling_Parameters_-_2017-08-18_-_FINAL.pdf [Accessed: 3 March 2020]

[37] WECC Renewable Energy Modeling Task Force, "Central Station PV Plant Model Validation Guideline," June 2015. [Online]. Available: https://www.wecc.org/Reliability/Central%20Station%20Photovoltaic%20Power%20Plant%20Model%20Validation%20Guideline%20June%2017%202015.pdf [Accessed: 24 March 2020]

[38] TenneT (AMN-GDS), "Verhaallijnen IP2020," May 2019.

[39] WECC Renewable Energy Modeling Task Force, "WECC Wind Plant Dynamic Modeling Guidelines," April 2014. [Online]. Available: https://www.wecc.org/reliability/wecc%20wind%20plant%20dynamic%20modeling%20guidelines.pdf [Accessed: 18 June 2020]

[40] TenneT (AMNGDS), "Flowchart_DynMod_v1," March 2019.

[41] GfK Belgium consortium, "Study on "Residential Prosumers in the European Energy Union"," May 2017. [Online]. Available: https://ec.europa.eu/commission/sites/beta-political/files/study-residential-prosumers-energy-union_en.pdf [Accessed: 22 June 2020]

[42] Jorrit Bos, "Critical Fault Clearing Time study 2019," February 2020.

[43] S. Wildenhues, J. L. Rueda, and I. Erlich, "Optimal allocation and sizing of dynamic var sources using heuristic optimization," *IEEE Transactions on Power Systems*, vol. 30, no. 5, pp. 2538–2546, 2015. [Online]. Available: https://ieeexplore.ieee.org/document/6920093 [Accessed: 5 August 2020]

[44] GMichał Kosmecki, Bogdan Sobczak, Jan Smoter, Maciej Wilk, "Dynamic model of Continental Europe 2019 Development of dispersed generation models DRAFT VERSION," 2020.